

**Flanders**  
State of  
the Art

13\_131\_19  
FHR reports

## Integraal Plan Boven-Zeeschelde

Sub report 19  
Effect of C-alternatives on Sand Transport

DEPARTMENT  
MOBILITY &  
PUBLIC  
WORKS

[www.flandershydraulicsresearch.be](http://www.flandershydraulicsresearch.be)

# Integraal Plan Boven-Zeeschelde

## Sub report 19 – Effect of C-alternatives on Sand Transport

Bi, Q.; Vanlede, J.; Smolders, S.

### Legal notice

Flanders Hydraulics Research is of the opinion that the information and positions in this report are substantiated by the available data and knowledge at the time of writing.  
 The positions taken in this report are those of Flanders Hydraulics Research and do not reflect necessarily the opinion of the Government of Flanders or any of its institutions.  
 Flanders Hydraulics Research nor any person or company acting on behalf of Flanders Hydraulics Research is responsible for any loss or damage arising from the use of the information in this report.

### Copyright and citation

© The Government of Flanders, Department of Mobility and Public Works, Flanders Hydraulics Research 2022  
 D/2021/3241/293

This publication should be cited as follows:

**Bi, Q.; Vanlede, J.; Smolders, S.** (2022). Integraal Plan Boven-Zeeschelde: Sub report 19 – Effect of C-alternatives on Sand Transport. Version 3.0. FHR Reports, 13\_131\_19. Flanders Hydraulics Research: Antwerp

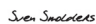

Reproduction of and reference to this publication is authorised provided the source is acknowledged correctly.

### Document identification

Customer:	Flanders Hydraulics Research	Ref.:	WL2022R13_131_19
Keywords (3-5):	Scaldis model, Sand transport, Scenario analysis		
Knowledge domains:	Hydraulics and sediment > Sediment > Non-cohesive sediment > Numerical modelling		
Text (p.):	41	Appendices (p.):	45
Confidential:	<input checked="" type="checkbox"/> No	<input checked="" type="checkbox"/> Available online	

Author(s):	Bi, Q.; Vanlede, J.
------------	---------------------

### Control

	Name	Signature
Reviser(s):	Smolders, S.	Getekend door:Sven Smolders (Signature) Getekend op:2022-02-17 14:26:47 +01:0 Reden:Ik keur dit document goed 
Project leader:	Vanlede, J.	Getekend door:Joris Vanlede (Signature) Getekend op:2022-03-03 15:11:39 +01:0 Reden:Ik keur dit document goed 

### Approval

Head of Division:	Bellafkih, K.	Getekend door:Abdelkarim Bellafkih (Sign) Getekend op:2022-02-17 14:18:19 +01:0 Reden:Ik keur dit document goed 
-------------------	---------------	----------------------------------------------------------------------------------------------------------------------------------------------------------------------------------------------------------------



## Abstract

A sand transport model for the Scheldt estuary was made in the framework of the integrated plan “Upper Sea Scheldt”. This model is called “Scaldis Sand” and was able to reproduce sand transport rates measured along the Sea Scheldt and was as such validated. In this report the Scaldis sand model is adopted to evaluate the effects of the C-alternatives on the sand transport with a focus on the Upper Sea Scheldt. A new mesh that is extended to accommodate the new measures of C alternatives is used in the model. The boundary forcing and other model settings are kept the same as in the model for the B alternatives. The net sand transport, the tidal asymmetry and the erosion/deposition are computed. The effects of the new measures on these variables are analysed and discussed in the report.



# Contents

Abstract .....	III
Contents .....	V
List of tables.....	VII
List of figures .....	VIII
1 Introduction.....	1
2 Units and reference plane .....	2
3 Summary of Scaldis sand transport model.....	3
3.1 Scaldis HD 2013 .....	3
3.2 Sand transport model in SISYPHE.....	4
3.2.1 Model parameters .....	4
3.2.2 Boundary conditions.....	5
3.2.3 Initial conditions .....	5
3.2.4 Bottom friction coefficient .....	5
3.2.5 Bottom update in hydrodynamic model switched off .....	6
4 Alternatives and scenarios .....	7
4.1 Bathymetry of the C-alternatives .....	7
4.1.1 The reference bathymetry and the bathymetry of C-alternatives.....	7
4.2 Scenarios: different boundary conditions.....	18
4.2.1 Tidal range scenarios .....	18
4.2.2 Sea level rise scenarios.....	19
4.2.3 Representative discharges.....	19
4.2.4 Modelling period .....	19
4.3 Overview of Model Runs .....	20
5 Methodology of scenario analysis.....	21
5.1 Erosion and sedimentation patterns.....	21
5.2 Net sand transport .....	21
5.3 Flow velocity and tidal (transport) asymmetry .....	22
6 Results .....	23
6.1 From 2013 to 2050 .....	23
6.2 2050REF_C.....	24
6.3 2050C1.....	28
6.4 2050C2.....	32

6.5	2050C3.....	36
7	Conclusion .....	40
	References.....	41
	Appendix 1. Polygons used in the result analysis.....	A1
	Polygons for 2050REF_C.....	A1
	Polygons for 2050C1.....	A4
	Polygons for 2050C2.....	A7
	Polygons for 2050C3.....	A10
	Appendix 2. Aggregated sedimentation and erosion.....	A13
	2050REF_C.....	A13
	2050C1.....	A16
	2050C2.....	A22
	2050C3.....	A28
	Appendix 3. Bed evolution in the Upper Sea Scheldt.....	A34
	2050REF_C.....	A34
	2050C1.....	A37
	2050C2.....	A40
	2050C3.....	A43

## List of tables

Table 1 – Overview of all measures in the C alternatives (IMDC, 2020) .....	8
Table 2 - Tidal range scenarios .....	18
Table 3 – Discharges imposed at tributaries in the Upper Sea Scheldt and at Terneuzen and Bath in the Western Scheldt .....	19
Table 4 – List of the different scenarios/alternatives runs.....	20



## List of figures

Figure 1 – The bathymetry used in the 2050REF_C .....	7
Figure 2 – Bathymetry of the Upper Sea Scheldt in 2050REF_C (km 1-13).....	10
Figure 3 – Bathymetry of the Upper Sea Scheldt in 2050REF_C (km 14-34).....	10
Figure 4 – Bathymetry of the Upper Sea Scheldt in 2050REF_C (km 35-56).....	11
Figure 5 – Bathymetry of the Upper Sea Scheldt in 2050REF_C (km 56-64).....	11
Figure 6 – Bathymetry of the Upper Sea Scheldt in 2050C1 (km 1-13).....	12
Figure 7 – Bathymetry of the Upper Sea Scheldt in 2050C1 (km 14-34).....	12
Figure 8 – Bathymetry of the Upper Sea Scheldt in 2050C1 (km 35-56).....	13
Figure 9 – Bathymetry of the Upper Sea Scheldt in 2050C1 (km 56-64).....	13
Figure 10 – Bathymetry of the Upper Sea Scheldt in 2050C2 (km 1-13).....	14
Figure 11 – Bathymetry of the Upper Sea Scheldt in 2050C2 (km 14-34).....	14
Figure 12 – Bathymetry of the Upper Sea Scheldt in 2050C2 (km 35-56).....	15
Figure 13 – Bathymetry of the Upper Sea Scheldt in 2050C2 (km 56-64).....	15
Figure 14 – Bathymetry of the Upper Sea Scheldt in 2050C3 (km 1-13).....	16
Figure 15 – Bathymetry of the Upper Sea Scheldt in 2050C3 (km 14-34).....	16
Figure 16 – Bathymetry of the Upper Sea Scheldt in 2050C3 (km 35-56).....	17
Figure 17 – Bathymetry of the Upper Sea Scheldt in 2050C3 (km 56-64).....	17
Figure 18 – The zone with changed bottom friction in the tidal range scenarios.....	18
Figure 19 – Map of the Scheldt estuary with main tributaries and most important locations.....	22
Figure 20 – Net sand transport over transects in the Sea Scheldt in 2013 and 2050 .....	23
Figure 21 – Tidal asymmetry based on the velocity over transects in the Sea Scheldt in 2013 and 2050 .....	24
Figure 22 – Time series of sand transport at different locations in the Sea Scheldt in the runs 2050REF_B_AOCN (blue line) and 2050REF_C_AOCN (red line).....	24
Figure 23 – Net sand transport capacity over cross-sections along the Sea Scheldt for a full spring/neap tidal cycle in 2050REF_C under different climate scenarios (AOCN, AminCL and AplusCH). .....	25
Figure 24 – Tidal asymmetry calculated over cross-sections along the Sea Scheldt in 2050REF_C under different climate scenarios (AOCN, AminCL and AplusCH).....	26
Figure 25 – Mean cross-sectionally averaged velocity along the Sea Scheldt in 2050REF_C under different climate scenarios (AOCN, AminCL and AplusCH).....	26
Figure 26 – Potential sedimentation and erosion map for the Upper Sea Scheldt. Scenario 2050REF_C_AOCN. ....	27
Figure 27 – Net sand transport capacity along the Sea Scheldt for a full spring/neap tidal cycle in 2050REF_C (dotted line) and 2050C1 (full line) under different climate scenarios (AOCN, AminCL and AplusCH).....	28
Figure 28 – Net sand transport capacity from km 0 to km 40 for a full spring/neap tidal cycle in 2050REF_C and 2050C1 under different climate scenarios (AOCN, AminCL and AplusCH). .....	28

Figure 29 – Tidal asymmetry along the Sea Scheldt under different climate scenarios in 2050REF\_C and 2050C1..... 29

Figure 30 – Mean cross-sectionally averaged velocity along the Sea Scheldt in 2050REF\_C and 2050C1 for a full spring/neap tidal cycle under different climate scenarios..... 30

Figure 31 – Effect of C1 alternative on the sedimentation/erosion in the Upper Sea Scheldt under AOCN condition..... 31

Figure 32 – Net sand transport capacity along the Sea Scheldt for a full spring/neap tidal cycle in 2050REF\_C (dotted line) and 2050C2 (full line) under different climate scenarios (AOCN, AminCL and AplusCH)..... 32

Figure 33 – Net sand transport capacity from km 0 to km 40 for a full spring/neap tidal cycle in 2050REF\_C (dotted line) and 2050C2 (full line) under different climate scenarios (AOCN, AminCL and AplusCH)..... 32

Figure 34 – Tidal asymmetry along the Sea Scheldt under different climate scenarios in 2050REF\_C and 2050C2..... 34

Figure 35 – Mean cross-sectionally averaged velocity along the Sea Scheldt in 2050REF\_C and 2050C2 for a full spring/neap tidal cycle under different climate scenarios..... 34

Figure 36 – Effect of C2 alternative on the sedimentation/erosion in the Upper Sea Scheldt under AOCN condition..... 35

Figure 37 – Net sand transport capacity over cross-sections along the Sea Scheldt for a full spring/neap tidal cycle in 2050REF\_C and 2050C3 under different climate scenarios (AOCN, AminCL and AplusCH). ..... 36

Figure 38 – Net sand transport capacity over cross-sections from km 0 to km 50 for a full spring/neap tidal cycle in 2050REF\_C and 2050C3 under different climate scenarios (AOCN, AminCL and AplusCH). ..... 36

Figure 39 – Tidal asymmetry along the Sea Scheldt under different climate scenarios in 2050REF\_C and 2050C3..... 38

Figure 40 – Mean cross-sectionally averaged velocity along the Sea Scheldt in 2050REF\_C and 2050C3 for a full spring/neap tidal cycle under different climate scenarios..... 38

Figure 41 – Effect of C3 alternative on the sedimentation/erosion in the Upper Sea Scheldt under AOCN condition..... 39

Figure 42 – Polygons for 2050\_REF\_C (polygons 1-13, 87-88)..... A1

Figure 43 – Polygons for 2050\_REF\_C (polygons 13-31, 85-86)..... A2

Figure 44 – Polygons for 2050\_REF\_C (polygons 32-58, 78-84)..... A3

Figure 45 – Polygons for 2050\_REF\_C (polygons 59-77)..... A3

Figure 46 – Polygons for 2050\_C1 (polygons 1-13, 87-88)..... A4

Figure 47 – Polygons for 2050\_C1 (polygons 13-31, 85-86)..... A5

Figure 48 – Polygons for 2050\_C1 (polygons 32-58, 79-84)..... A6

Figure 49 – Polygons for 2050\_C1 (polygons 59-78)..... A6

Figure 50 – Polygons for 2050\_C2 (polygons 1-13, 91-92)..... A7

Figure 51 – Polygons for 2050\_C2 (polygons 13-31, 89-90)..... A8

Figure 52 – Polygons for 2050\_C2 (polygons 32-58, 79-88)..... A9

Figure 53 – Polygons for 2050\_C2 (polygons 59-78)..... A9

Figure 54 – Polygons for 2050\_C3 (polygons 1-13, 90-91)..... A10

Figure 55 – Polygons for 2050\_C3 (polygons 13-31, 88-89)..... A11

Figure 56 – Polygons for 2050\_C3 (polygons 32-58, 79-87)..... A12

Figure 57 – Polygons for 2050\_C3 (polygons 59-78)..... A12

Figure 58 – Potential sedimentation and erosion map for the Upper Sea Scheldt. Scenario 2050REF\_C\_A0CN. .... A13

Figure 59 – Potential sedimentation and erosion map for the Upper Sea Scheldt. Scenario 2050REF\_C\_AminCL..... A14

Figure 60 – Potential sedimentation and erosion map for the Upper Sea Scheldt. Scenario 2050REF\_C\_AplusCH. .... A15

Figure 61 – Potential sedimentation and erosion map for the Upper Sea Scheldt. Scenario 2050C1\_A0CN. .... A16

Figure 62 – Effect of C1 alternative on the sedimentation/erosion in the Upper Sea Scheldt under A0CN condition..... A17

Figure 63 – Potential sedimentation and erosion map for the Upper Sea Scheldt. Scenario 2050C1\_AminCL. .... A18

Figure 64 – Effect of C1 alternative on the sedimentation/erosion in the Upper Sea Scheldt under A0CN condition..... A19

Figure 65 – Potential sedimentation and erosion map for the Upper Sea Scheldt. Scenario 2050C1\_AplusCH. .... A20

Figure 66 – Effect of C1 alternative on the sedimentation/erosion in the Upper Sea Scheldt under A0CN condition..... A21

Figure 67 – Potential sedimentation and erosion map for the Upper Sea Scheldt. Scenario 2050C2\_A0CN. .... A22

Figure 68 – Effect of C2 alternative on the sedimentation/erosion in the Upper Sea Scheldt under A0CN condition..... A23

Figure 69 – Potential sedimentation and erosion map for the Upper Sea Scheldt. Scenario 2050C2\_AminCL. .... A24

Figure 70 – Effect of C2 alternative on the sedimentation/erosion in the Upper Sea Scheldt under AminCL condition..... A25

Figure 71 – Potential sedimentation and erosion map for the Upper Sea Scheldt. Scenario 2050C2\_AplusCH. .... A26

Figure 72 – Effect of C2 alternative on the sedimentation/erosion in the Upper Sea Scheldt under AplusCH condition..... A27

Figure 73 – Potential sedimentation and erosion map for the Upper Sea Scheldt. Scenario 2050C3\_A0CN. .... A28

Figure 74 – Effect of C3 alternative on the sedimentation/erosion in the Upper Sea Scheldt under A0CN condition..... A29

Figure 75 – Potential sedimentation and erosion map for the Upper Sea Scheldt. Scenario 2050C3\_AminCL. .... A30

Figure 76 – Effect of C3 alternative on the sedimentation/erosion in the Upper Sea Scheldt under AminCL condition..... A31

Figure 77 – Potential sedimentation and erosion map for the Upper Sea Scheldt. Scenario 2050C3\_AplusCH. .... A32

Figure 78 – Effect of C3 alternative on the sedimentation/erosion in the Upper Sea Scheldt under AplusCH condition. .... A33

Figure 79 – Bed evolution in the Upper Sea Scheldt after a spring-neap cycle (2050REF\_C\_A0CN)..... A34

Figure 80 – Bed evolution in the Upper Sea Scheldt after a spring-neap cycle (2050REF\_C\_AminCL)..... A35

Figure 81 – Bed evolution in the Upper Sea Scheldt after a spring-neap cycle (2050REF\_C\_AplusCH) ..... A36

Figure 82 – Difference of bed evolution in the Upper Sea Scheldt after a spring-neap cycle (2050C1\_A0CN-2050REF\_C\_A0CN)..... A37

Figure 83 – Difference of bed evolution in the Upper Sea Scheldt after a spring-neap cycle (2050C1\_AminCL-2050REF\_C\_AminCL) ..... A38

Figure 84 – Difference of bed evolution in the Upper Sea Scheldt after a spring-neap cycle (2050C1\_AplusCH-2050REF\_C\_AplusCH)..... A39

Figure 85 – Difference of bed evolution in the Upper Sea Scheldt after a spring-neap cycle (2050C2\_A0CN-2050REF\_C\_A0CN)..... A40

Figure 86 – Difference of bed evolution in the Upper Sea Scheldt after a spring-neap cycle (2050C2\_AminCL-2050REF\_C\_AminCL) ..... A41

Figure 87 – Difference of bed evolution in the Upper Sea Scheldt after a spring-neap cycle (2050C2\_AplusCH-2050REF\_C\_AplusCH)..... A42

Figure 88 – Difference of bed evolution in the Upper Sea Scheldt after a spring-neap cycle (2050C3\_A0CN-2050REF\_C\_A0CN)..... A43

Figure 89 – Difference of bed evolution in the Upper Sea Scheldt after a spring-neap cycle (2050C3\_AminCL-2050REF\_C\_AminCL) ..... A44

Figure 90 – Difference of bed evolution in the Upper Sea Scheldt after a spring-neap cycle (2050C3\_AplusCH-2050REF\_C\_AplusCH)..... A45



# 1 Introduction

A sand transport model, as a part of a high-resolution sediment transport model for the whole Scheldt estuary is developed and validated in the project: “Integraal Plan Boven-Zeeschelde”. The details of the sand model for the Scheldt estuary is reported in Smolders et al. (2019a).

The main objectives of this sand transport model is to study future (2050) scenarios/alternatives of the Scheldt estuary by quantifying the effects compared to the reference case, e.g. the effects on bedload transport and the sediment flux through zones of interest.

The present report describes the model results with new future bathymetry alternatives in the tidal-influenced zones of the estuary, i.e. the Upper Sea Scheldt. These new alternatives are called C-alternatives and developed with the following mindset (Vansteenkiste and Adams, 2020):

- **C1 alternative:** Tackles the most prominent nautical bottlenecks (Km 0 – Ringvaart, km 10 – Wetteren, km 15 till 17 – Hoogland and Uitbergen, Km 30 – Kasteeltje, km 40 – Kramp). Looking for opportunities in the river and redefining the Sigma plan to improve habitat and to reduce the increase in tidal amplitude (from climate change and due to nautical changes).
- **C2 alternative:** Tackles also less prominent nautical bottlenecks and defines additional measures for the most prominent bottlenecks. Includes additional opportunities in the valley (depolderings, side channels) to improve habitat and to reduce the increase in tidal amplitude.
- **C3 alternative:** Yet additional nautical measures for a limited number of locations (Uitbergen, Paardenweide, Kasteeltje) and additional measures (larger depolderings, additional depoldering at Weert, undeeptening at Temse) aiming at providing additional (climate) resilience while also improving habitat conditions.

All the C alternatives are designed based on the sustainable bathymetry for 2050 (IMDC, 2015). The overview of the implemented measures is described in Bi et al. (2020a).

## 2 Units and reference plane

Time is expressed in CET (Central European Time).

Depth, height and water levels are expressed in meter TAW (Tweede Algemene Waterpassing).

Bathymetry and water levels are positive above the reference plane.

The horizontal coordinate system is RD Parijs.

## 3 Summary of Scaldis sand transport model

### 3.1 Scaldis HD 2013

The Scaldis model is a 3D hydrodynamic model that was developed within the framework of the project Integrated Plan for Upper Sea Scheldt (FHR project 13\_131). There was a need for a numerical model with higher mesh resolution in the upstream part of the Scheldt estuary. An unstructured mesh has the advantage to be very flexible in changing mesh resolution in specified areas. Therefore the Scaldis model was developed in the TELEMAC software, which is based on a finite element method.

The computational grid includes the Belgian coastal zone, extended to Dunkirk in France and Westenschouwen in the Netherlands. The grid includes the Eastern Scheldt as well. The grid size varies between 400 and 150 m in this part of the model. In the Western Scheldt and estuary mouth area the grid size decreases leading to cell sizes of 120 to 80 m. The grid includes all tributaries reaching as far as the tidal influence. The grid size keeps decreasing all the way till the upstream boundary in Merelbeke where the cell size become 5-7 m. All flood control areas of the Sigma Plan are included in the grid. The 2D grid consists of 553,057 nodes. The 3D mesh consists of prisms eventually cut into tetrahedrons and is automatically constructed from the 2D mesh. A sigma transformation is used for the vertical location of these 5 layers. Layer 1 is the bottom layer and the following layers are always situated on 0.12, 0.30, 0.60 and 1.00 fraction of the water depth.

The bathymetry is interpolated from measured data from 2013 or the closest date available. For more detailed information we refer to the calibration report of the Scaldis model from Smolders et al. (2016).

The downstream boundary is located in the North Sea. A water level is imposed on this boundary. This boundary contains 469 nodes. On every node a water level time series with 10 minute interval is imposed. These time series are extracted from the regional ZUNO model of the southern North Sea. A correction of the harmonic components was calculated based on the comparison of the harmonic components of the ZUNO results and measurements over a period of 1 year (Maximova et al., 2015). Differences in harmonic components (ZUNO vs. measurements) are found for stations in the Belgian and Dutch Coastal zone for the  $M_2$ ,  $M_4$ ,  $S_2$  phases and the  $Z_0$  component. After extraction of time series from the ZUNO model the time series of the boundary conditions of the Scaldis model are “harmonically corrected” with the obtained correction terms (+4° for  $M_2$ , -6° for  $M_4$ , +7° for  $S_2$  phase and -21 cm for  $Z_0$ ). This means that the time series are decomposed in harmonic components and a residual term. The harmonic components are corrected, and the signal is resynthesized. The subroutine BORD3D.f was changed to read and impose the appropriate time series for each boundary node.

There are 8 liquid boundaries with prescribed discharges for Merelbeke (Melle), Dender, Zenne, Dijle, Kleine Nete, Grote Nete, Canal Ghent – Terneuzen and the Canal of Bath.

Wind influence is not included in the hydrodynamic model. It is assumed to be incorporated in the boundary conditions downstream.

Salinity is applied as an active tracer. This means that density effects are taken into account in the model. time series with 10 minute interval are imposed on the downstream boundary. The downstream boundary for salinity was generated from the CSM-ZUNO model train, and subsequently corrected based on the comparison of the simulated and measured salinity time series at Vlakte van de Raan (located in the larger mouth area of the Scheldt Estuary). No tracer (Salinity) values are set for the upstream boundary conditions. No salinity is entering the domain through these boundaries in the Scaldis 3D HD model. The model starts from an initial salinity field: a map is made based on a combination of salinity measurements (Western Scheldt) and corrected model results from ZUNO (coastal area). This initial salinity map is read at the start of a simulation. The values of the 2D map are copied to the other four layers in the model.



The model runs with a time step of 4 seconds. A cold start is done with a constant water level throughout the entire model domain and the boundary imposed water levels and discharges are smoothed for the first tidal cycle. Manning's equations is used for the bottom roughness and these values vary along the estuary and were used to calibrate the hydrodynamic model. Negative depths are clipped to zero with flux control to keep the model stable. The RANS equations are solved also on the tidal flats with corrections. As a vertical turbulence model the mixing length model of Nezu and Nakagawa was used. The horizontal turbulence model is a Smagorinski model. Coriolis is activated with a coefficient value of 1.13522E-04.

For the study of sand transport in the Upper Sea Scheldt, the Scaldis HD 2013 is slightly adapted. The simulation period is one spring-neap cycle, in which the upstream discharges are kept constant. Readers are referred to §4 for detailed information.

## 3.2 Sand transport model in SISYPHE

### 3.2.1 Model parameters

The sediment module SISYPHE is coupled with the 3D hydrodynamic module TELEMAC-3D. No parameter changes were done in the hydrodynamic model Scaldis, described in Smolders et al. (2016).

In SISYPHE, the module is coupled with the hydrodynamics every time step. Engelund and Hansen (1967) was chosen as the transport equation. The formula is used in the sediment grain size range of  $D_{50} = [0.2 - 1]$  mm. This formula is derived for river flow (Engelund and Hansen, 1967). The formula given by Engelund and Hansen estimates the total transport,  $\vec{Q}_0$ , in the direction of the flow velocity,  $\vec{v}$ :

$$|\vec{Q}_0| = \frac{0.05\alpha|v|^5}{\sqrt{g}s^2C^3d_{50}} \quad (1)$$

where  $\alpha$  is a calibration coefficient (order 1);  $|v| = \sqrt{u^2 + v^2}$  is the magnitude of the flow velocity [m/s];  $s = (\rho_s - \rho)/\rho$  is the relative density with  $\rho_s$  and  $\rho$  the sediment and water density, respectively [-];  $C$  is the Chézy friction coefficient [ $m^{1/2}/s$ ]; and  $d_{50}$  is the median grain size [m]. Furthermore, to account for the bed slope effects, the correction method of Flokstra and Koch (1981) is available in Sisyphé (keyword: FORMULA FOR DEVIATION = 1) and multiplies the above equation by a factor:

$$|\vec{Q}| = |\vec{Q}_0| \left(1 - \beta \frac{\partial z_b}{\partial s}\right) \quad (2)$$

where  $\beta$  is a bed slope coefficient (keyword: BETA = 1.3);  $s$  is the coordinate in the flow direction and  $z_b$  is the bed level.

This formula is implemented in Sisyphé in the subroutine bedload\_engel.f. The formula is implemented as follows:

$$\Phi_b = C_{engel} \sqrt{\frac{(C_1 * TOB)^5}{\max(CF, 1.E - 6)}} \quad (3)$$

with

$$C_{engel} = 0.1 \sqrt{s * g * d^3} \quad (4)$$

and

$$C_1 = \frac{1}{(s * \rho * g * d)} \quad (5)$$

and

$$CF = \frac{2n^2g}{h^{\frac{1}{3}}} \quad (6)$$

and

$$TOB = 0.5 * \rho * CF * |v|^2 \quad (7)$$

where  $\Phi_b$  is the dimensionless current induced sediment transport rate; TOB is the bed shear stress [Pa]; CF is the quadratic friction coefficient;  $s = (\rho_s - \rho) / \rho$  is the relative density [-]; g is the gravitational acceleration constant [m/s<sup>2</sup>]; d is the sediment grain size [m];  $|v| = \sqrt{u^2 + v^2}$  is the magnitude of the flow velocity [m/s]; n is the Manning friction coefficient [m<sup>1/3</sup>/s]; h is the water depth [m]; and  $\rho$  is the water density [kg/m<sup>3</sup>]. CF can have a different formula depending on the type of friction coefficient that was chosen in the model. For Scaldis a Manning bottom friction coefficient was chosen and the corresponding formula for CF is given here (equation 3.6).

The velocity magnitude  $|v|$  that is used for computing the bed shear stress is derived from the near bed velocity (velocity on the bottom plane) from TELEMAC-3D. This is more accurate than using a 2DH model. In fact, it is one of the advantages of coupling SISYPHE with a 3D hydrodynamic model.

Suspended load transport is not activated in SISYPHE because the Engelund and Hansen transport equation is a total load equation. The morphological factor is set to 1. The sediment grain size is equal to 150  $\mu$ m. Only a single sediment fraction is taken into account over the entire model domain. There is an unlimited amount of sediment available in the model (= 100 m of sediment layer thickness).

The simulation will run for 15 days (a full spring-neap tidal cycle) and output is written to a results file every half hour. the time step is four seconds.

Slope effects are taken into account by default. Secondary currents is not active when coupled with a 3D hydrodynamic model. The 3D flow patterns are given to the SISYPHE module, and, near bottom velocity is used in SISYPHE for the erosion/deposition processes.

### 3.2.2 Boundary conditions

Sediment can leave the domain freely. No sediment enters the model domain through the boundaries. To prevent the model from resulting into unwanted erosion at the inflow boundaries, a fixed bed elevation (zero evolution) was defined in the boundary conditions file (.cli). This can be achieved by assigning LIEBOR=5 for the inflow nodes (8th column in .cli file).

### 3.2.3 Initial conditions

The hydrodynamic model has two days to spin up. After these two days the model is started again from the last time step of the spin up simulation and the sediment module SISYPHE is coupled. A uniform sediment layer is available throughout the entire model domain. By default the initial sediment layer thickness is 100 m. This means that the model runs with an unlimited sediment supply, and the results represent (effects on) the transport capacity

### 3.2.4 Bottom friction coefficient

In the hydrodynamic model a Manning bottom friction coefficient was spatially varied to calibrate the water levels and flow velocities in the model. By default the sediment module uses the bottom friction coefficient of the hydrodynamic module to calculate the bed shear stresses to estimate sediment motion. But during calibration of the hydrodynamic model the variation in bottom friction coefficient is used to compensate also for non-physical properties of the model, like numerical diffusion. Taking these values of the bottom friction coefficient would not be correct for sediment transport. Therefore a fixed value for the Manning bottom friction coefficient was used for the entire model domain for the sediment transport. In the subroutine

coefro\_sisyphe.f a fixed value for the bottom friction coefficient was introduced. The Manning coefficient was set to  $0.02 \text{ m/s}^{1/3}$ . In the subroutine tob\_sisyphe.f changes were made to make sure the fixed bottom friction coefficient was used in the calculations of the bed shear stress.

### 3.2.5 Bottom update in hydrodynamic model switched off

The sediment module calculates a certain sand transport and the related bottom changes. By default these bottom changes are updated in the bottom file of the hydrodynamic model every time step. But the focus of the sand transport model is on sand transport and not on morphology. Therefore the update of the bottom in the hydrodynamic model is switched off in the code. The mass balance and bottom changes are still recorded in the sediment module and are given as output, but the sand transport is always calculated based on the hydrodynamics with a fixed initial bathymetry.

## 4 Alternatives and scenarios

The calibrated sand transport model is used to evaluate the effects of different alternatives (specified morphology of the Scheldt estuary in a specific state and at a specific time), under different scenarios (a range of boundary conditions to take into account sea level rise, increasing or decreasing tidal amplitude, high or low river discharge). This chapter will give an overview of all scenarios that will be analysed with the sand transport model.

### 4.1 Bathymetry of the C-alternatives

#### 4.1.1 The reference bathymetry and the bathymetry of C-alternatives

For implementing the three different C alternatives (C1, C2 and C3) in the SCALDIS model, a new reference grid is created based on the original 2050REF grid used in the B-alternatives (**2050REF\_B**). This new reference grid, named **2050REF\_C**, is then used as the basis for implementing the C alternatives.

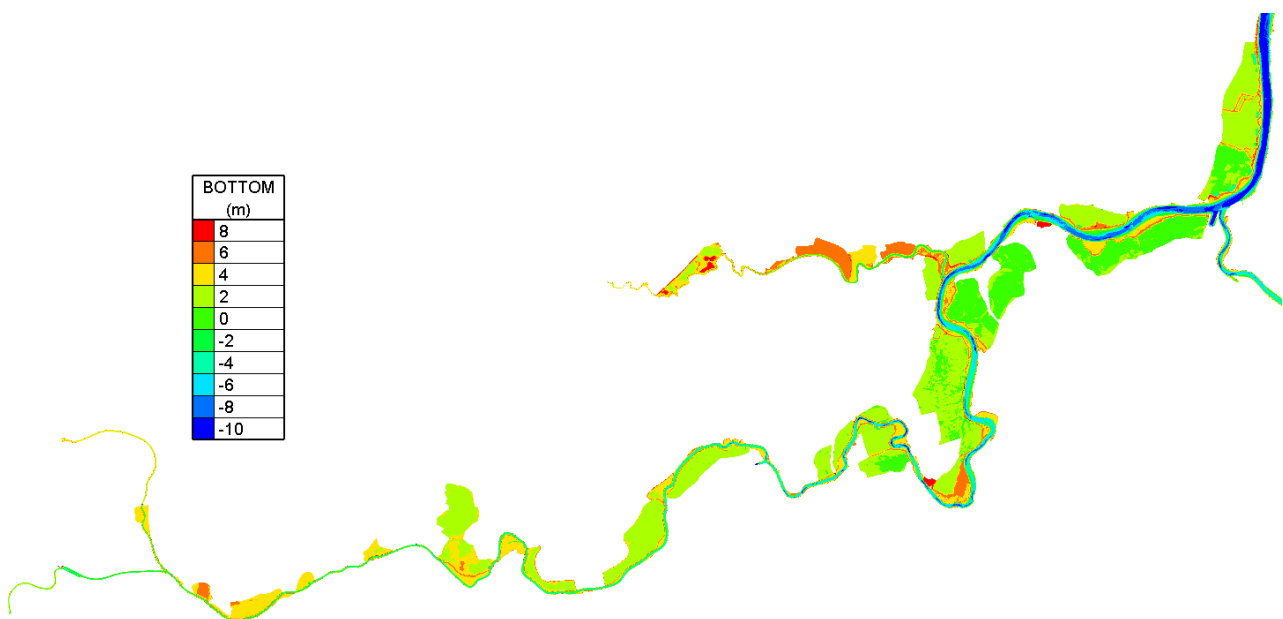


Figure 1 – The bathymetry used in the 2050REF\_C

The new reference grid is obtained by extending and refining the 2050REF\_B mesh in the Upper Sea Scheldt in order to include the maximum outline of all C alternatives. For the rest of the domain except in the Ringvaart (a widened and deepened Ringvaart is applied to the 2050REF\_C and all the C alternatives later), the grid remains unmodified, in order to allow the reuse of the boundary data. In the extended areas in the Upper Sea Scheldt, the finest grid resolution is about 7 m, and the coarsest resolution is about 50 m.

The new reference grid is able to accommodate the adaptations of the navigation channel, the new development of intertidal nature and the additional de-embankments and FCAs (with and without CRT), which are considered in any of the C alternatives.

The sustainable bathymetry in the 2050REF\_B grid with the deepening and widening of the Ringvaart is mapped to the new reference grid 2050REF\_C (Figure 1), except for the extended areas. For the extended areas, the background bathymetry without any modification from the C alternatives (provided by IMDC) is

used as the data source. The background bathymetry does not contain any measure for 2050, it represents the current situation.

When incorporating the C alternatives, the new bathymetry from C1, C2 and C3 is mapped to the 2050REF\_C grid, respectively. The overview of the implemented measures in the C alternatives is presented in Table 1. The bathymetries of the 2050REF\_C and the C alternatives are shown below .

Table 1 – Overview of all measures in the C alternatives (IMDC, 2020)

	Distance to Merelbeke [km]	Overview measures			MHW	MLW
		C1	C2	C3	[m TAW]	[m TAW]
<b>Ringvaart</b>	0-3	Deepening and widening (also present in 2050REF_C)			5.05	2.44
<b>Veerhoek</b>	4.5	-	Widening + pull back of dyke		5.05	2.44
<b>Melleham</b>	5.5	Limited tidal interaction	CRT without FCA	Depoldering	5.05	2.44
<b>Bommels</b>	6.5	-	Widening + pull back of dyke		5.06	2.37
<b>Voorde</b>	9	Bend modifications + intertidal nature			5.07	2.28
<b>Wetteren</b>	11	-	Improved navigation (cfr VaG) by installing sheet piles		5.08	2.23
<b>DS Wetteren</b>	12.5	Depoldering			5.08	2.23
<b>FCA Wijmeers</b>	15	-	Additional FCA in the north		5.08	2.12
<b>Wijmeers (Hoogland)</b>	16	Bend cut off (C1: variant 1, C2: variant 2, C3: variant 3) + intertidal nature+FCA			5.10	2.10
<b>Uitbergen</b>	19	Bend cut off + intertidal nature+depoldering (C1: variant 1, C2: variant 2, C3: variant 3)			5.10	2.02
<b>Paardenweide (Wichelen)</b>	21	-	-	Bend cut off+depoldering	5.10	1.95
<b>Oude Broekmeer</b>	24-27	-	Depoldering variant 1 + side channel	Depoldering variant 2 + side channel	5.17	1.63
<b>Appels (Scheldebreek)</b>	28	Improved navigation by smoothing the bend (cfr Chafing)			5.20	1.50
<b>Scheldebreek</b>	28	FCA Scheldebreek converted into FCA-CRT			5.20	1.50
<b>Sint-Onolfspolder</b>	28-30	-	Depoldering variant 1 + side channel variant 1	Depoldering variant 1 + side channel variant 2	5.20	1.50
<b>Kasteeltje</b>	31	Bend smoothing + intertidal nature (C1: variant 1, C2: variant 2, C3: variant 3)			5.27	1.24
<b>Dender</b>	32.5	-	Improved navigation by widening channel		5.3	1.12
<b>Grembergen broek – Armenput</b>	35-38	-	Depoldering		5.34	1.02
<b>Waterleiding</b>	38	Improved navigation (cfr Chafing) by widening channel			5.38	0.91

	Distance to Merelbeke [km]	Overview measures			MHW	MLW
		C1	C2	C3	[m TAW]	[m TAW]
<b>Roggeman</b>	39	-	Depoldering variant 1	Depoldering variant 2	5.40	0.85
<b>Kockham (Kramp)</b>	40	Bend cut off + intertidal nature (C1: variant 1; C2-C3: variant 2)			5.44	0.75
<b>Wal-Zwijn</b>	44-48	FCA with CRT	FCA with CRT	FCA with CRT	5.50	0.59
<b>Blankaart</b>	49	FCA	Depoldering variant 1	Depoldering variant 2	5.55	0.40
<b>Akkershoofd</b>	50	-	-	Depoldering together with Blankaart	5.54	0.38
<b>Tielrode Broek</b>	55	New connection with Durme + partly depoldering Tielrode Broek			5.52	0.31
<b>Weert</b>	51-56	-	-	Depoldering	5.52	0.31
<b>Temse to Rupel</b>	57-64	Local fill-in		Local fill-in + reducing channel depth	5.46	0.15
<b>Schouselbroek</b>	59	-	Depoldering + new side channel		5.47	0.19
<b>Schellandpolder</b>	61	-	Depoldering + new side channel		5.47	0.16
<b>Oudbroekpolder</b>	63	-	Depoldering + new side channel		5.45	0.13

### Reference bathymetry

The bathymetry of the 2050REF\_C is shown in Figure 2 - Figure 5. There are no new measures defined in this reference case.

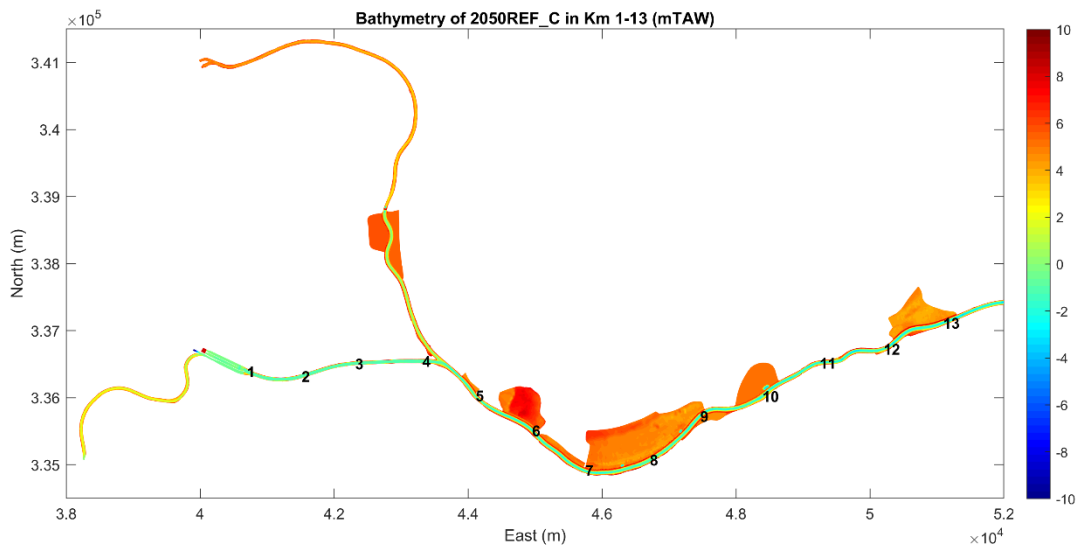


Figure 2 – Bathymetry of the Upper Sea Scheldt in 2050REF\_C (km 1-13)

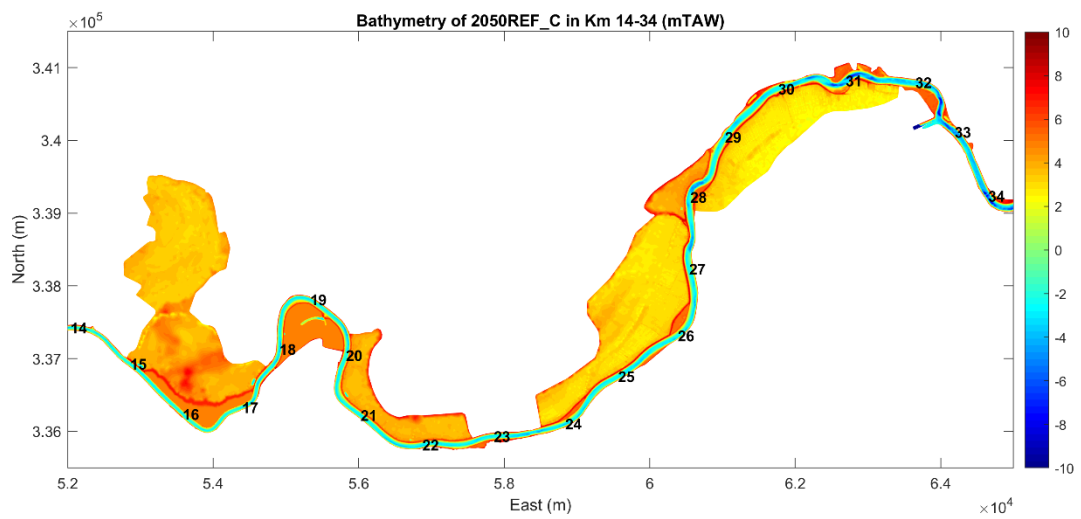


Figure 3 – Bathymetry of the Upper Sea Scheldt in 2050REF\_C (km 14-34)

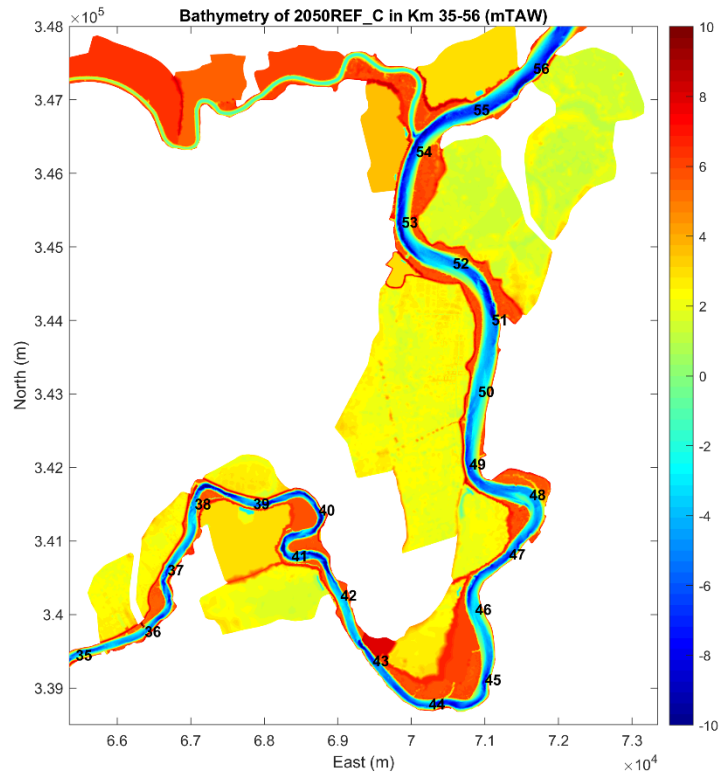


Figure 4 – Bathymetry of the Upper Sea Scheldt in 2050REF\_C (km 35-56)

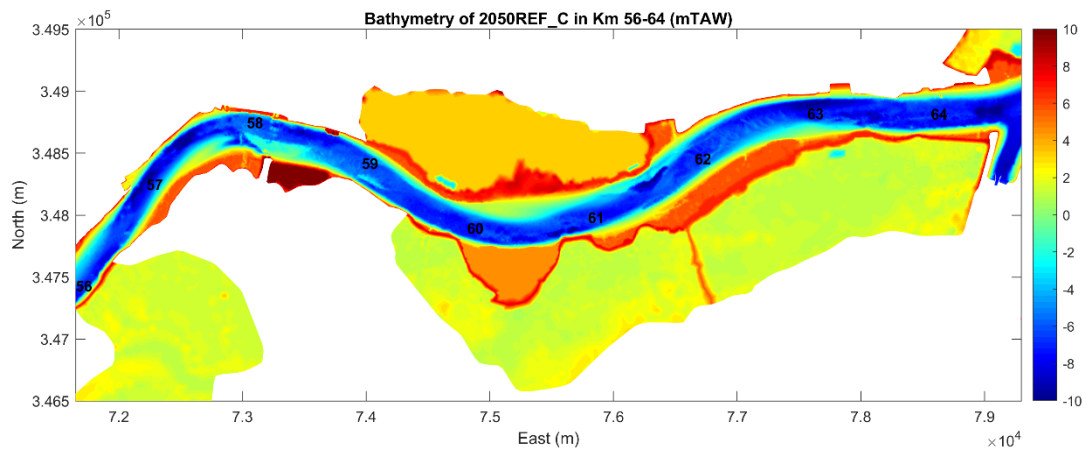


Figure 5 – Bathymetry of the Upper Sea Scheldt in 2050REF\_C (km 56-64)



### C1 bathymetry

The bathymetry used of the C1 alternative is shown in Figure 6 - Figure 9. The new measures implemented in the C1 alternative are listed in Table 1.

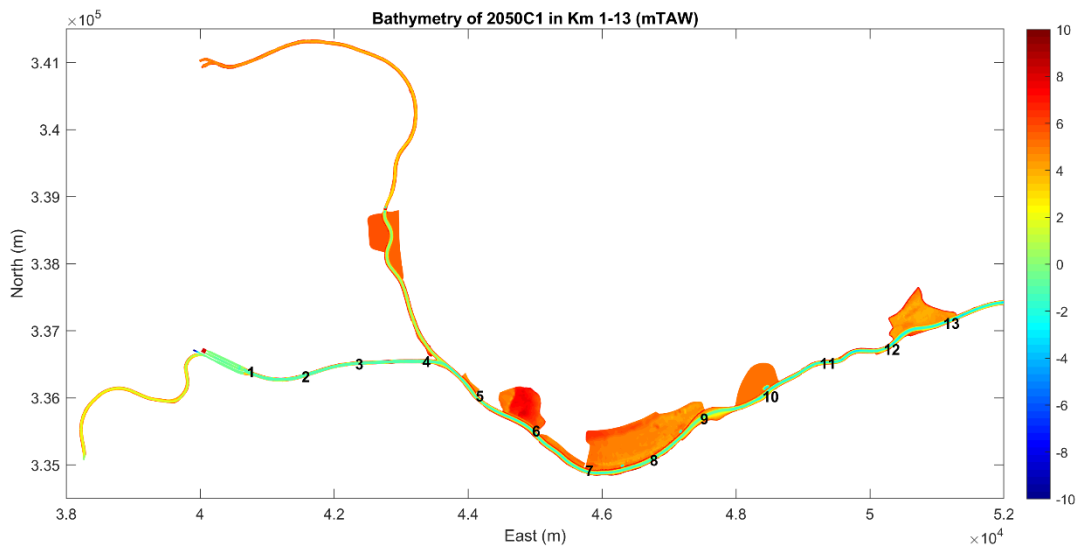


Figure 6 – Bathymetry of the Upper Sea Scheldt in 2050C1 (km 1-13)

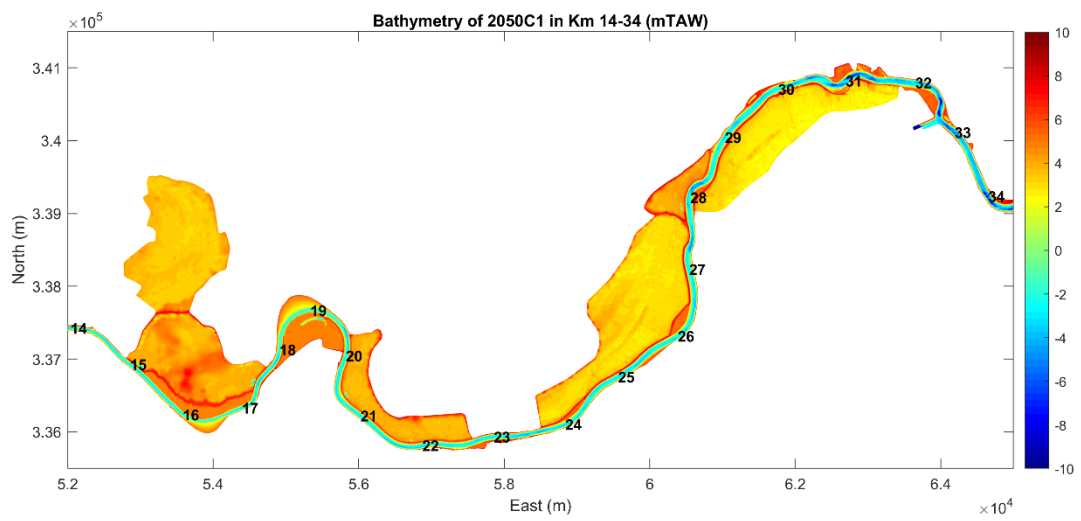


Figure 7 – Bathymetry of the Upper Sea Scheldt in 2050C1 (km 14-34)

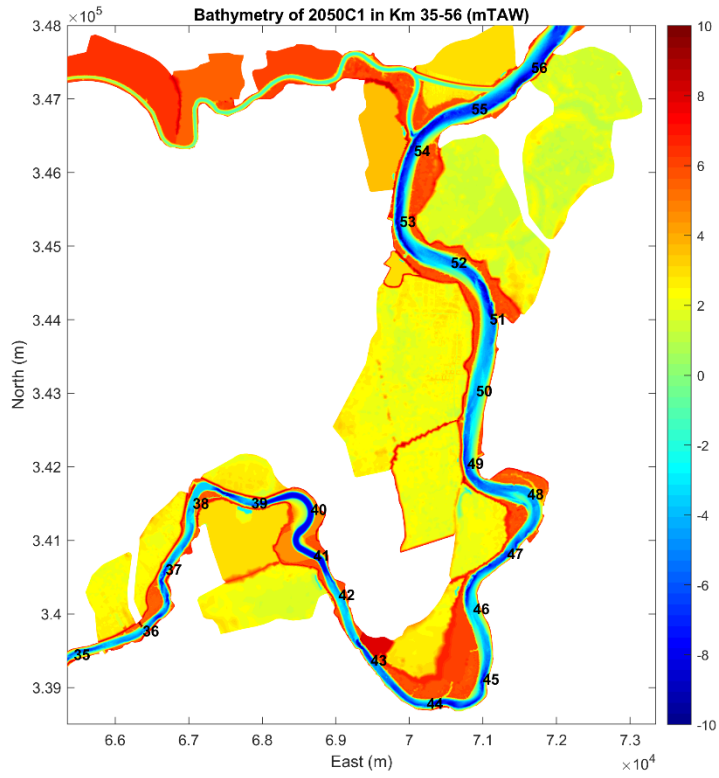


Figure 8 – Bathymetry of the Upper Sea Scheldt in 2050C1 (km 35-56)

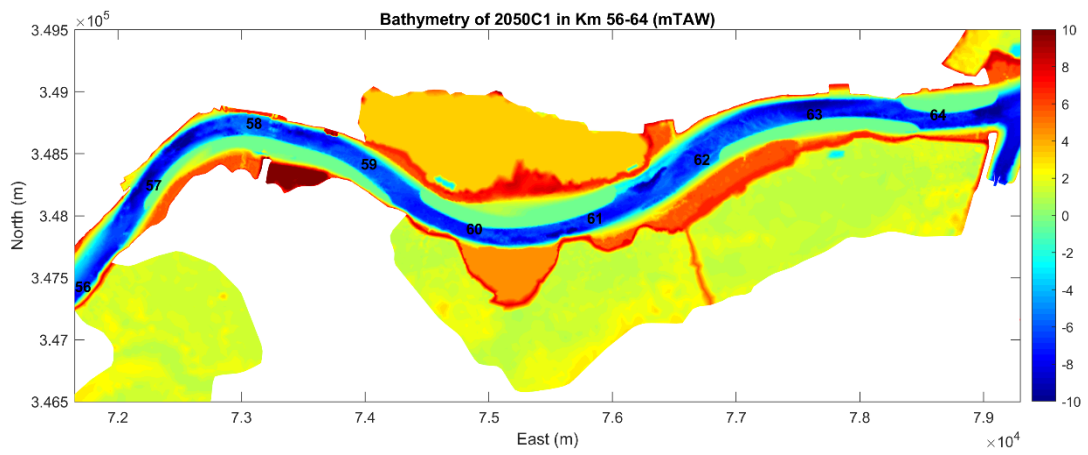


Figure 9 – Bathymetry of the Upper Sea Scheldt in 2050C1 (km 56-64)

### C2 bathymetry

The bathymetry used of the C2 alternative is shown in Figure 10 - Figure 13. The new measures implemented in the C2 alternative can be seen in Table 1.

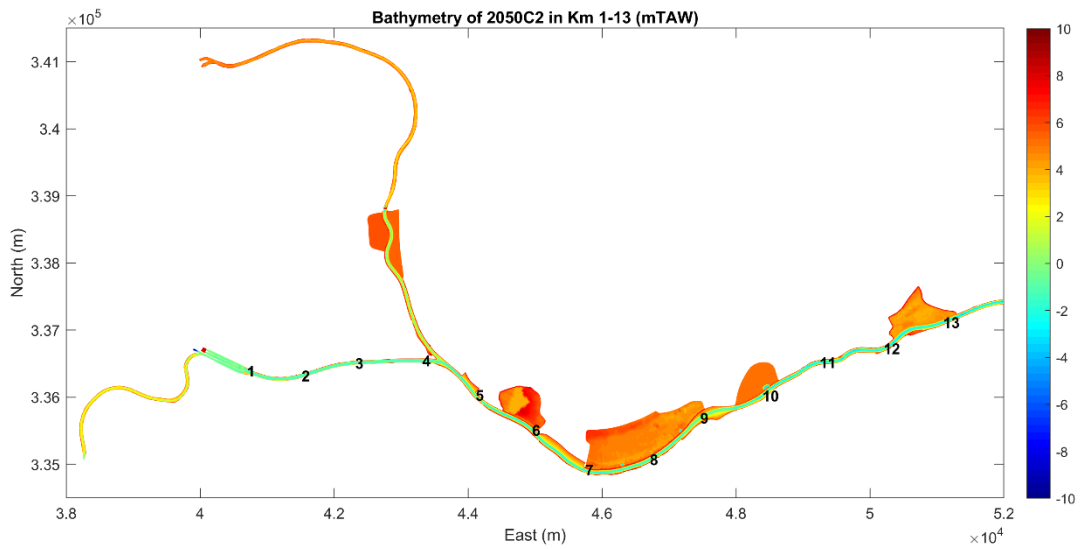


Figure 10 – Bathymetry of the Upper Sea Scheldt in 2050C2 (km 1-13)

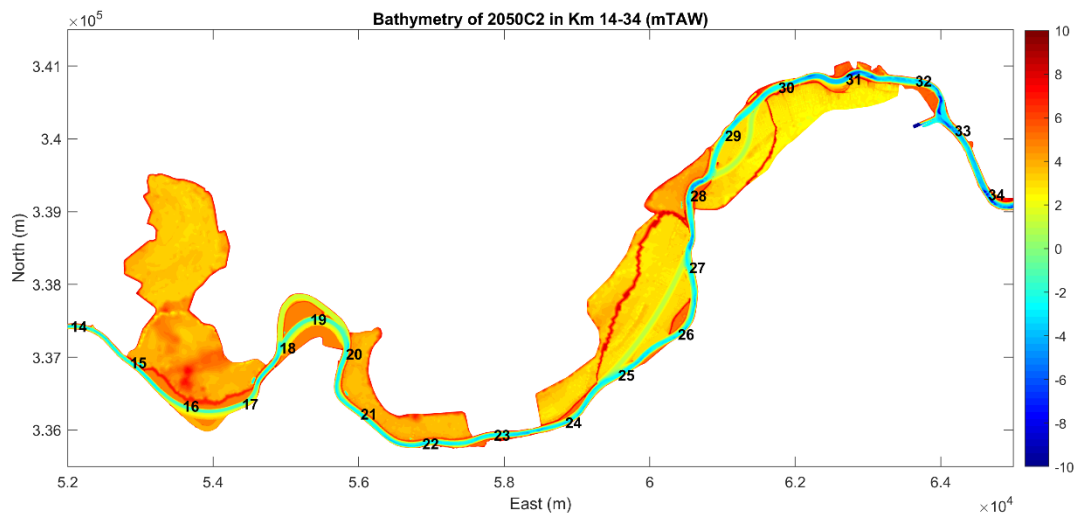


Figure 11 – Bathymetry of the Upper Sea Scheldt in 2050C2 (km 14-34)

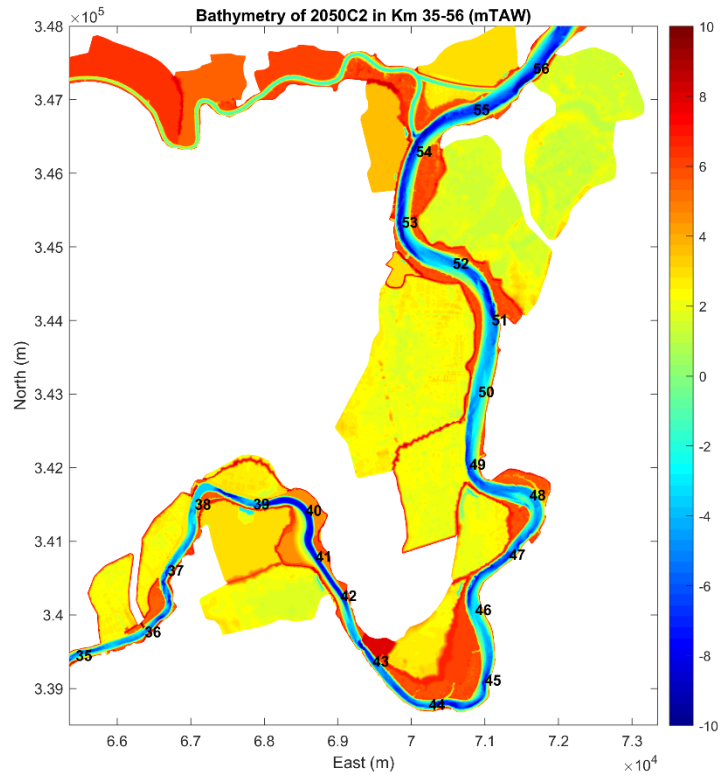


Figure 12 – Bathymetry of the Upper Sea Scheldt in 2050C2 (km 35-56)

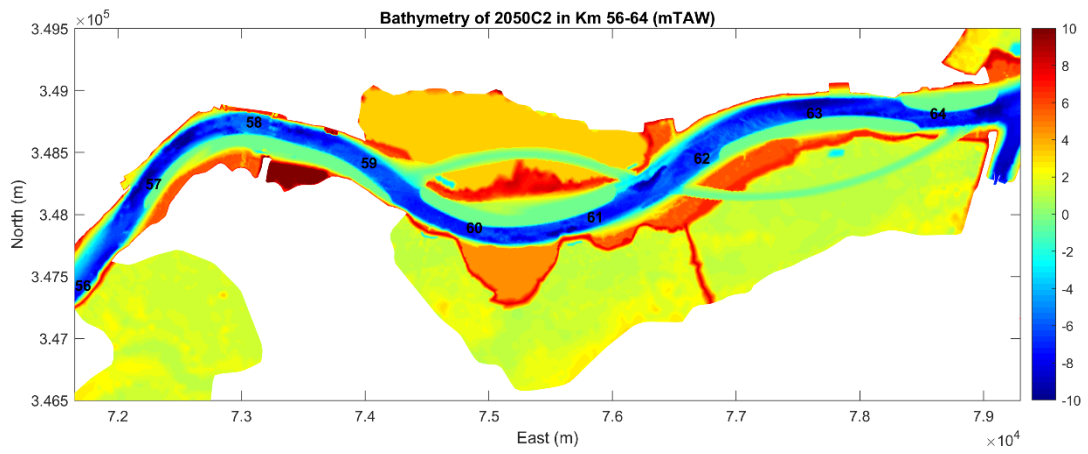


Figure 13 – Bathymetry of the Upper Sea Scheldt in 2050C2 (km 56-64)

### C3 bathymetry

The bathymetry used of the C3 alternative is shown in Figure 14 - Figure 17. The C3 alternative has the most new measures implemented, a list is shown in Table 1.

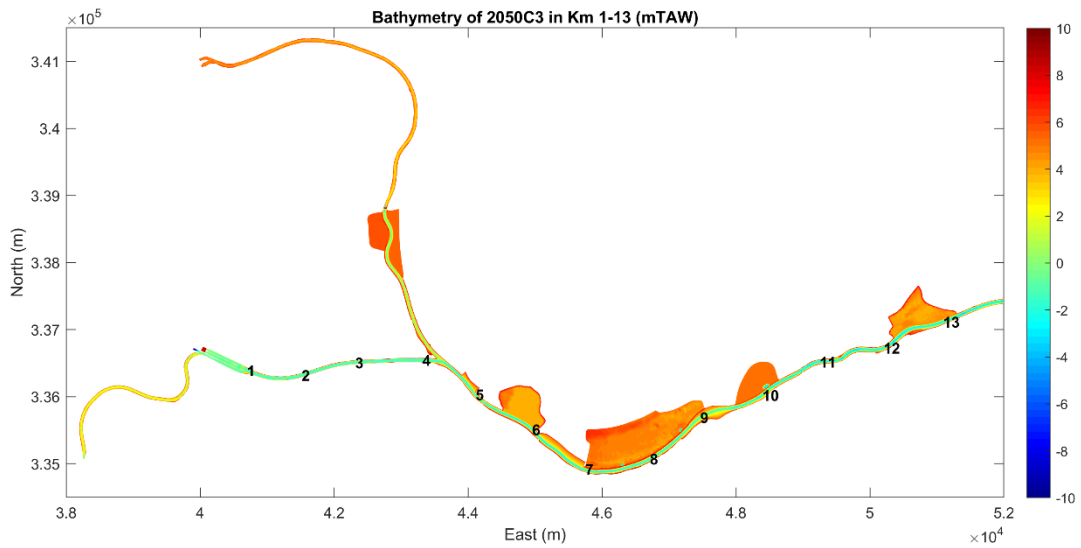


Figure 14 – Bathymetry of the Upper Sea Scheldt in 2050C3 (km 1-13)

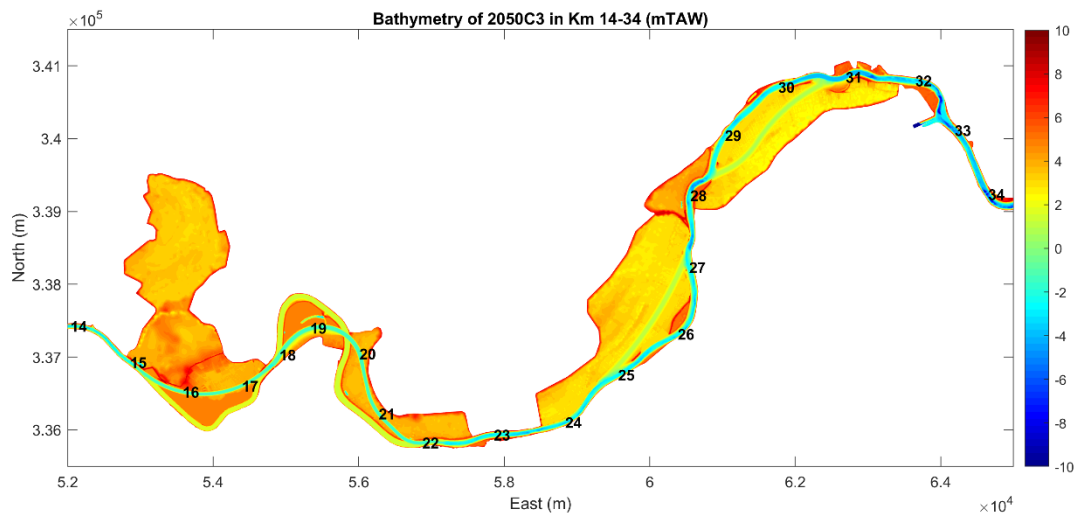


Figure 15 – Bathymetry of the Upper Sea Scheldt in 2050C3 (km 14-34)

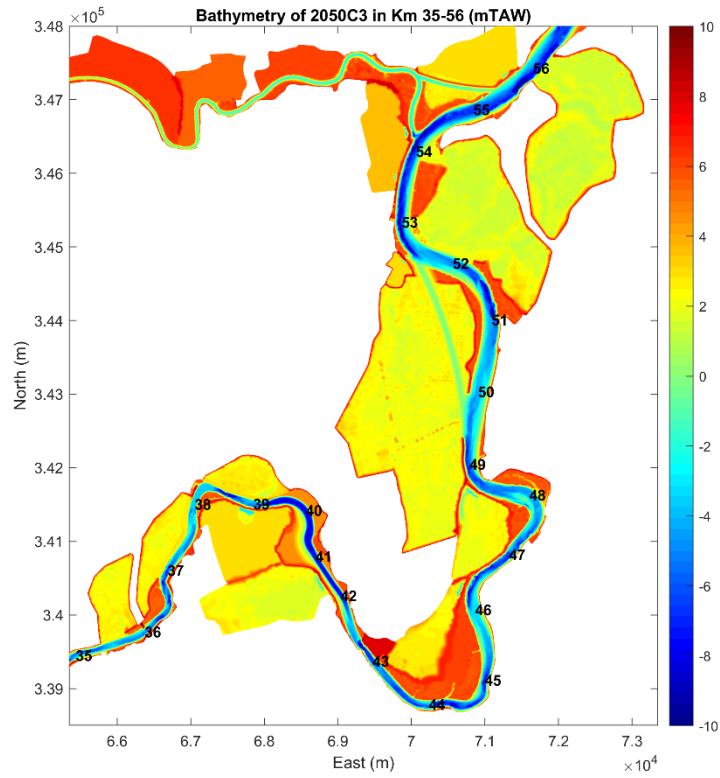


Figure 16 – Bathymetry of the Upper Sea Scheldt in 2050C3 (km 35-56)

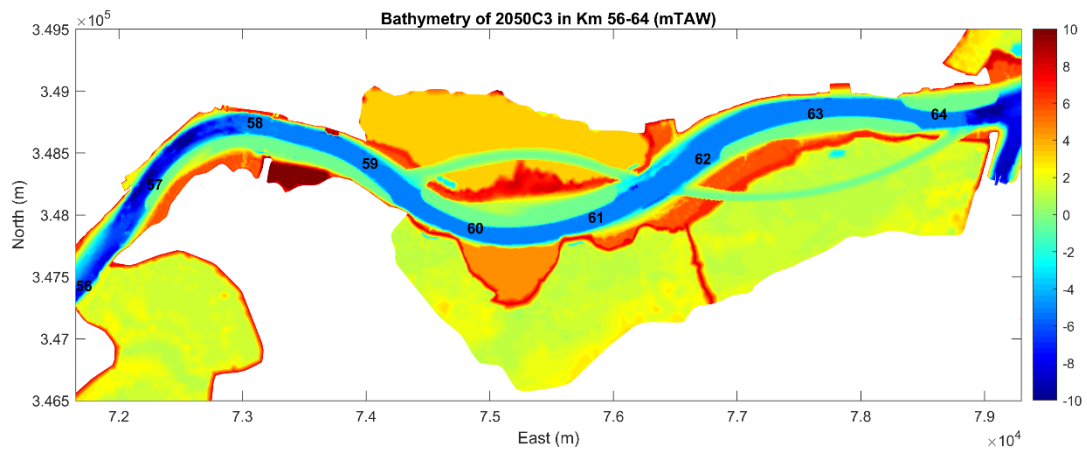


Figure 17 – Bathymetry of the Upper Sea Scheldt in 2050C3 (km 56-64)

## 4.2 Scenarios: different boundary conditions

This section describes the different scenarios. Each scenario consists of different boundary conditions, i.e. upstream discharge, tidal range, and sea level rise at the seaward boundary.

### 4.2.1 Tidal range scenarios

The SCALDIS model is used to evaluate the effect of increased and reduced tidal range near Schelle and further upstream in the Upper Sea Scheldt. In this study, tidal range scenarios **A+**, **A0** and **A-** have been implemented in both the hydrodynamic model and the sand model. In these three scenarios, the tidal amplitude at Schelle is equal to 5.70, 5.40 and 5.00 m, respectively (Table 2).

Table 2 - Tidal range scenarios

Scenario	Bottom friction	Tidal amplitude at Schelle (m)
<b>A+</b>	The bottom friction for hydrodynamics in the Western Scheldt is lowered.	5.70
<b>A0</b>	The bottom friction for hydrodynamics in the Western Scheldt remains as in the SCALDIS hydrodynamic model.	5.40 (current tidal range)
<b>A-</b>	The bottom friction for hydrodynamics in the Western Scheldt is increased.	5.00

The increase and decrease of the tidal range is realised in the model by changing the roughness (Manning coefficient) in the Western Scheldt. The zone with altered bottom roughness is indicated in Figure 18. By changing the roughness, the tidal propagation is influenced.

For the scenario “A+”, the Manning coefficient at each point in the red zone is decreased by 0.00426; for the scenario “A-”, the Manning coefficient at each point in the red zone is increased by 0.00554.

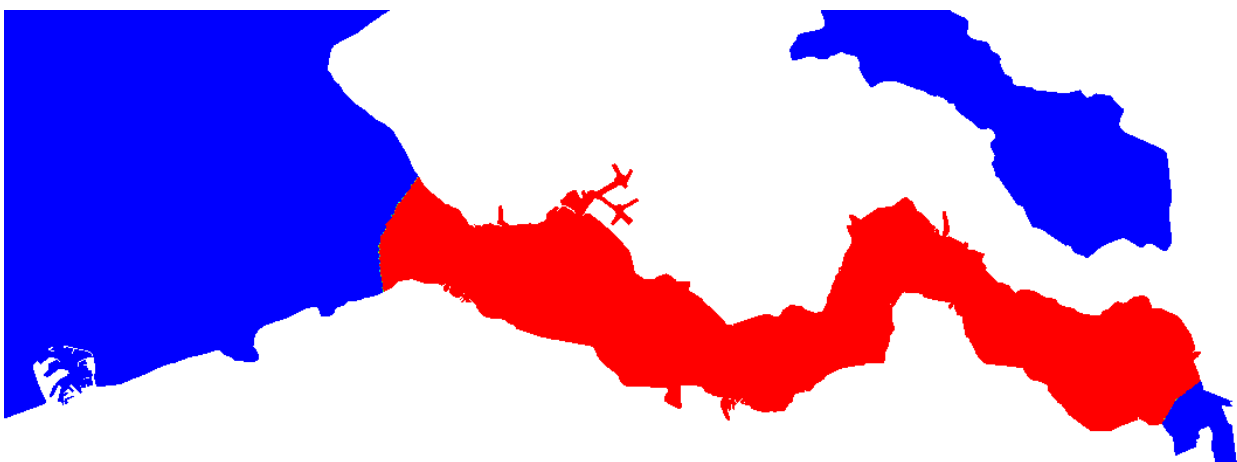


Figure 18 – The zone with changed bottom friction in the tidal range scenarios (red indicates the area with changes).

#### 4.2.2 Sea level rise scenarios

The following sea level rise scenarios are modelled in different runs for 2050:

- The “current” situation (**CN**, +0 cm in 2050);
- The “low” scenario (**CL**, +15 cm in 2050);
- The “high” scenario (**CH**, +40 cm in 2050).

The downstream boundary conditions for “CL” and “CH” scenarios are generated from CSM-ZUNO model, instead of adding the values directly on the water levels at the boundary.

The “current” situation CN is always used in the reference cases for comparison, and never combined with the change of tidal range. The tidal range scenario A+ is combined with the sea level rise CH. The tidal range scenario A- is combined with the sea level rise CL. More information about the scenarios is given in IMDC/INBO/UA/WL (2015).

#### 4.2.3 Representative discharges

There are two different sets of synthetic discharges used as the upstream boundary conditions in the model scenarios. One is based on the current situation of 2013 (QN2013), and the other one is made for the future scenario in 2050 (QN2050). QN2050 is matched with AminCL and AplusCH, while QN2013 is matched with AOCN.

These two sets of upstream discharges are based on a statistical analysis for the current and future scenarios (IMDC, 2015). They consist of typical average discharges for the tributaries in the upstream and at the open boundaries at Terneuzen and Bath. As shown in Table 3, the discharges at Melle, Dender and Rupel (the sum of Zenne, Dijle, Grote Nete and Kleine Nete) have different values in Q2013 and in Q2050. It can be seen that the discharges become larger for Melle and Dender in 2050, while the Rupel basin has a smaller average discharge compared to the current situation. For each boundary, the synthetic discharge stays constant throughout the simulation period.

Table 3 – Discharges imposed at tributaries in the Upper Sea Scheldt and at Terneuzen and Bath in the Western Scheldt

Tributary	Terneuzen	Melle	Dender	Zenne	Dijle	Grote Nete	Kleine Nete	Bath
Q2013	23.00	34.70	11.10	15.92	34.60	8.30	10.38	35.00
Q2050	23.00	41.60	12.30	14.63	31.80	7.63	9.54	35.00

The list of model runs are summarized in § 4.2.4.

#### 4.2.4 Modelling period

All the runs have a simulation period of 17 days, including a pure hydrodynamic spin up period of 2 days. For the AOCN runs, the simulation period is from 2013/07/29 22:20:00 to 2013/08/17 22:20:00. For the rest of the runs, the 2050 future scenarios are applied, with the simulation period from 2050/08/09 22:00:00 to 2050/08/28 22:00:00.



### 4.3 Overview of Model Runs

Twelve model runs are devised to study the effects of C-alternatives on the sand transport. The overview of model runs is listed in Table 4.

Table 4 – List of the different scenarios/alternatives runs

Code	Year	Bathymetry (alternatives)	Discharge	Amplitude correction	Sea level scenario
2050REF_C_A0CN	2050	REF_C	QN2013	A0	CN
2050REF_C_AminCL			QN2050	A-	CL
2050REF_C_AplusCH			QN2050	A+	CH
2050C1_A0CN	2050	C1	QN2013	A0	CN
2050C1_AminCL			QN2050	A-	CL
2050C1_AplusCH			QN2050	A+	CH
2050C2_A0CN	2050	C2	QN2013	A0	CN
2050C2_AminCL			QN2050	A-	CL
2050C2_AplusCH			QN2050	A+	CH
2050C3_A0CN	2050	C3	QN2013	A0	CN
2050C3_AminCL			QN2050	A-	CL
2050C3_AplusCH			QN2050	A+	CH

(A0, A+, A-): Different tidal range scenarios.

(CN, CL, CH): Sea level rise scenarios.

## 5 Methodology of scenario analysis

In the scenarios analysis, sand transport (bedload) is calculated over transects and mass balances are made in polygons. The reference runs are 2050REF\_C\_A0CN, 2050REF\_C\_AminCL and 2050REF\_C\_AplusCH. The results obtained in the C-alternative (C1, C2 and C3) runs are compared with the reference cases for each climate scenario (A0CN, AminCL and AplusCH).

Differences in sand transport are explained in terms of the measures in the alternatives, and their effect on the flow velocity and the sand transport. The calculated sand transport in the model represents the transport capacity. This is because the sand transport assumes an unlimited bed layer thickness, and there is no morphological feedback. This also implies that the sand transport model only captures the initial effects of a measure, and not the new morphodynamic equilibrium.

For analyzing the C scenarios, the modelled results for a spring-neap cycle are used, the first two days are considered as spin-up period, thus excluded from the analysis.

### 5.1 Erosion and sedimentation patterns

Erosion and sedimentation patterns over 1 spring/neap cycle are shown at the resolution of the model grid in Appendix 3.

The mass balance is aggregated over the boxes of the ecosystem model (Bi et al., 2020b). The lines that separate the boxes are chosen as transects for the sand transport (see section 5.2). The same transects and boxes are also used in the other reports within this project, so consistency is guaranteed between the different scenario reports (HD, sand and mud). The polygons and the transects in each C-alternative are shown in Appendix 1

### 5.2 Net sand transport

For every time step of the model output (= every 30 minutes) the sand transport over different transects along the Scheldt estuary is calculated. These transports are averaged out over a spring/neap tidal cycle (14.76 days) to get the net sand transport capacity. Downstream transport is positive, and upstream transport is negative.

Plots are made with on the x-axis the distance of the transect from Merelbeke and on the y-axis the net sand transport capacity for the specific transect. An overview map of the estuary is given in Figure 19 with some key locations and their distance along the navigation channel to Merelbeke.

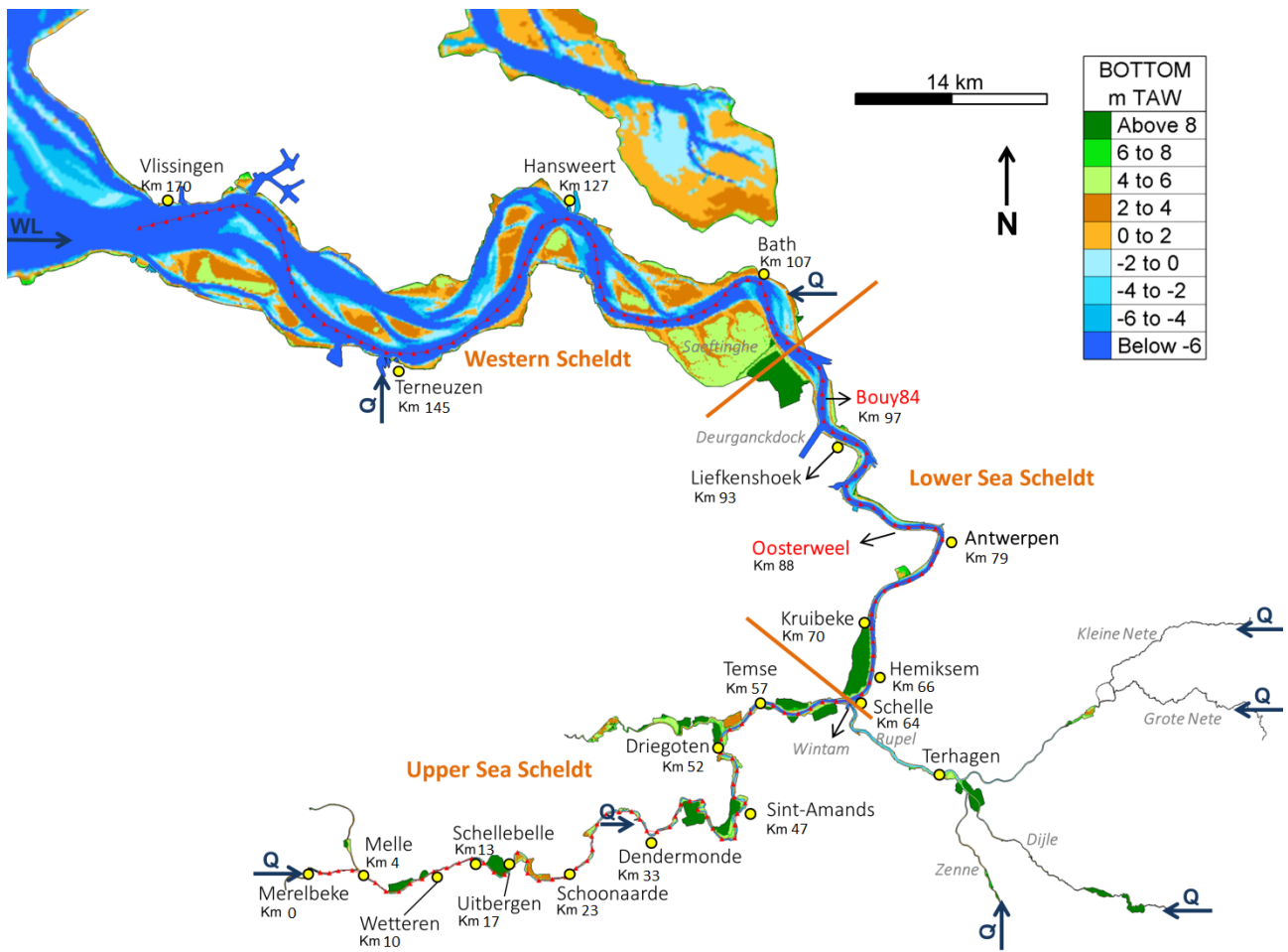


Figure 19 – Map of the Scheldt estuary with main tributaries and most important locations

### 5.3 Flow velocity and tidal (transport) asymmetry

Flow velocity is the most important explanatory variable for sand transport capacity. In this report, the cross sectional averaged flow velocity is used.

Since in the Engelund and Hansen sediment transport equation (see section 3.2), flow velocity is raised to the power five, the tidal asymmetry is expressed as the ratio between the integrated flood flow velocity to the power five over the integrated ebb flow velocity to the power five:  $\frac{\int (V_{flood})^5}{\int (V_{ebb})^5}$ . A ratio higher than one represents flood dominated transport.

## 6 Results

### 6.1 From 2013 to 2050

The Scaldis sand model was calibrated against the measurements in 2013. The model total sand transport in the Sea Scheldt shows a good agreement to the point measurements. Moreover, the net sand transport over different transects also shows a good agreement to the sediment balance derived from 10-year observation (Smolders et al. 2019a). One of the limitations in the sand model is that it assumes unlimited bed layer supply, hence, the sand transport computed by the model should be interpreted as sand transport capacity. In reality, sand transport would be supply-limited.

The effects on the sand transport from 2013 to 2050 is analyzed and described in Smolders et al. (2019b). The only difference between these two runs is the bathymetry, which is changed from the current (2013) bathymetry to the sustainable bathymetry (2050). The changes in bathymetry between the 2013 and 2050 model are rather small (Smolders et al. 2017). Therefore, the main effects from 2013 to 2050 are also small, both in terms of net sand transport and of transport asymmetry. The direction of the net transport capacity remains the same everywhere, except around km 60 (from Merelbeke) where the flood dominated transport in 2013 changes to an ebb dominated transport in 2050 (see Figure 20). This is caused by the de-embankment at Groot Schoor in the 2050 bathymetry.

The effect on tidal asymmetry (see the description in §5.3) also is small (see Figure 21). Downstream of km 33 the 2050 simulation is slightly more ebb dominant than the 2013 simulation. Upstream from km 33 the 2050 simulation becomes slightly more flood dominant than the 2013 simulation.

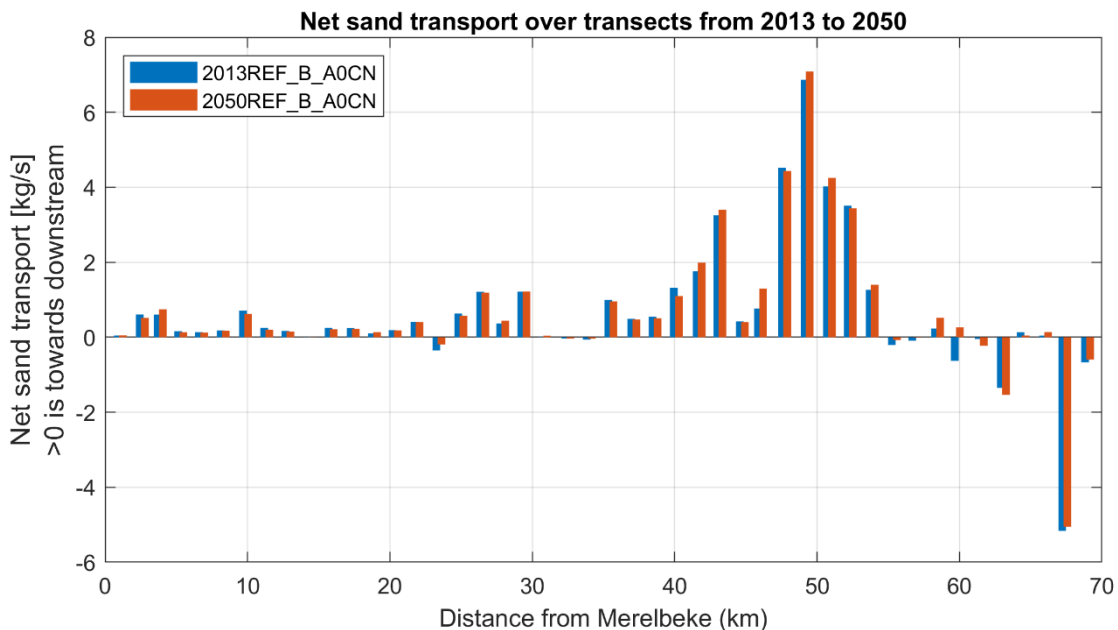


Figure 20 – Net sand transport over transects in the Sea Scheldt in 2013 and 2050 (Smolders et al. ,2019)

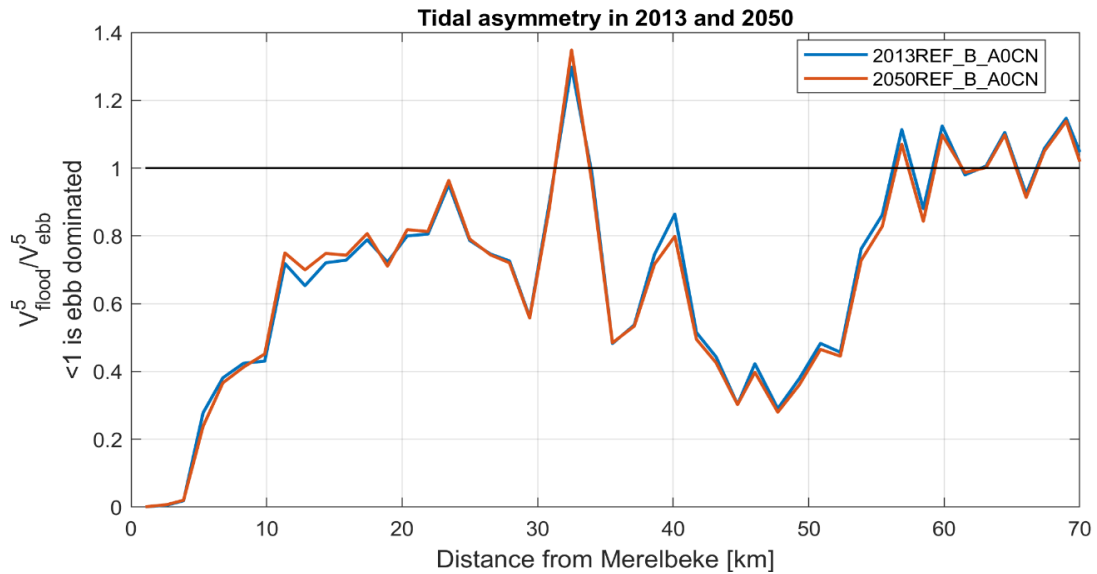


Figure 21 – Tidal asymmetry based on the velocity over transects in the Sea Scheldt in 2013 and 2050

## 6.2 2050REF\_C

In order to the numeric comparison with the C-alternatives, a new reference run called 2050REF\_C\_AOCN is created. The model inputs and boundary forcing are the same as in the runs 2050REF\_B\_AOCN. The only difference between the two is in the mesh. As described in §4.1.1, from 2050REF\_B\_AOCN mesh to 2050REF\_C\_AOCN mesh, the bathymetry stays unchanged, but the 2050REF\_C mesh is extended in order to include additional areas for the new measures (only activated in C-alternative runs). Note that the results of 2050REF\_C\_AOCN has an output internal of 10 min, instead of 1 h in 2050REF\_B\_AOCN, so in principle the sand transport computed by the 2050REF\_C\_AOCN run should have higher accuracy.

Figure 22 shows the comparison of timeseries of the sand transport at different locations in the Sea Scheldt between the runs 2050REF\_B\_AOCN and 2050REF\_C\_AOCN. As expected, the discrepancies in the results between the two runs are negligible.

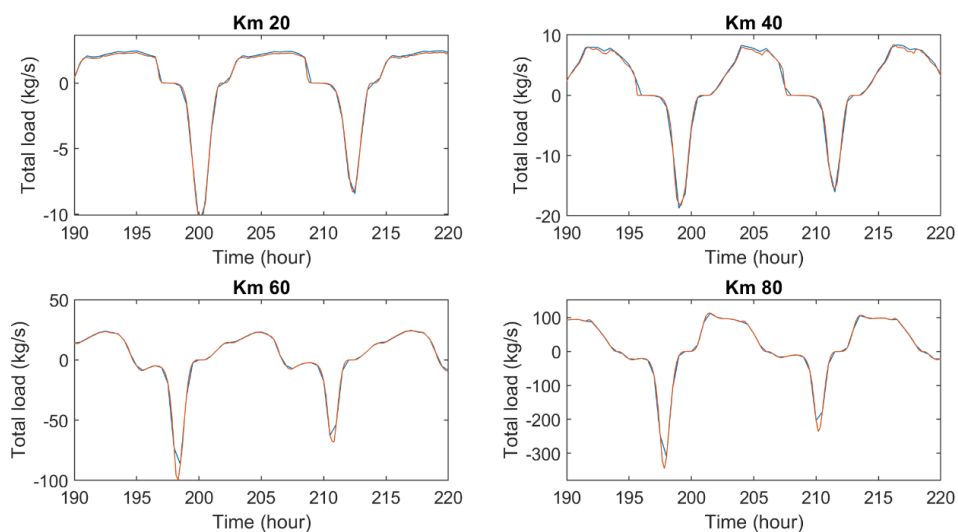


Figure 22 – Time series of sand transport at different locations in the Sea Scheldt in the runs 2050REF\_B\_AOCN (blue line) and 2050REF\_C\_AOCN (red line).

This section describes the results of the reference runs 2050REF\_C\_A0CN, 2050REF\_C\_AminCL and 2050REF\_C\_AplusCH. The detailed analysis of the 2050 reference runs is described in Smolders et al. (2019b).

The net sand transport capacity for 2050REF\_C under different climate scenarios is shown in Figure 23. In general, the net sand transport capacity is larger in the downstream and smaller in the upstream, and in most of the areas it is ebb dominated, except that it becomes flood dominant between km 60-70 under A0CN.

Comparing the results under different climate scenarios, one can see that the most noticeable effect is from the scenario AplusCH, under which the net sand transport capacity increases in the downstream direction in the Lower Sea Scheldt. The influence of AminCL on the net transport capacity is less pronounced, which could mean that the effects of decreasing tidal amplitude and sea level rise cancel each other out to some degree. In both climate scenarios, the differences of the net transport capacity compared to A0CN are less than 1 kg/s from km 0 to km 39.

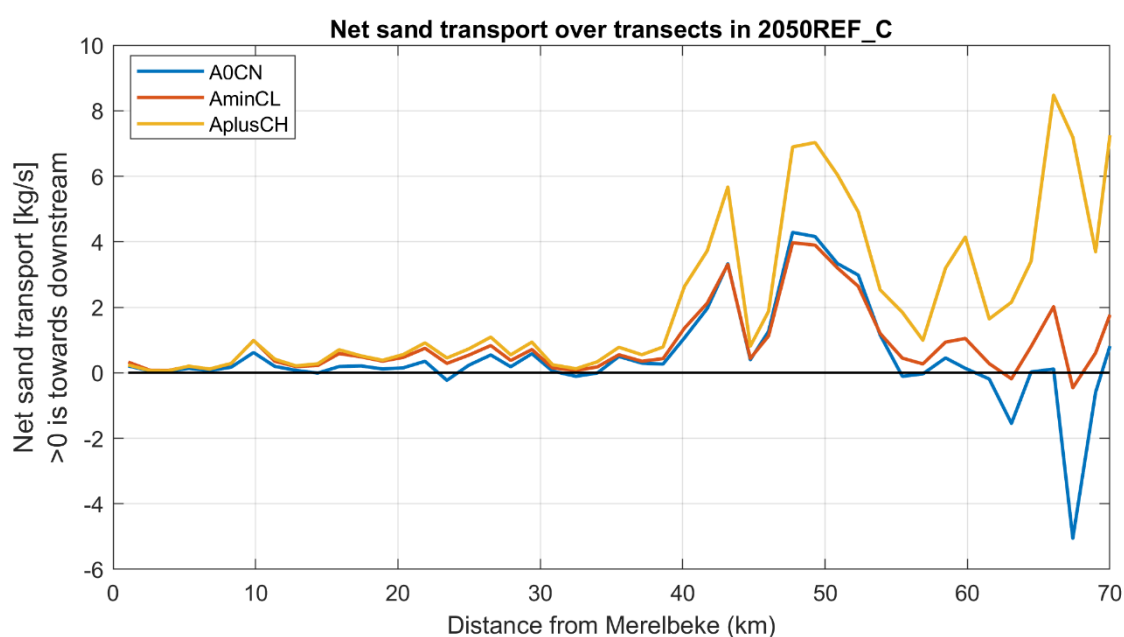


Figure 23 – Net sand transport capacity over cross-sections along the Sea Scheldt for a full spring/neap tidal cycle in 2050REF\_C under different climate scenarios (A0CN, AminCL and AplusCH). A positive value means downstream transport.

The ebb or flood dominance in sand transport can be partly explained by the tidal asymmetry in Figure 24.

In general, the Upper Sea Scheldt is ebb dominant with regards to sand transport. Under both scenarios AminCL and AplusCH, the transport asymmetry becomes more ebb dominant. However, under A0CN scenario, the locations around km 32 and km 57-69 shows slight flood dominance.

At km 55, the sign of tidal asymmetry changes in the A0CN scenario. This results in convergence of sediment transport and hence sedimentation, which can be seen in Figure 26. In AminCL and AplusCH, due to the combined effects of changing tidal amplitude and sea level rise, the sand transport remains ebb dominant in km 60-70.

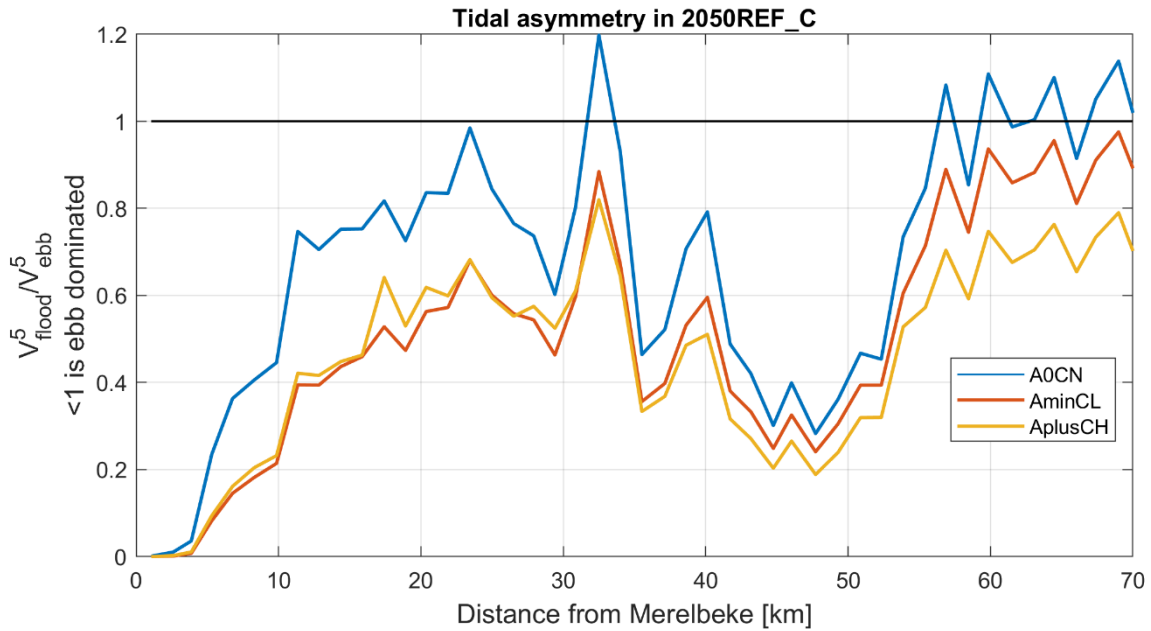


Figure 24 – Tidal asymmetry calculated over cross-sections along the Sea Scheldt in 2050REF\_C under different climate scenarios (A0CN, AminCL and AplusCH). A value below 1 means ebb dominated.

The mean cross-sectionally averaged velocity over a spring-neap tidal cycle is calculated and plotted in Figure 25. From km 0 towards downstream, the mean cross-sectionally averaged velocity is decreasing as a result of the increase of the transect areas from upstream to downstream to carry the upstream discharge.

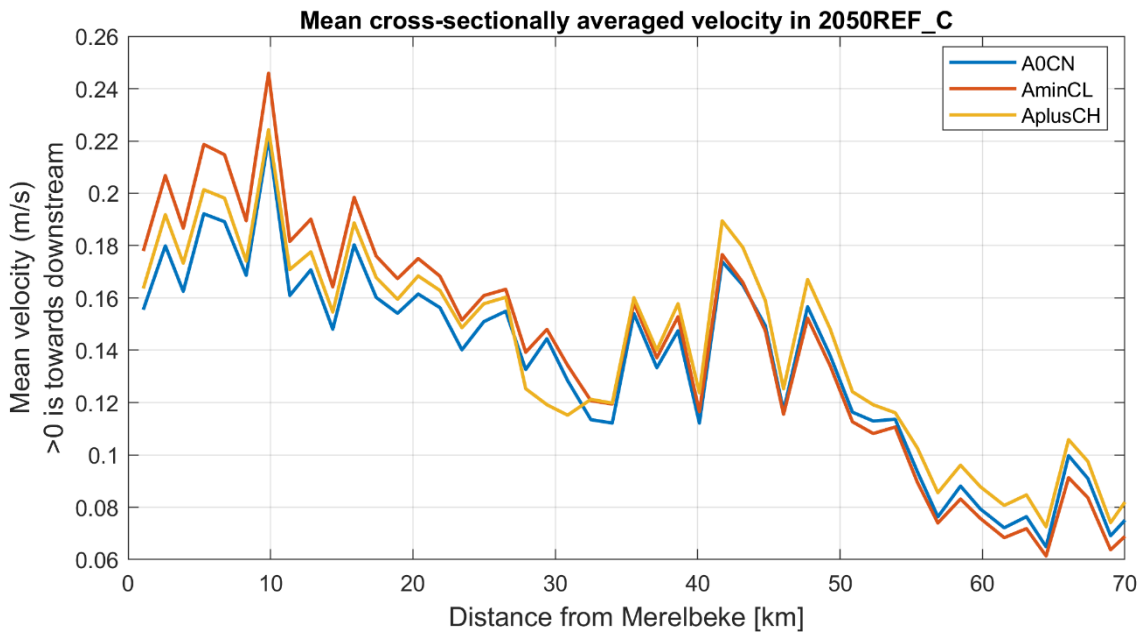


Figure 25 – Mean cross-sectionally averaged velocity along the Sea Scheldt in 2050REF\_C under different climate scenarios (A0CN, AminCL and AplusCH).

The maps of bed evolution (at each node) after a spring-neap cycle in the Upper Sea Scheldt is plotted and shown in Appendix 3. However, the spatial patterns of bed evolution is rather scattered, it is not clear to see the main trend of sedimentation/erosion in a specific area, hence, the bed evolution is aggregated into polygons. The same polygons are used for all alternatives, and also for the mud and sand scenario analysis in

order to facilitate comparison. Figure 26 shows for different polygons in the Upper Sea Scheldt the potential sedimentation and erosion after a year based on the results bed evolution of a full spring/neap tidal cycle (15 days).

We take channel and intertidal area in one morphological analysis volume. This is related to the data availability. The most important validation dataset for the sand transport model is the sediment balance, which also has morphological cells that contain channel plus intertidal area. The erosion/sedimentation is expressed in  $\text{Ton}/\text{m}^2/\text{year}$  for each polygon in order to compensate the influence of the polygon areas on the visualization. This is done for the rest of the alternatives as well.

The red color indicates potential sedimentation and the blue color indicates potential erosion in that polygon. In the red polygons more maintenance dredging can be expected. The general patterns observed here can be linked to the changes in the net sand transport capacity, which in turn is linked to the tidal asymmetry.

There is no obvious sedimentation found in the depoldering or intertidal areas, as the bed evolution occurs mainly in the main channel (see e.g. Figure 79).

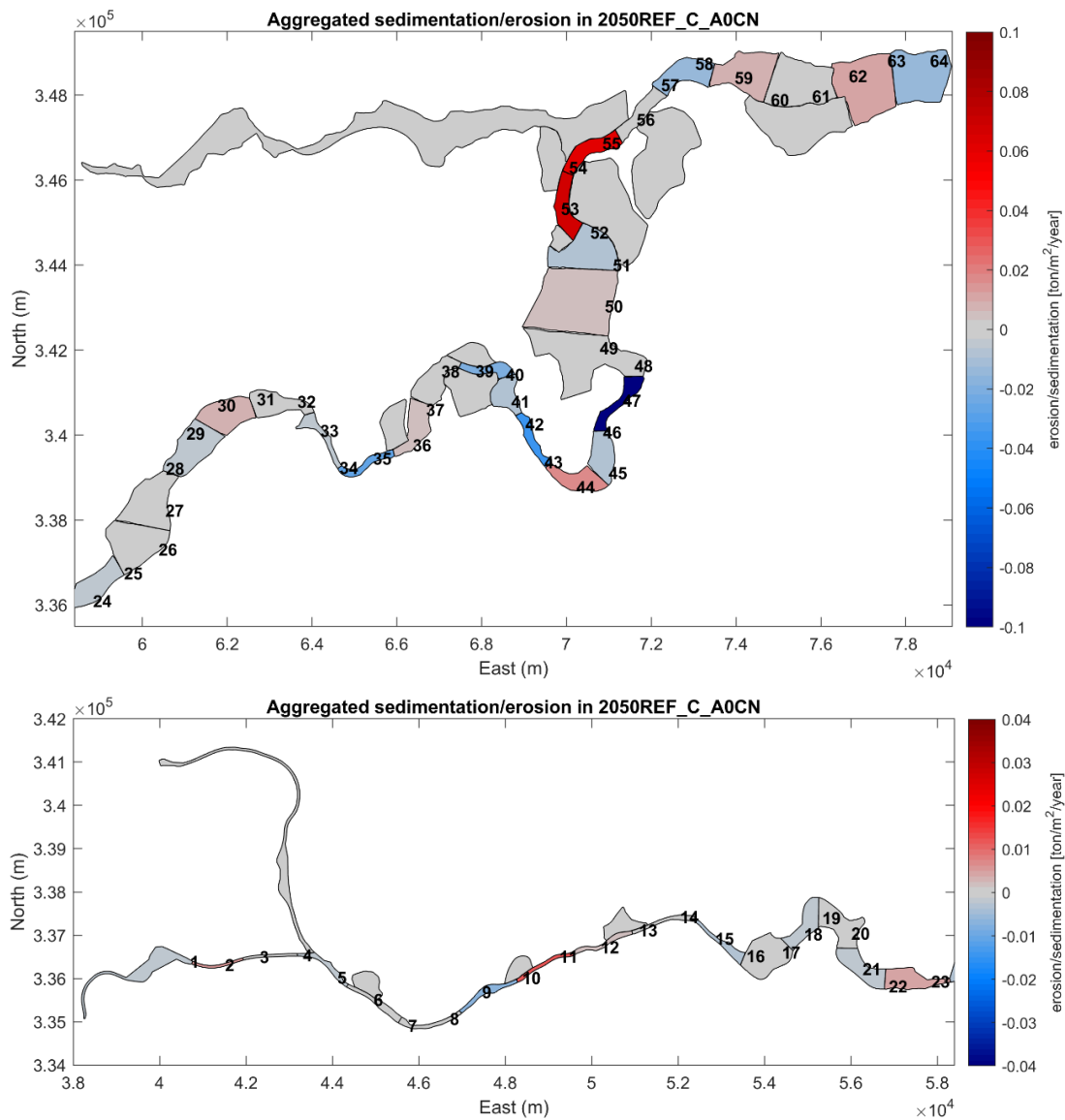


Figure 26 – Potential sedimentation and erosion map for the Upper Sea Scheldt. Scenario 2050REF\_C\_A0CN. Erosion in blue and sedimentation in red. Numbers indicate the distance (km) from Merelbeke.



### 6.3 2050C1

The net sand transport capacity along the Sea Scheldt is assessed by comparing the different climate and tide amplification scenarios to their reference cases. To be more specific, 2050C1\_A0CN is compared to 2050REF\_C\_A0CN, 2050C1\_AminCL to 2050REF\_C\_AminCL and 2050C1\_AplusCH to 2050REF\_C\_AplusCH. In this way, the consistency of the effect on the net sand transport capacity under different climate scenarios can be evaluated.

The net sand transport capacity over the transects along the Sea Scheldt is computed and plotted in Figure 27. Notice that the net transport capacity is much smaller in the upstream region from km 0 to km 40. In order to better reveal the effect of C1 upstream, a zoom-in figure is provided (Figure 28).

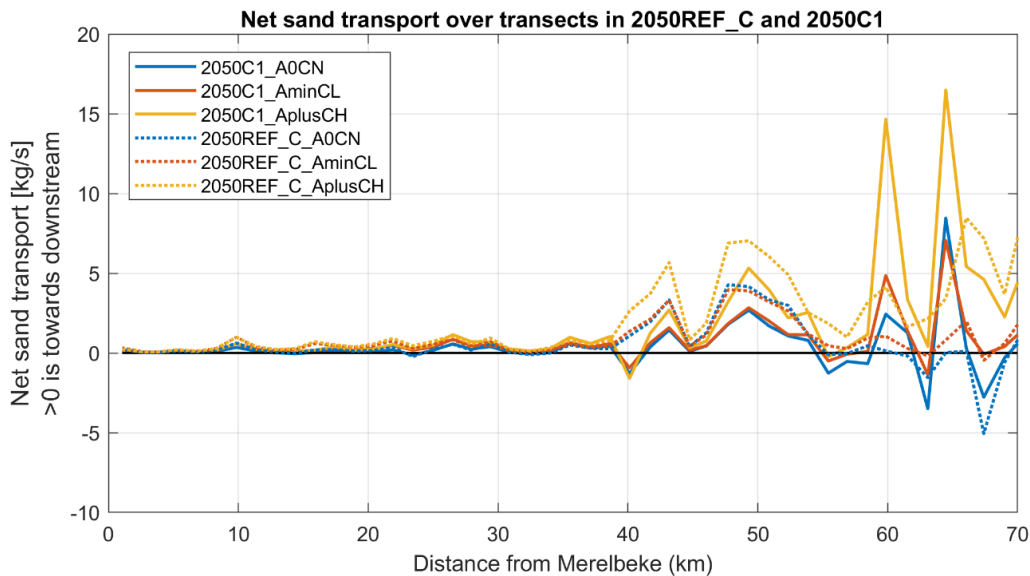


Figure 27 – Net sand transport capacity along the Sea Scheldt for a full spring/neap tidal cycle in 2050REF\_C (dotted line) and 2050C1 (full line) under different climate scenarios (A0CN, AminCL and AplusCH). A positive value means downstream transport.

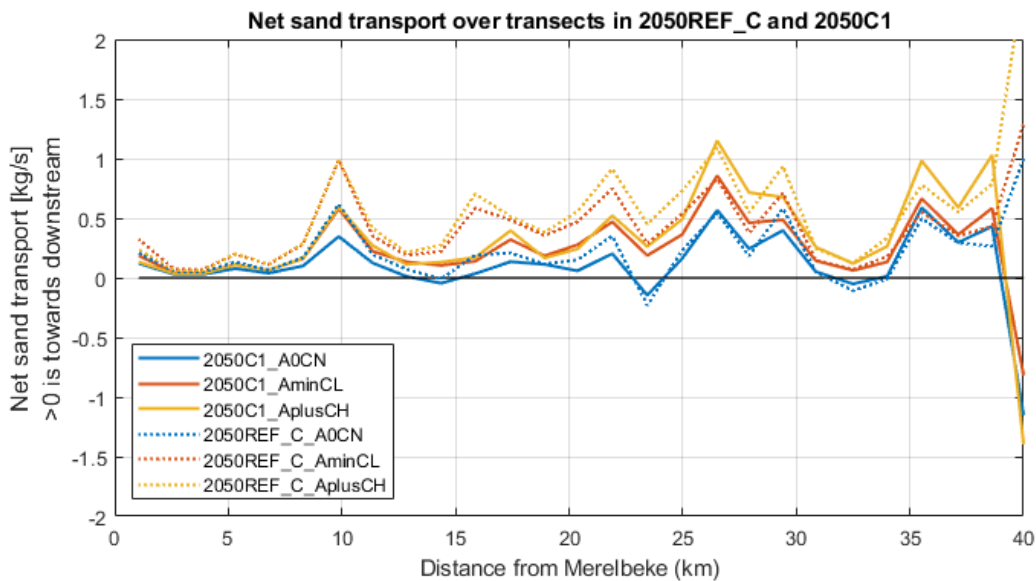


Figure 28 – Net sand transport capacity from km 0 to km 40 for a full spring/neap tidal cycle in 2050REF\_C and 2050C1 under different climate scenarios (A0CN, AminCL and AplusCH). A positive value means downstream transport.

Upstream of km 65, the effects of C1 on the net transport capacity are mainly local.

- From km 0 to km 40, some local influences of the new measures can be observed. For example, the bend modification at Voorde (km 9) , and the bend cut off plus the new intertidal area at Wijmeers (km 16) and Uitbergen (km 19) decrease the net sand transport capacity towards downstream. This is mainly due to the decrease of the mean velocity (see Figure 30). Moreover, the FCA-CRT at Scheldebroek (km28) also leads to the reduction of net sand transport locally. The other measures do not heavily affect the net sand transport.
- The measure at Uitbergen (km 19) has a local effect on tidal asymmetry, but this effect is not as pronounced in the net sediment transport
- The measure at the Kramp (km 40-41) has locally an important effect on the velocity (decrease), on the tidal asymmetry (more ebb dominant) and on the net sand transport overall decrease, combined with a local switch from ebb dominant to flood dominant, which indices a local convergence zone.
- From km 40 to km 59, a new connection to Durme is developed and Tielrode Broek is partly depoldered (km 55), FCA Blankaart is combined with FCA-CRT Wal-Zwijn (km 49), and the navigation channel is straightened at Kramp (km 40-41). All these new measures make this region generally less ebb dominant (except at km 40 the main channel becomes more ebb dominant), meanwhile the mean velocity also lowers (Figure 29 and Figure 30). The combined effects lead to a reduced downstream net transport capacity.
- At km 60 and km 64, a local narrowing of the channel is implemented in this area. The consequence is a locally larger mean velocity, and also a more ebb-dominant channel (Figure 29 and Figure 30). These two changes in hydrodynamics result in locally higher downstream net transport capacity.

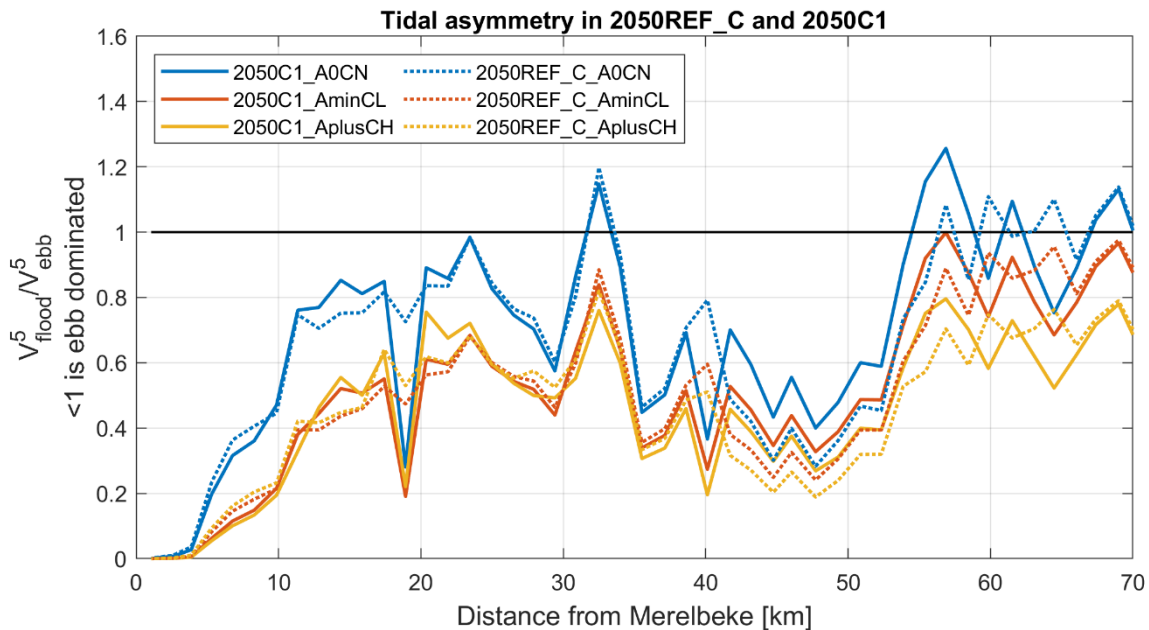


Figure 29 – Tidal asymmetry along the Sea Scheldt under different climate scenarios in 2050REF\_C and 2050C1. A value below 1 means ebb dominant, and above 1 means flood dominant.

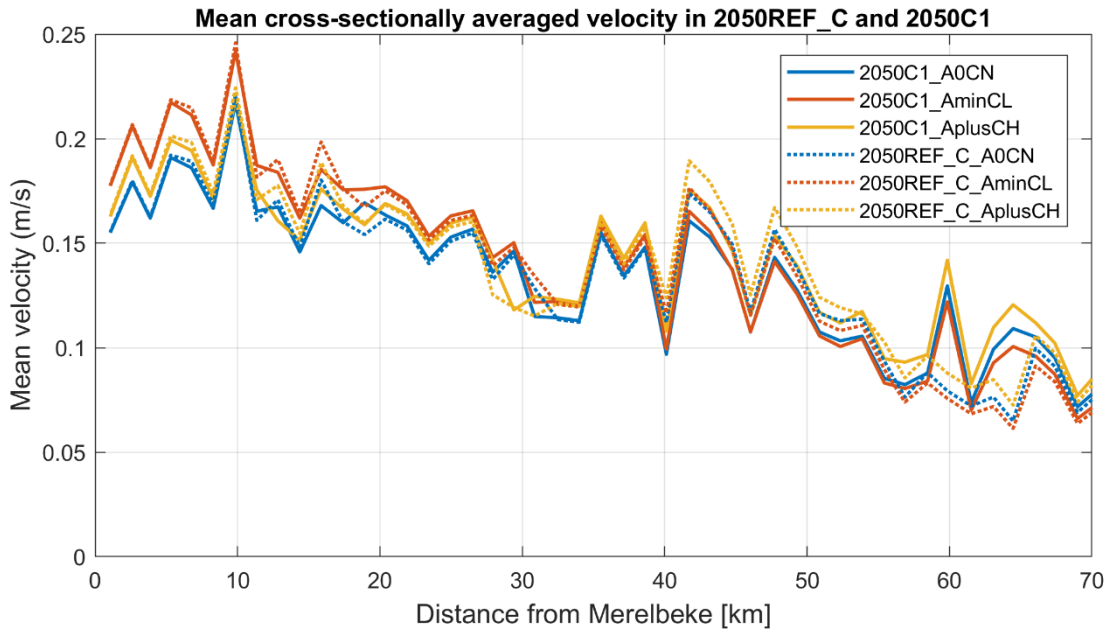


Figure 30 – Mean cross-sectionally averaged velocity along the Sea Scheldt in 2050REF\_C and 2050C1 for a full spring/neap tidal cycle under different climate scenarios. A positive value means more flood dominance or less ebb dominance.

The sedimentation/erosion in the Sea Scheldt expressed in tons per year is computed over a spring-neap cycle. The effect of C1 alternative on the sedimentation/erosion is calculated by comparing the C1 runs to their respective reference runs. The effects on the sedimentation/erosion are in general consistent under different climate scenarios, although some affected regions can be extended under more severe scenarios, e.g. AplusCH.

For readability, here we only show the differences of aggregated sedimentation/erosion in the polygons with REF under the A0CN scenario (Figure 31). The aggregated sedimentation/erosion maps under A0CN, AminCL and AplusCH scenarios can be found in Appendix 2 and the detailed maps of bed evolution at each node can be seen in Appendix 3.

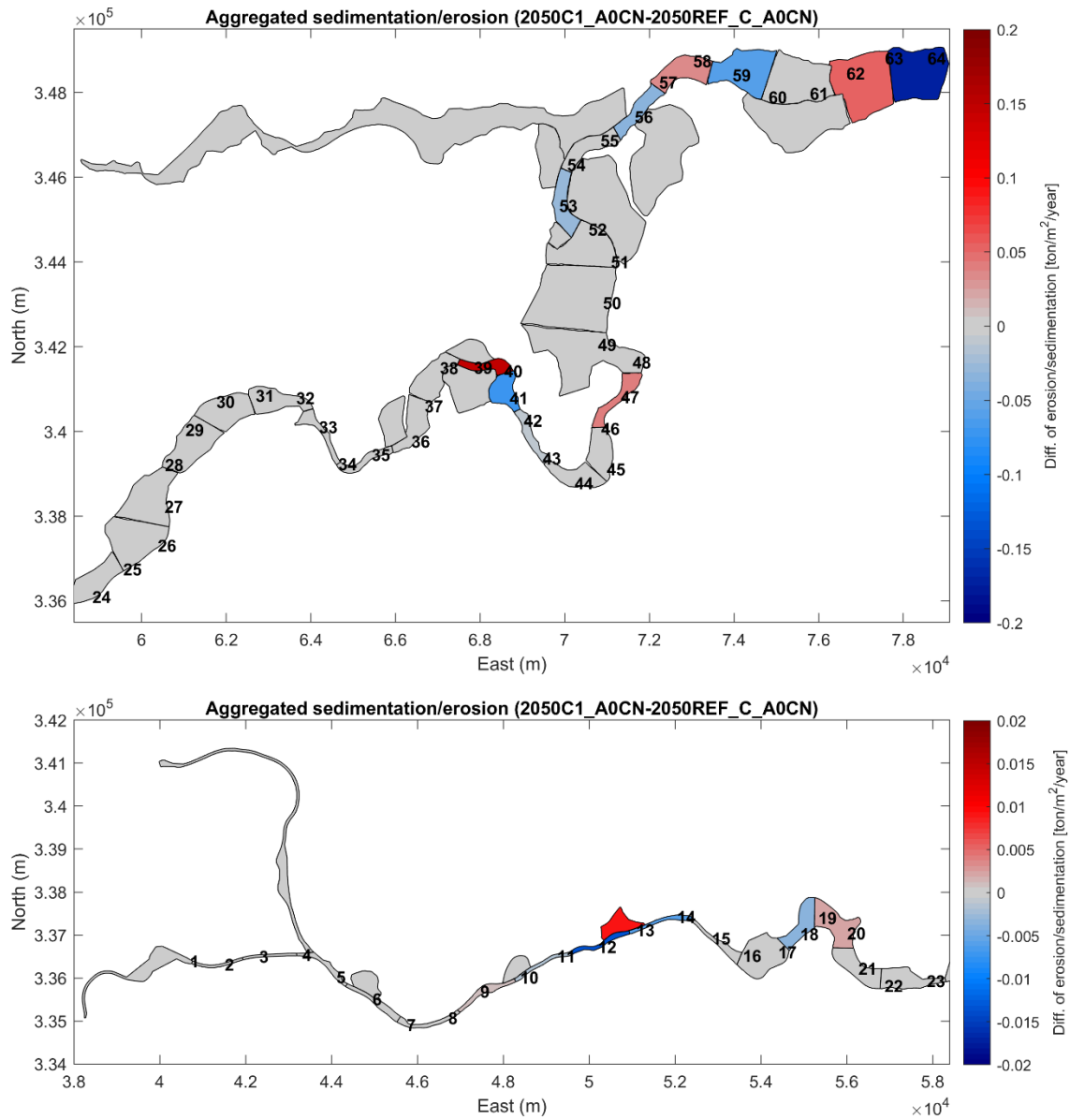


Figure 31 – Effect of C1 alternative on the sedimentation/erosion in the Upper Sea Scheldt under AOCN condition. Red indicates more sedimentation or less erosion. Numbers indicate the distance (km) from Merelbeke.

## 6.4 2050C2

The effect of C2 alternative on the net sand transport capacity is assessed in a similar way as for C1 alternative. Figure 32 shows the net sand transport capacity over the transects in the Sea Scheldt under three climate scenarios, i.e. A0CN, AminCL and AplusCH, and Figure 33 shows a zoomed-in figure from km 0 to km 40. The effect of C2 on the net transport capacity is consistent across different climate scenarios in the Sea Scheldt.

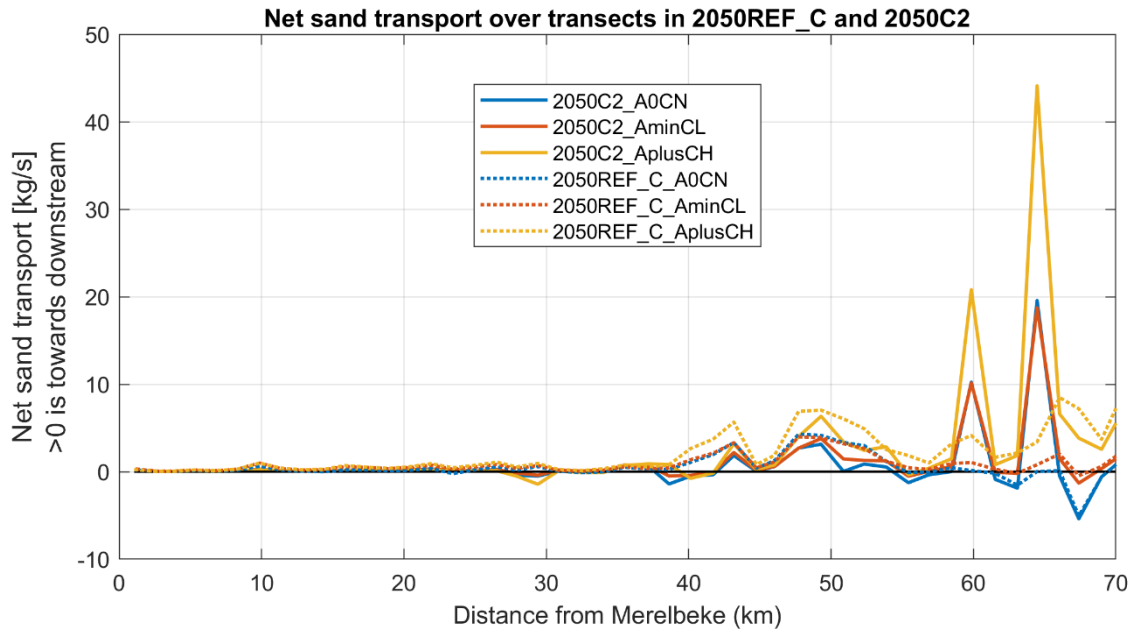


Figure 32 – Net sand transport capacity along the Sea Scheldt for a full spring/neap tidal cycle in 2050REF\_C (dotted line) and 2050C2 (full line) under different climate scenarios (A0CN, AminCL and AplusCH). A positive value means downstream transport.

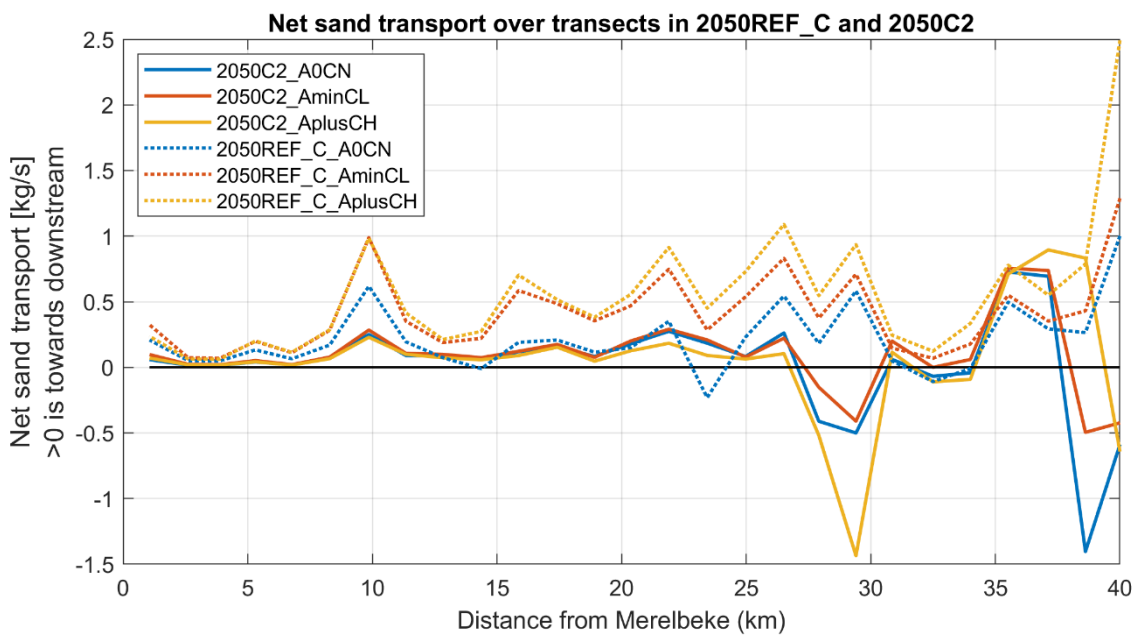


Figure 33 – Net sand transport capacity from km 0 to km 40 for a full spring/neap tidal cycle in 2050REF\_C (dotted line) and 2050C2 (full line) under different climate scenarios (A0CN, AminCL and AplusCH). A positive value means downstream transport.

From Figure 32 and Figure 33 we can see that in the region km 0-65, the influence of C2 on the net sand transport capacity (main trend) can be linked to the following measures:

- Upstream of km 25, the channel becomes more ebb dominant but the mean velocity decreases as a consequence of depoldering and the creation of intertidal areas. As a result, the net sand transport capacity becomes lower. The most noticeable changes can be linked to the bend cut off plus the new intertidal area at Uitbergen (km 19) and Wijmeers (km 16), and bend modification at Voorde (km 9).
- From km 25 to km 30, Oude Broekmeer (km 26) and Sint-Onolfspolder (km 29) are depoldered and side channels are constructed. In this region, the tidal asymmetry changes its sign in the main channel from more ebb dominance to flood dominance, and the mean velocity decreases, which makes the net transport capacity smaller towards downstream from km 25 to km 27, eventually changes its direction to upstream transport between km 27 to km 30. This sediment convergence zone leads locally to more sedimentation between km 27 and km 29.
- From km 39 to km 41, a more intensive variant of the bend straightening combined with the development of intertidal nature is defined near Kramp (km 40). Also, Roggeman (km 39) is depoldered. These new measures lead to less ebb dominance or even flood dominance, and mean velocity also becomes lower in the channel. As a result, net transport capacity changes its direction to upstream. This induces a local convergence zone for sand, as in C1.
- At km 49, Blankaart becomes depoldered area in C2 alternative. Figure 34 and Figure 35 indicate that the main channel becomes less ebb dominant, and the mean velocity decreases. Hence, we also observe a decrease in the downstream net sand transport capacity.
- At km 55, a new connection to Durme is developed and Tielrode Broek is partly depoldered. Figure 34 shows the main channel becomes slightly flood dominant under AOCN and less ebb dominant under AminCL and AplusCH at this location. The mean velocity also increases as seen in Figure 35. Hence, with these changes in hydrodynamics, the net transport capacity changes direction to towards upstream here. The altered connection to Durme in C2 leads locally to more sedimentation. The new connection shows sedimentation near its downstream entrance as seen in Figure 85.
- From km 60 to km 64, local narrowing is carried out from Temse to the Rupel mouth. In addition, new side channels are constructed in Schouselbroek and Schelland/Oudbroekpolder. The combination of these two kinds of measures result in an increase in mean velocity along the transects and more ebb dominance in the main channel (Figure 34 and Figure 35). This explains the increase in the downstream net sand transport capacity seen in this zone.

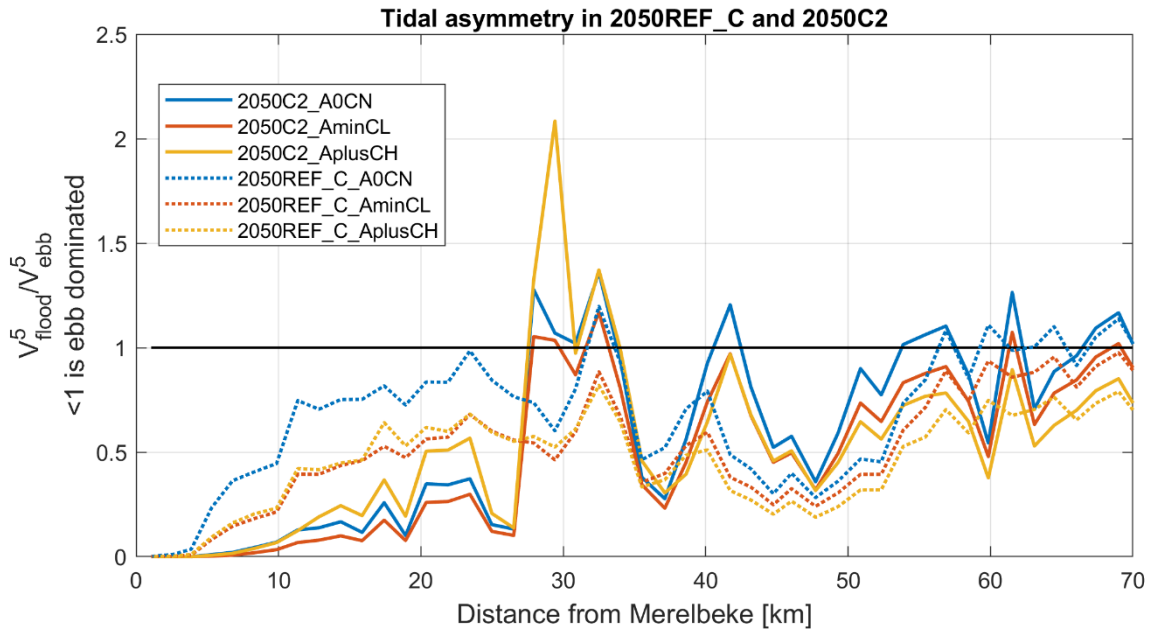


Figure 34 – Tidal asymmetry along the Sea Scheldt under different climate scenarios in 2050REF\_C and 2050C2. A value below 1 means ebb dominated, and above 1 means flood dominant.

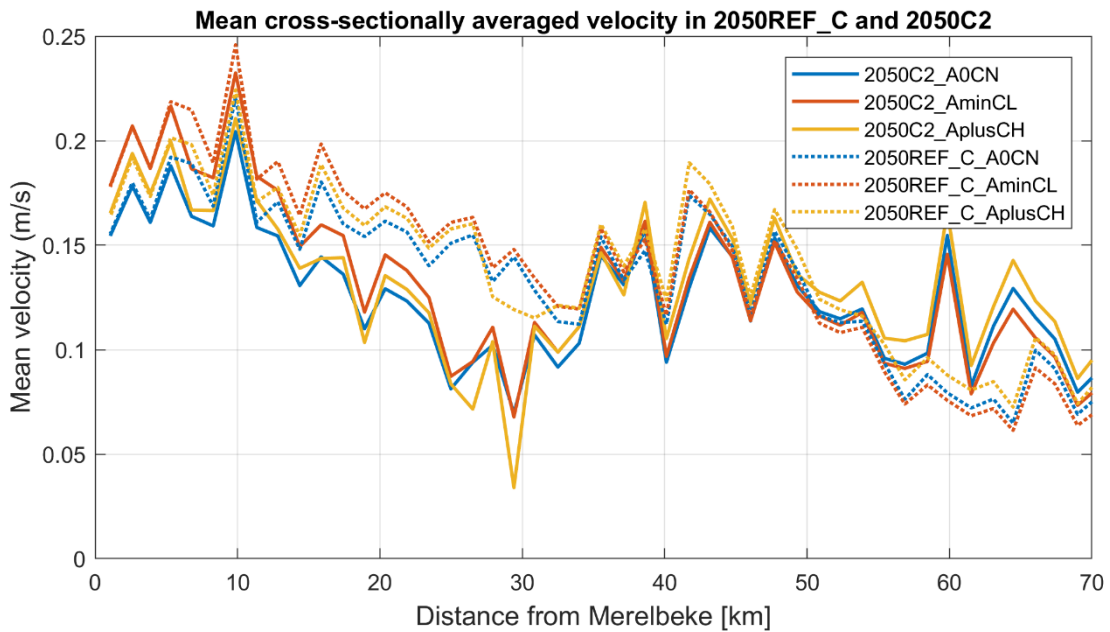


Figure 35 – Mean cross-sectionally averaged velocity along the Sea Scheldt in 2050REF\_C and 2050C2 for a full spring/neap tidal cycle under different climate scenarios. A positive value means more flood dominance or less ebb dominance.

The sedimentation/erosion in the Sea Scheldt expressed in tons per year is computed over a spring-neap cycle. The effect of the C2 alternative on the sedimentation/erosion is calculated by comparing the C2 runs to their respective reference runs.

For readability, here we only show the differences of aggregated sedimentation/erosion in the polygons with REF under the A0CN scenario (Figure 36). The aggregated sedimentation/erosion maps under A0CN, AminCL and AplusCH scenarios can be found in Appendix 2 and the detailed maps of bed evolution at each node can be seen in Appendix 3.

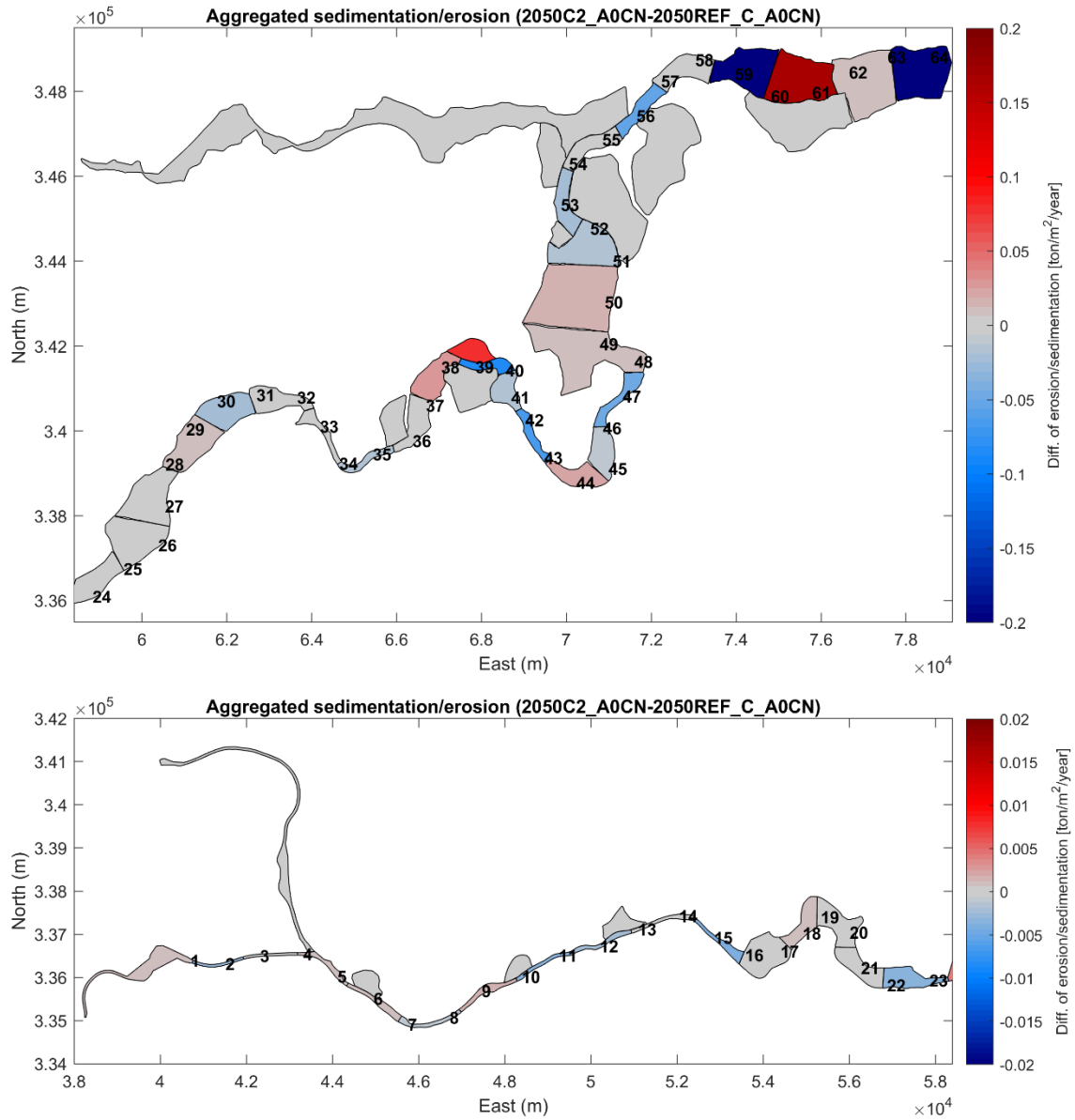


Figure 36 – Effect of C2 alternative on the sedimentation/erosion in the Upper Sea Scheldt under AOCN condition. Red indicates more sedimentation or less erosion.



## 6.5 2050C3

The effect of C3 alternative on the net sand transport capacity under different climate scenarios (A0CN, AminCL and AplusCH) is assessed in a similar way as for the C1 alternative. The net sand transport capacity over the transects in the Sea Scheldt under three climate scenarios is shown in Figure 37 and Figure 38.

As observed in other C alternatives, the effects of the new measures on the net transport capacity are similar across different scenarios. In the Upper Sea Scheldt, the influences are mainly local, meaning that the net sand transport capacity changes depending on the location and the type of the measures.

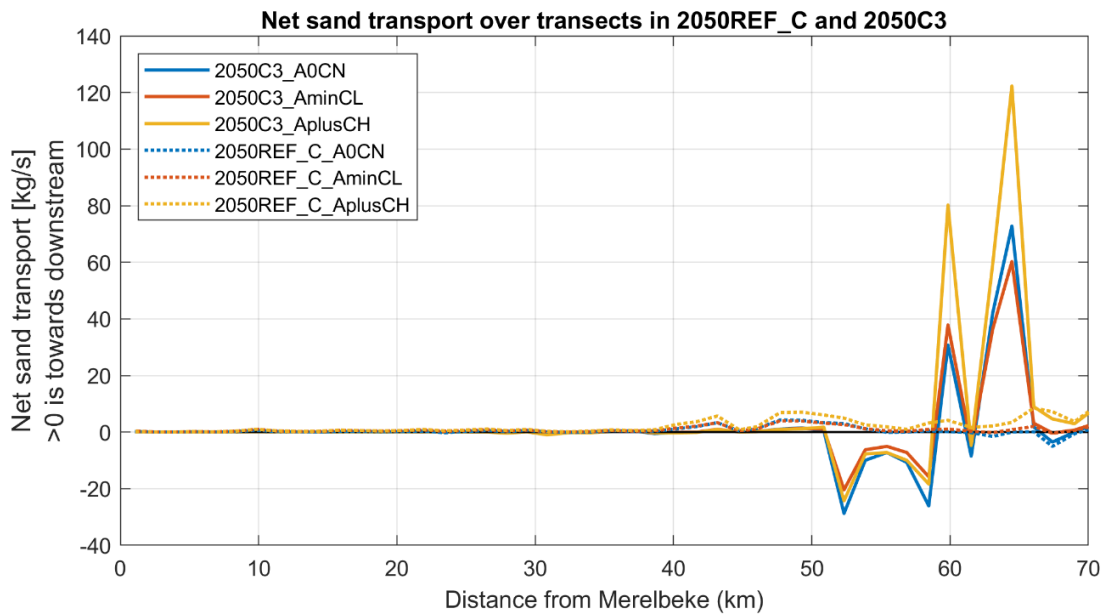


Figure 37 – Net sand transport capacity over cross-sections along the Sea Scheldt for a full spring/neap tidal cycle in 2050REF\_C and 2050C3 under different climate scenarios (A0CN, AminCL and AplusCH). A positive value means downstream transport.

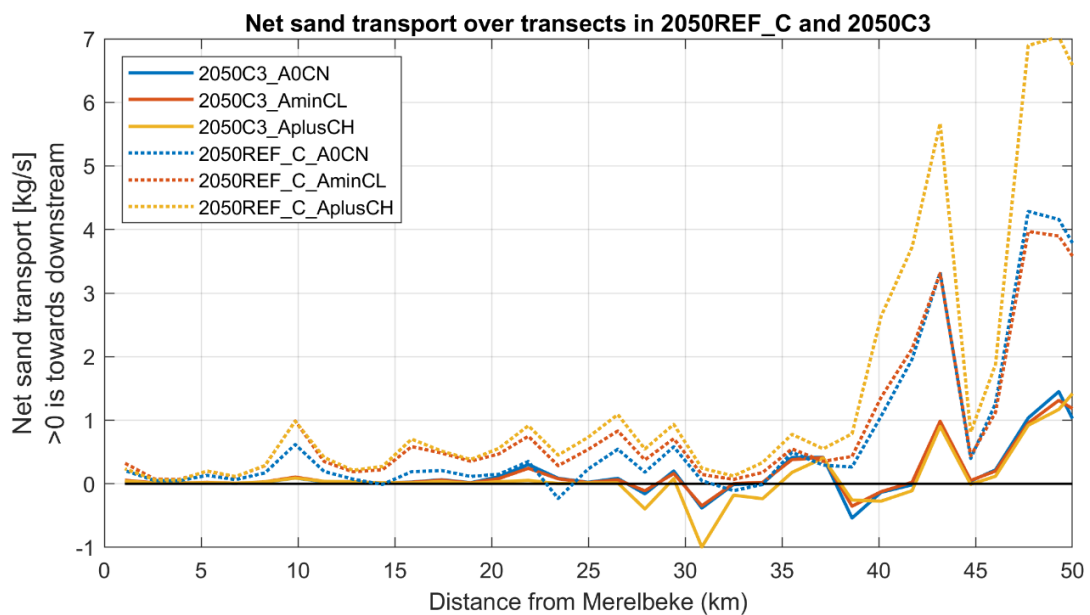


Figure 38 – Net sand transport capacity over cross-sections from km 0 to km 50 for a full spring/neap tidal cycle in 2050REF\_C and 2050C3 under different climate scenarios (A0CN, AminCL and AplusCH). A positive value means downstream transport.

- From km 0 to km 24, the tidal asymmetry indicates this region becomes more ebb dominant, but in the meantime the mean velocity is also reduced due to the increase of the wet surface area (Figure 39 and Figure 40), as a result, the net transport capacity is still towards downstream but the amount is lower. The relevant measures are the bend cut off plus the new intertidal area at Paardenweide (km 22), Uitbergen (km 19) and Wijmeers (km 16), and bend modification at Voorde (km 9).
- From km 25 to km 37, due to the implementation of large depoldered areas, e.g. Oude Broekmeer (km 26), Sint-Onolfspolder (km 29), Grembergen broek (km 36) and Armenput (km 37), the main channel becomes less ebb dominant in general, and at km 28 and km 30-34 it even becomes flood dominant (Figure 39). In addition, the mean velocity also decreases due to the increase of wet surface (Figure 40). These two changes result in an overall decrease in the downstream net sand transport capacity in this region, and at km 28 and km 30-34, the net sand transport capacity changes its direction to upstream. This sign reversal will cause local sediment accumulation.
- From km 38 to km 49, as seen in Figure 39, the biggest change in the tidal asymmetry in this region happens at km 41-42, where the bend straightening combined with new development of intertidal nature is carried out at Kramp. As a result, the main channel becomes less ebb dominant and the mean velocity decreases (Figure 40). Moreover, Roggeman is depoldered with the dyke more to the north (km 39), which also decreases the mean velocity in the channel. Therefore, lower downstream net sand transport capacity can be observed in this region from km 42 to km 49, and the net transport capacity changes its direction from downstream to upstream, again leading to local sediment accumulation.
- From km 50 to km 59, one can see that the net sand transport capacity reverses its direction from downstream transport to upstream transport when comparing to the reference case. Several large depoldered areas are defined in this region, e.g. Weert at km 53 and km 56, Blankaart and Akkershoofd at km 49-52. As in the other two C alternatives, this area also has a new connection to Durme and the partly depoldered Tielrode Broek. The new measures affect the hydrodynamics in the main channel, resulting in a strong flood dominant section (Figure 39).
- The depoldering Weert in C3 alternative attracts sedimentation, so the main channel nearby loses sediment. This is visible in the lateral area at km 52 and 56 in Figure 41.
- From km 60 to km 64, the net sand transport capacity in the main channel increases drastically. In the C3 alternative, the main channel is not only narrowed but also undeepened in this region. Similar to the C2 alternative, two side channels are excavated in Schouselbroek and Schelland/Oudbroekpolder. Due to these measures, the channel becomes more ebb dominant and the mean velocity increases (Figure 39 and Figure 40). Because the sand transport formula is scaled with velocity to the power of five, the changes triggers large effects in the net sand transport capacity.

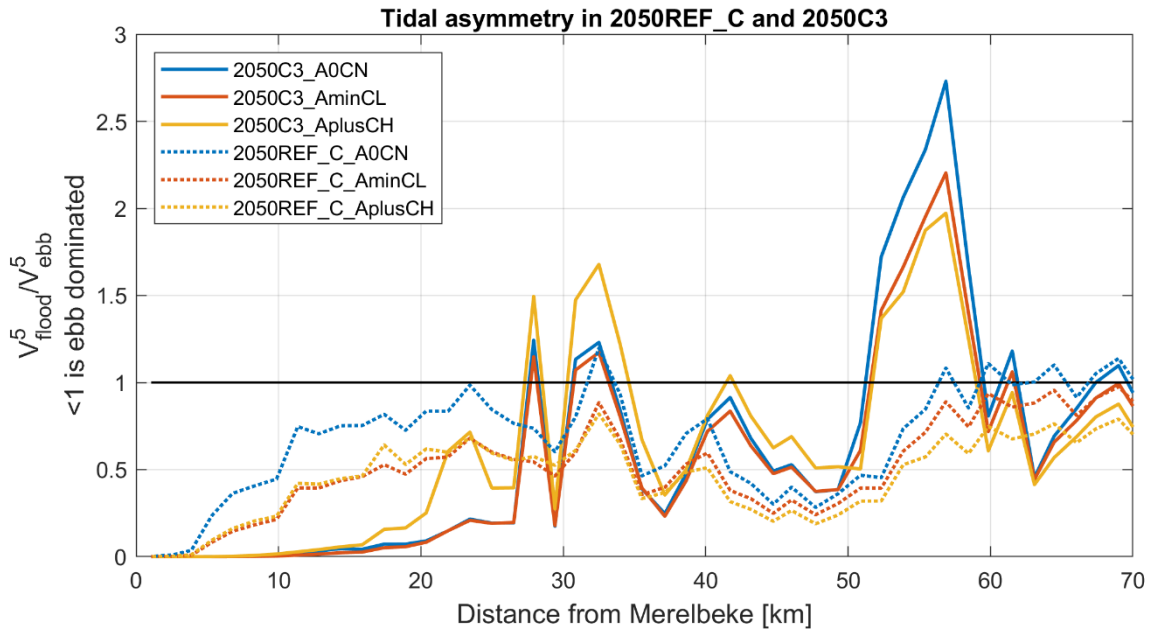


Figure 39 – Tidal asymmetry along the Sea Scheldt under different climate scenarios in 2050REF\_C and 2050C3. A value below 1 means ebb dominant, and above 1 means flood dominant.

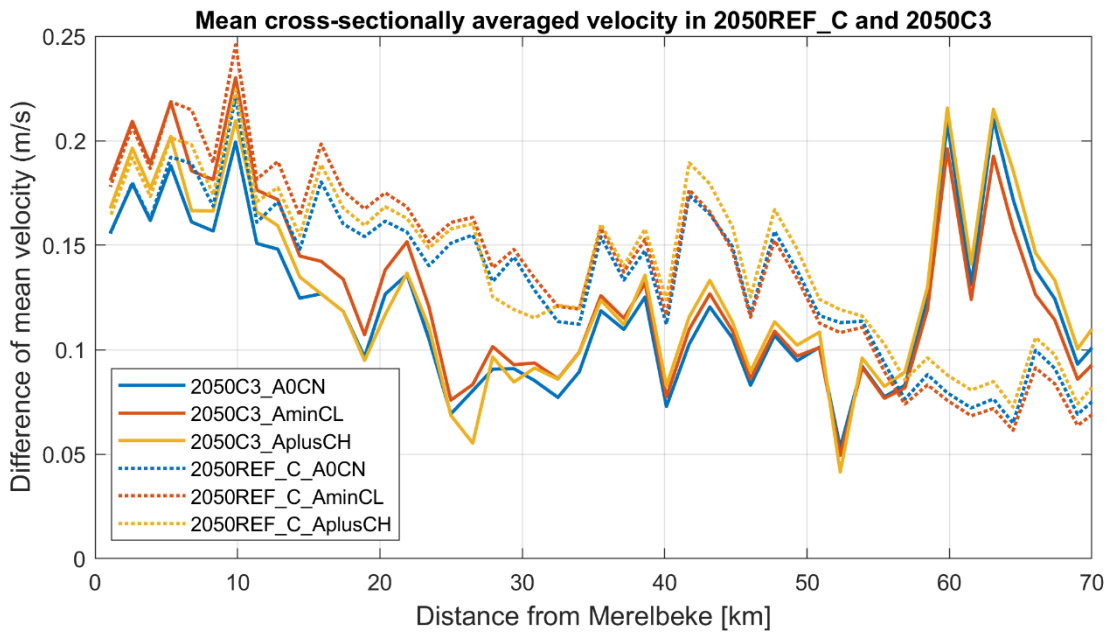


Figure 40 – Mean cross-sectionally averaged velocity along the Sea Scheldt in 2050REF\_C and 2050C3 for a full spring/neap tidal cycle under different climate scenarios. A positive value means more flood dominance or less ebb dominance.

The sedimentation/erosion in the Sea Scheldt expressed in tons per year is computed over a spring-neap cycle. The effect of the C2 alternative on the sedimentation/erosion is calculated by comparing the C2 runs to their respective reference runs.

For readability, here we only show the aggregated sedimentation/erosion in the polygons and an analysis of the differences with REF under the AOCN scenario. The aggregated sedimentation/erosion maps under AOCN, AminCL and AplusCH scenarios can be found in Appendix 2 and the detailed maps of bed evolution at each node can be seen in Appendix 3.

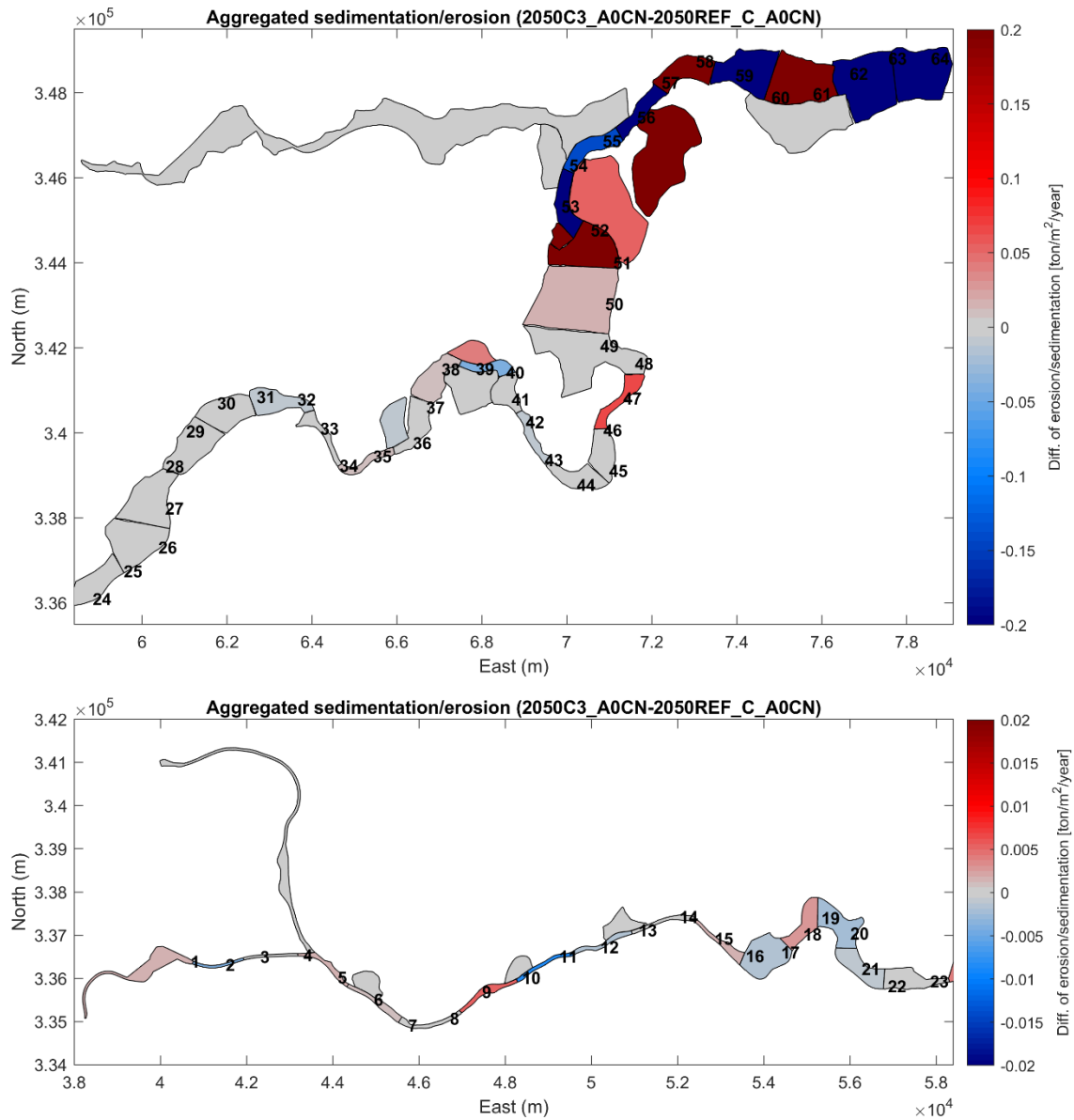


Figure 41 – Effect of C3 alternative on the sedimentation/erosion in the Upper Sea Scheldt under A0CN condition. Red indicates more sedimentation or less erosion.

## 7 Conclusion

The sand transport model is used to study the effects of the C alternatives on the sand transport. One of the advantages of using a 3D model is that the near bottom velocity is used for computing the sand transport instead of depth-averaged velocity in a 2D model.

The results are analyzed and presented in Chapter 6. The effects are evaluated under different climate scenarios, i.e. AOCN, AminCL and AplusCH. The effects of C alternatives on tidal asymmetry and mean velocity are also analyzed and linked to the changes of the net sand transport capacity. The following conclusions can be drawn from the analysis:

- The detailed sed/ero maps in Appendix 3 show that the sand transport mainly occurs in the main channels. The sedimentation/erosion in the lateral system is minor or negligible due to the fact that the velocity in these shallow areas cannot mobilize the sand effectively. This is important in the interpretation of the aggregated sedimentation/erosion maps.
- For the depoldered areas, significant sedimentation only happens in the entrance of Weert in the C3 alternative. In other C alternatives, no obvious sedimentation is observed. This is because, unlike mud, sand is more difficult to be mobilized in the shallow area when velocity is relatively low.
- The results also show that, for the areas with secondary channels, sedimentation is usually happens near the downstream entrance. This is because the flood velocity is higher at the downstream entrance, then it decreases towards upstream. During the ebb, velocity is relatively lower and cannot flush the sediment out (Appendix 3).
- In general, the development of additional intertidal nature along the main channel will increase the wet surface, hence, decrease the velocity. Additional depoldered areas tend to influence the tidal asymmetry and make the main channel less ebb dominant or even locally reverse it to flood dominant. This can locally induce convergence zones for sand, which could imply a local maintenance need to keep the channel navigable. This is visible for instance with the depoldering of Blankaart and Akkershoofd (around km 50) in C3.
- The effects of the C alternatives on the sand transport capacity are robust under different climate scenarios. This is because the effects of C alternatives on the hydrodynamics (e.g. water level, velocity) are consistent under different climate scenarios (Bi et al. 2021), and the sand transport is highly correlated with the hydrodynamic conditions, especially the velocity.
- Channel straightening/undeeptening/narrowing typically increases the velocity, while the channel widening decreases the velocity. The combined effects on the velocity and tidal asymmetry lead to the changes in the net sand transport capacity.
- Because the alternatives are a combination of many measures simultaneously, the modeled effects are sometimes difficult to attribute to individual measures. For that you would need to have runs for each measure separately, since the effects of the measures can overlap. This could be done in a follow-up study.

Finally, it is worth repeating that the sand model does not aim to predict long-term effects due to the fact that it assumes unlimited bed supply and no feedback of the bed evolution on the hydrodynamics.

## References

**Bi, Q.; Smolders, S.; Vanlede, J.; Mostaert, F.** (2020a). Integraal Plan Bovenzeeschede: Sub report 13 – Implementation of C alternatives. Version 1.0. FHR Reports, 13\_131\_13. Flanders Hydraulics Research: Antwerp.

**Bi, Q.; Smolders, S.; Vanlede, J.; Mostaert, F.** (2020b). Integraal Plan Bovenzeeschede: Sub report 15 – Tracer Calculations for Determining the Dispersion Coefficients for the Ecological Model in the C alternatives. Version 0.1. FHR Reports, 13\_131\_15. Flanders Hydraulics Research: Antwerp.

**Bi, Q.; Vanlede, J.; Smolders, S.; Mostaert, F.** (2021). Integraal Plan Bovenzeeschede: Sub report 16 – Effect of the C-alternatives on the Hydrodynamics. Version 1.0. FHR Reports, WL2020R13\_131\_16. Flanders Hydraulics Research: Antwerp.

**IMDC** (2015). Bepalen van randvoorwaarden voor de referentiesituatie (2050) m.b.t. debiet en waterstand. IMDC Report, I/NO/11448/15.128/TFR/. IMDC: Antwerp.

**Smolders, S.; Maximova, T.; Vanlede, J.; Plancke, Y.; Verwaest, T.; Mostaert, F.** (2016). Integraal Plan Bovenzeeschede: Subreport 1 – SCALDIS: a 3D Hydrodynamic Model for the Scheldt Estuary. Version 5.0. WL Rapporten, 13\_131. Flanders Hydraulics Research: Antwerp, Belgium.

**Smolders, S.; Maximova, T.; Vandenbruwaene, W.; Coen, L.; Vanlede, J.; Verwaest, T.; Mostaert, F.** (2017). Integraal Plan Bovenzeeschede: Deelrapport 5 – Scaldis 2050. Version 4.0. FHR Reports, 13\_131\_5. Flanders Hydraulics Research: Antwerp.

**Smolders, S.; De Maerschack, B.; Plancke, Y.; Vanlede, J.; Mostaert, F.** (2019a). Integraal Plan Boven-Zeeschede: Sub report 10 – Scaldis Sand: a sand transport model for the Scheldt estuary. Version 2.0. FHR Reports, 13\_131\_10. Flanders Hydraulics Research: Antwerp.

**Smolders, S.; Plancke, Y.; Vanlede, J.; Mostaert, F.** (2019b). Integraal Plan Boven-Zeeschede: Sub report 11 – Effect of B-alternatives on Sand Transport. Version 3.0. FHR Reports, 13\_131\_11. Flanders Hydraulics Research: Antwerp.

**IMDC.** (2020). Definition of the C alternatives (v1.4). IMDC Report, I/NO/11448/19.226/JVS/RAD. IMDC: Antwerp



# Appendix 1. Polygons used in the result analysis

## Polygons for 2050REF\_C

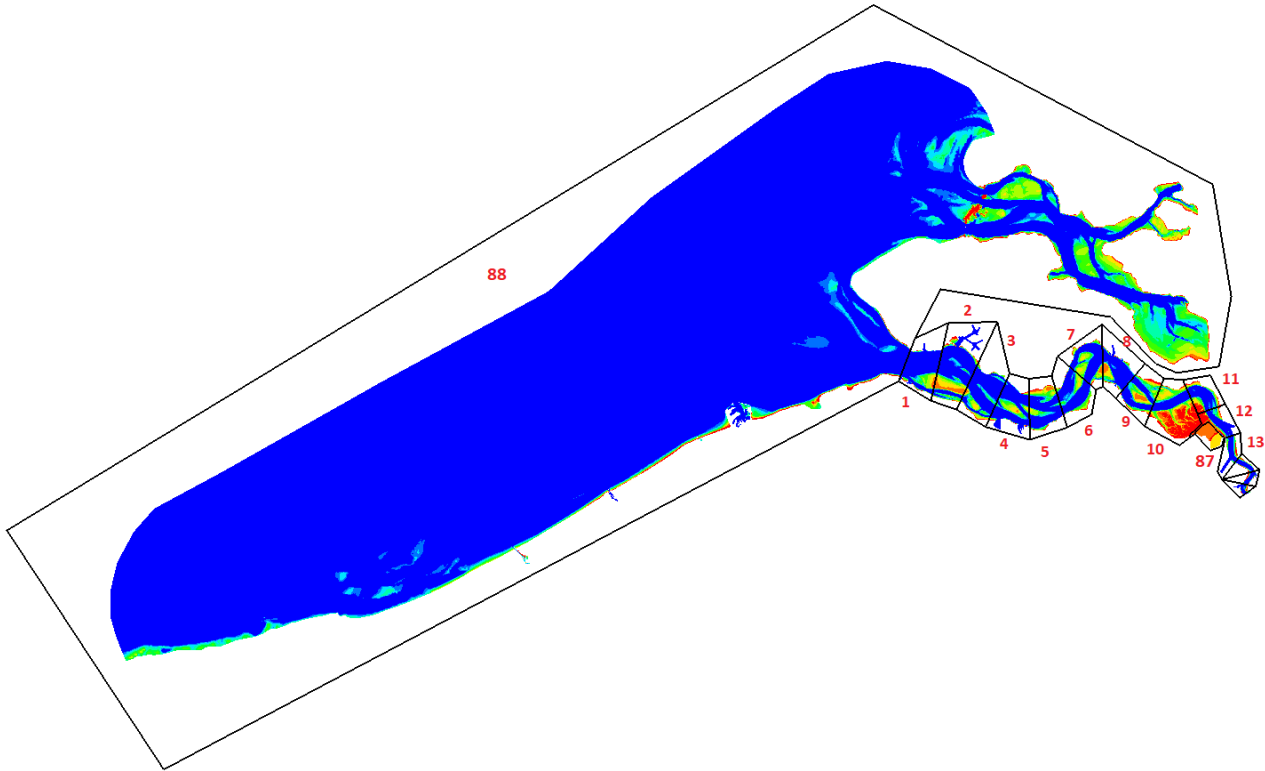
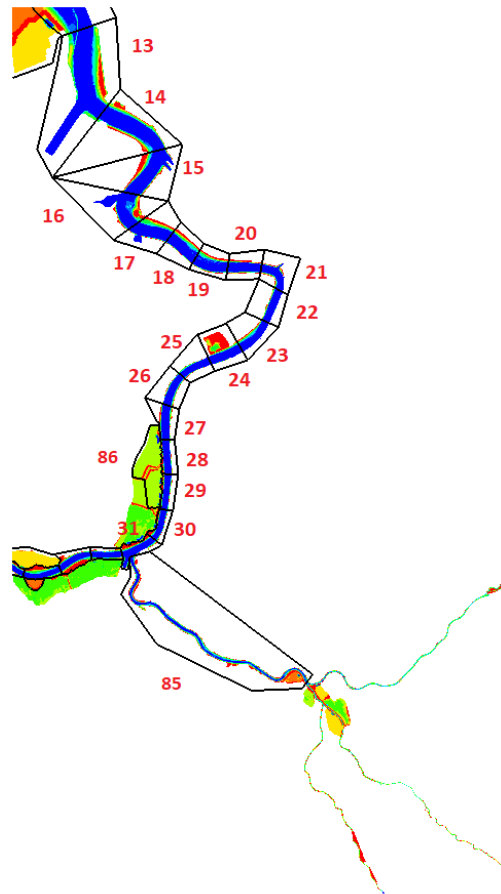


Figure 42 – Polygons for 2050\_REF\_C (polygons 1-13, 87-88)





---

Figure 43 – Polygons for 2050\_REF\_C (polygons 13-31, 85-86)

---

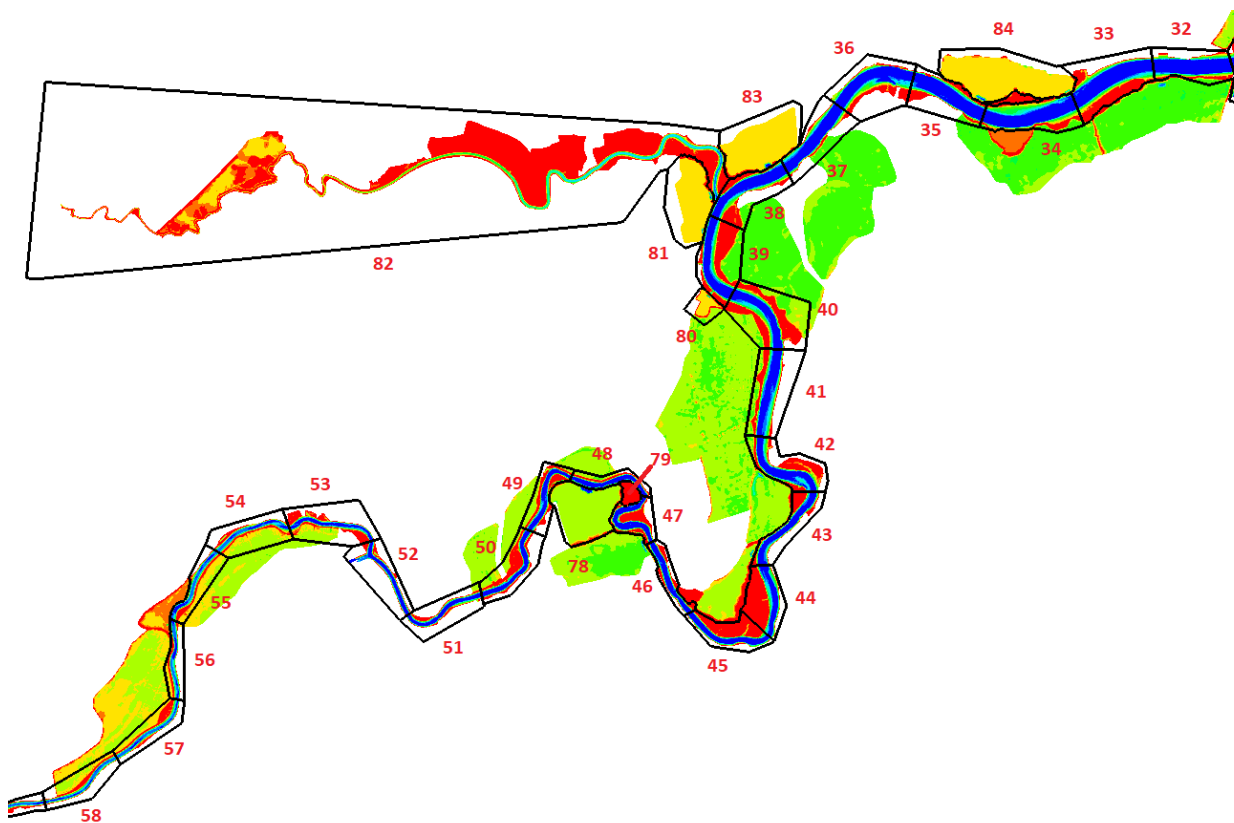


Figure 44 – Polygons for 2050\_REF\_C (polygons 32-58, 78-84)

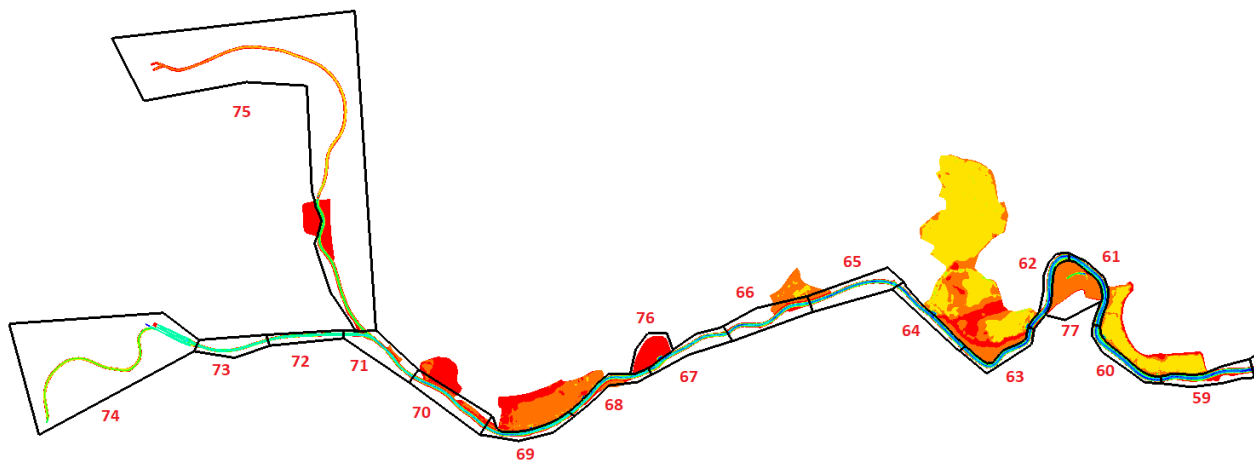


Figure 45 – Polygons for 2050\_REF\_C (polygons 59-77)

## Polygons for 2050C1

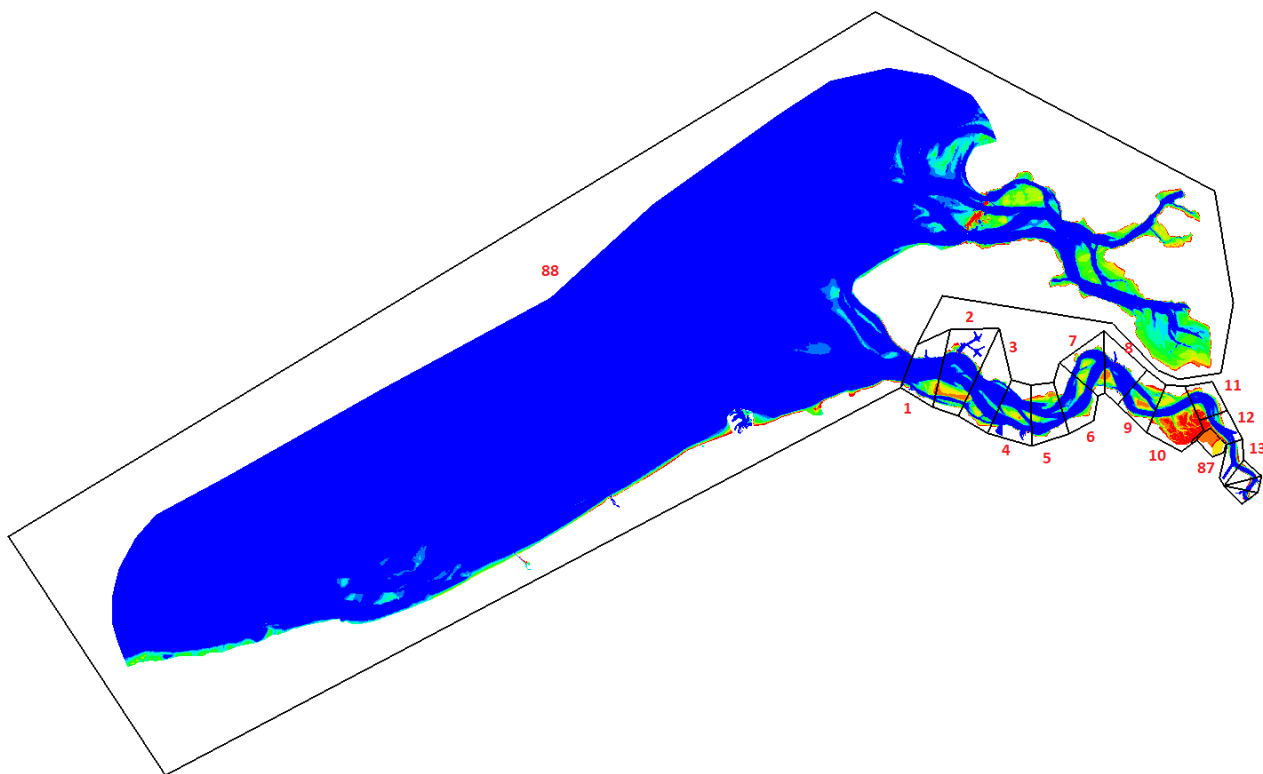


Figure 46 – Polygons for 2050\_C1 (polygons 1-13, 87-88)

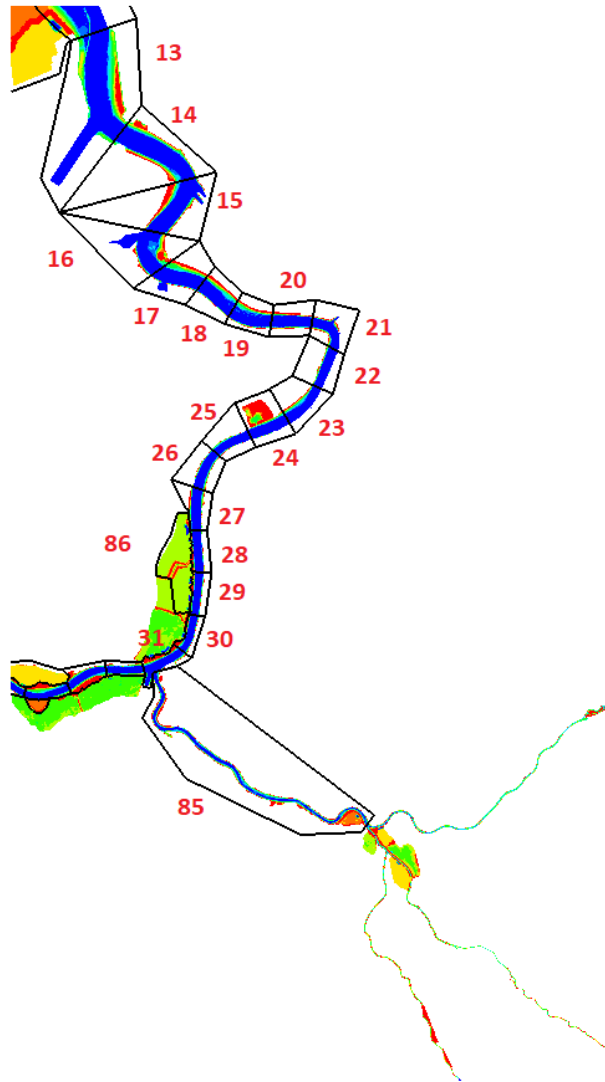


Figure 47 – Polygons for 2050\_C1 (polygons 13-31, 85-86)

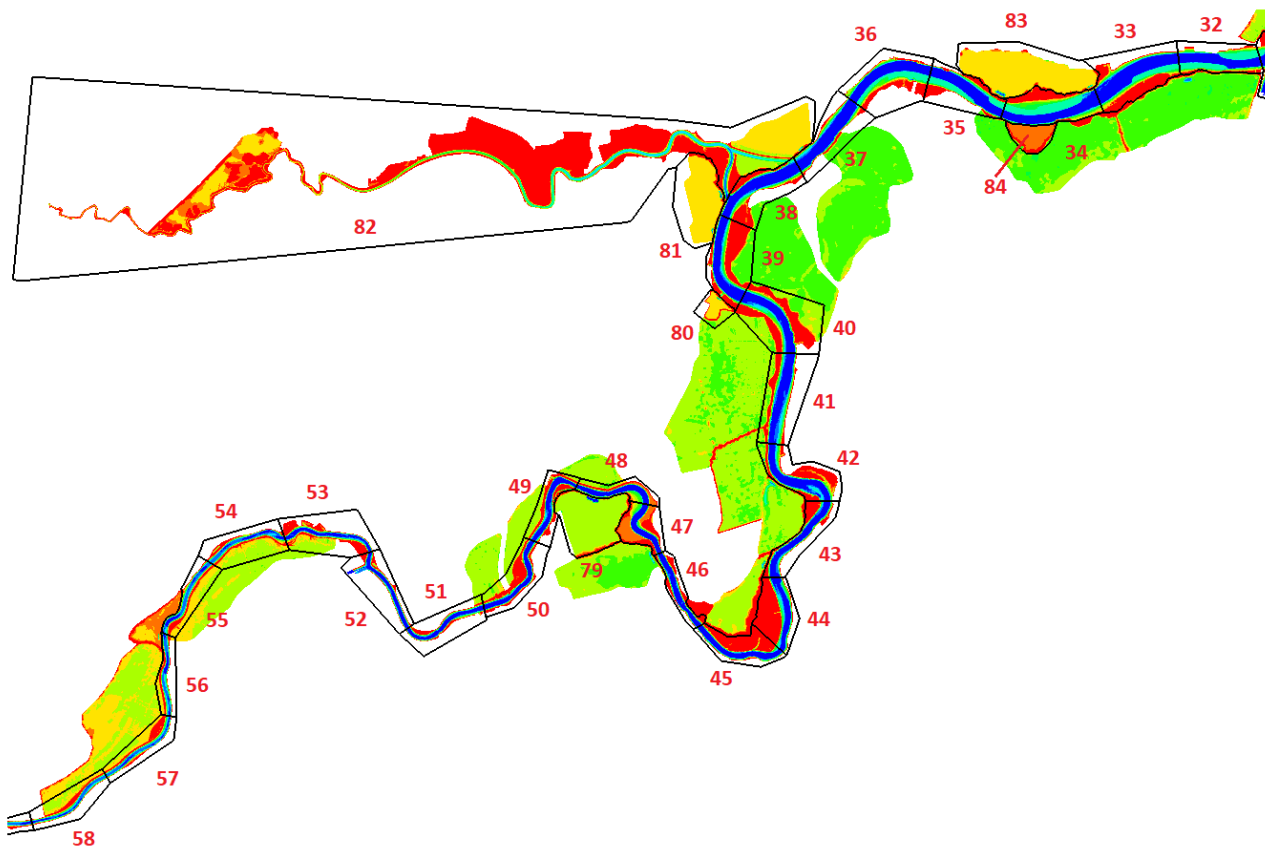


Figure 48 – Polygons for 2050\_C1 (polygons 32-58, 79-84)

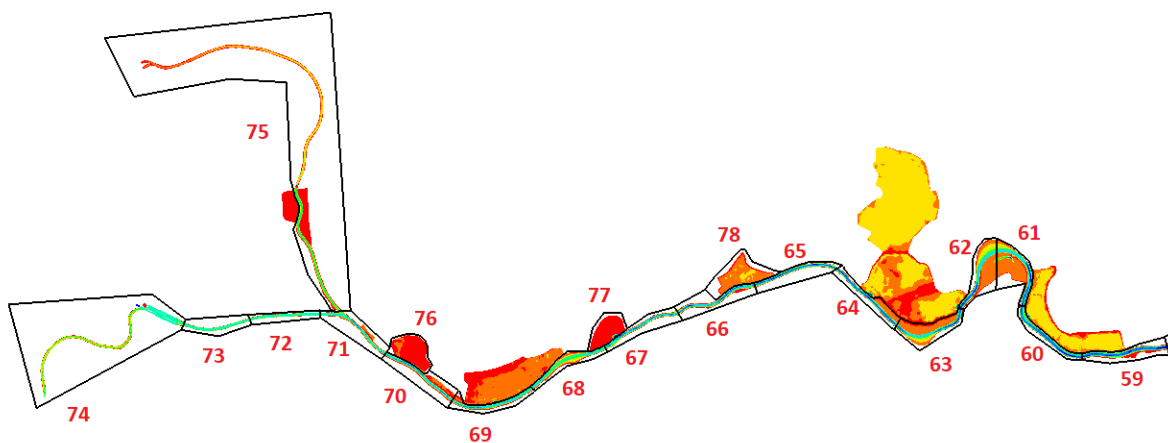


Figure 49 – Polygons for 2050\_C1 (polygons 59-78)

## Polygons for 2050C2

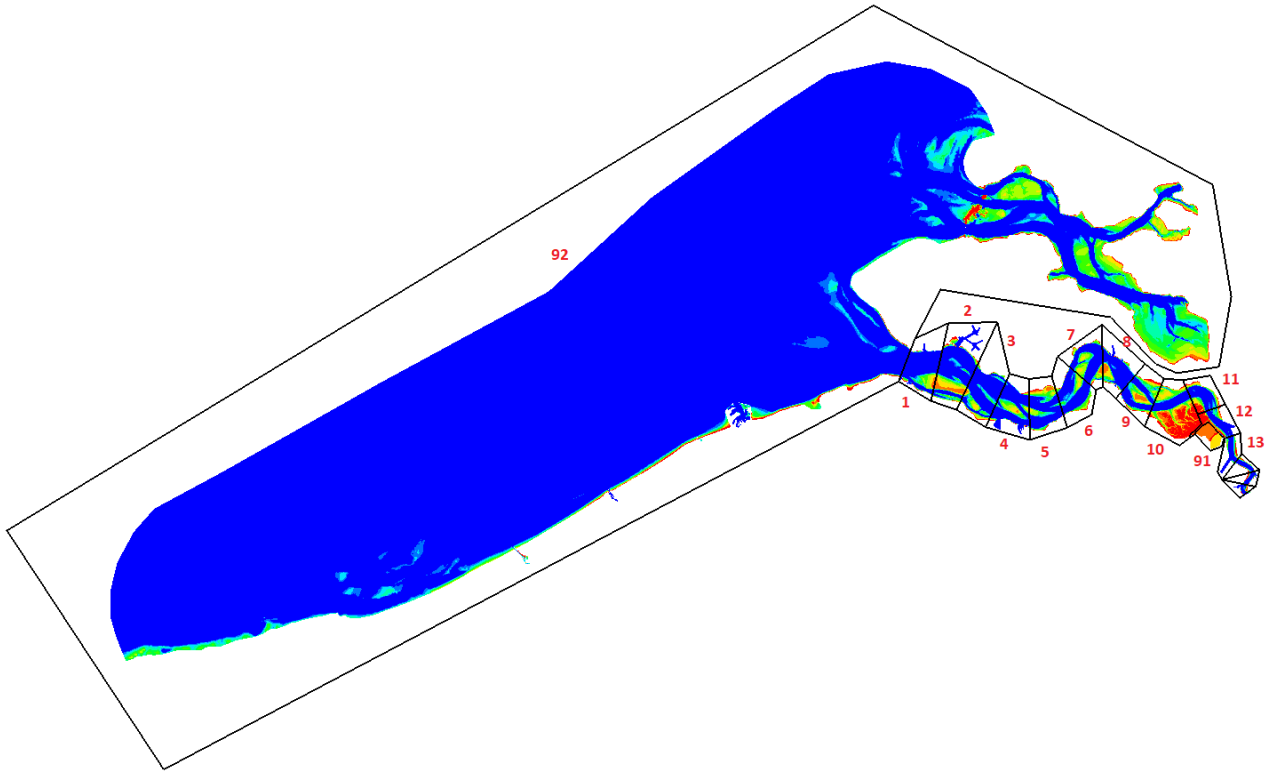


Figure 50 – Polygons for 2050\_C2 (polygons 1-13, 91-92)

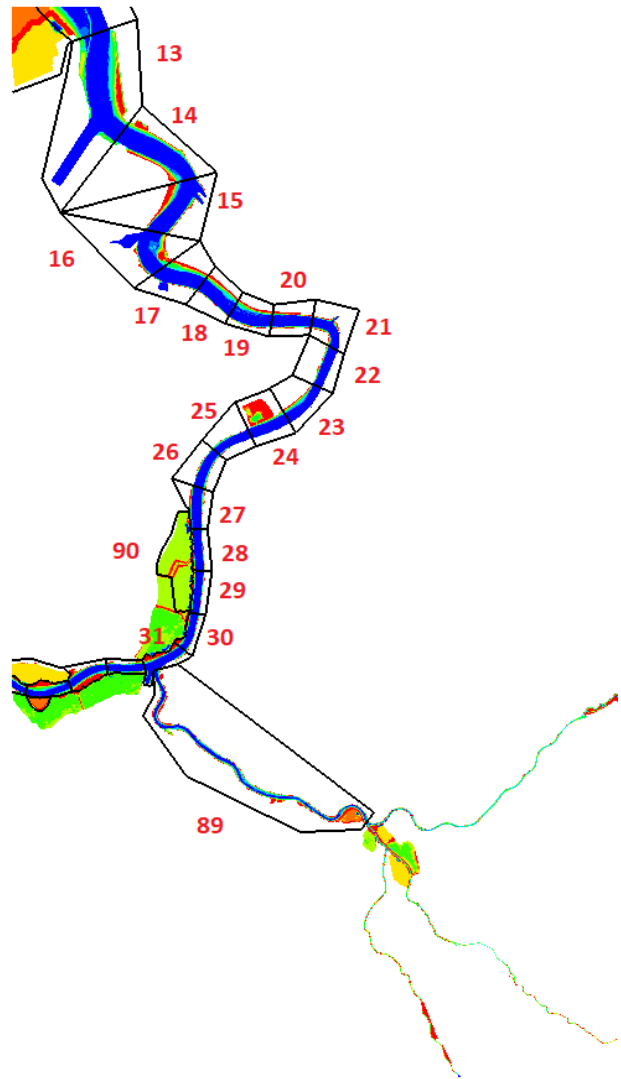


Figure 51 – Polygons for 2050\_C2 (polygons 13-31, 89-90)

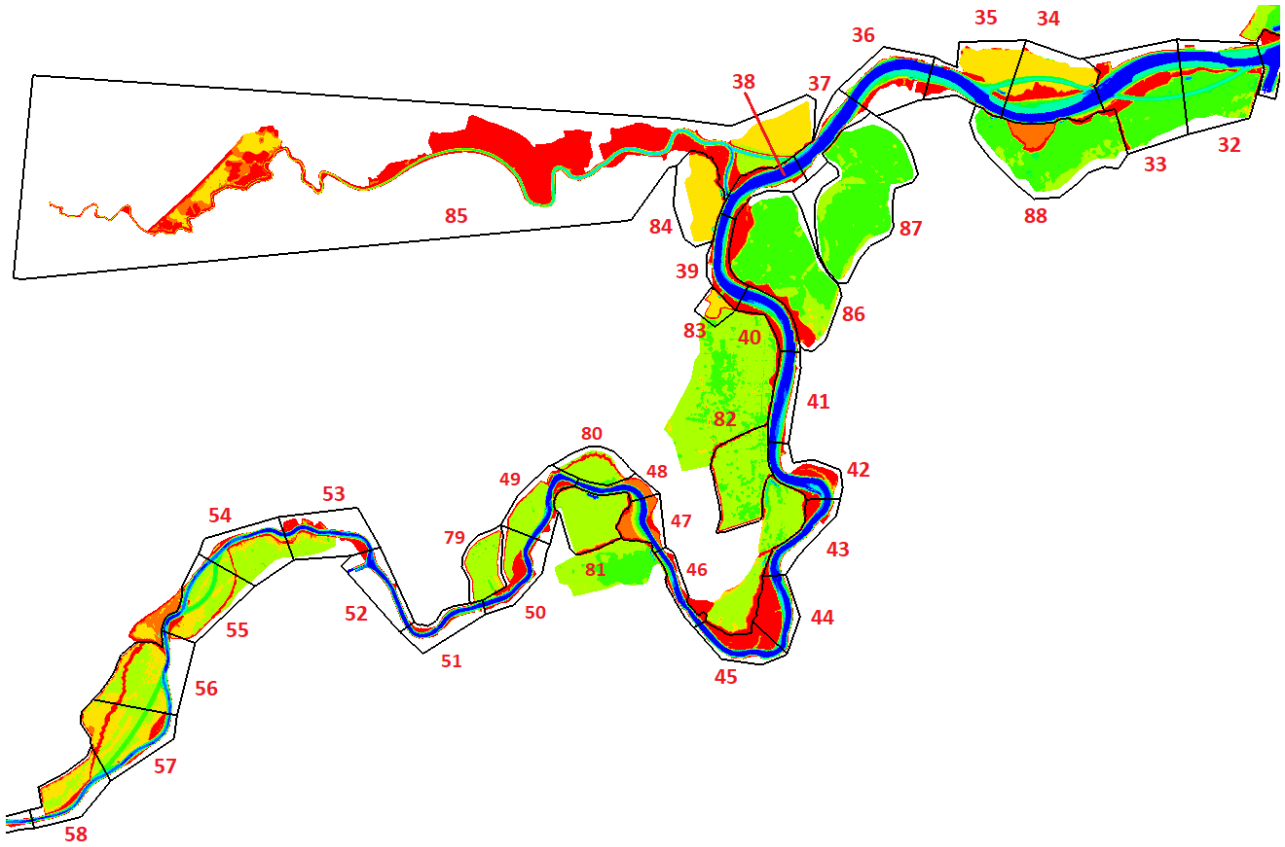


Figure 52 – Polygons for 2050\_C2 (polygons 32-58, 79-88)

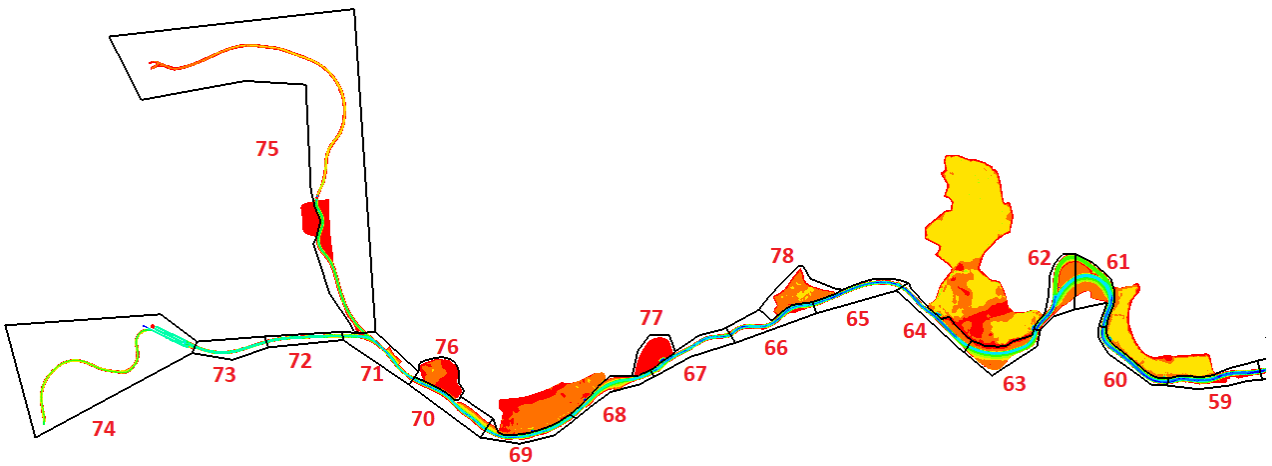


Figure 53 – Polygons for 2050\_C2 (polygons 59-78)



## Polygons for 2050C3

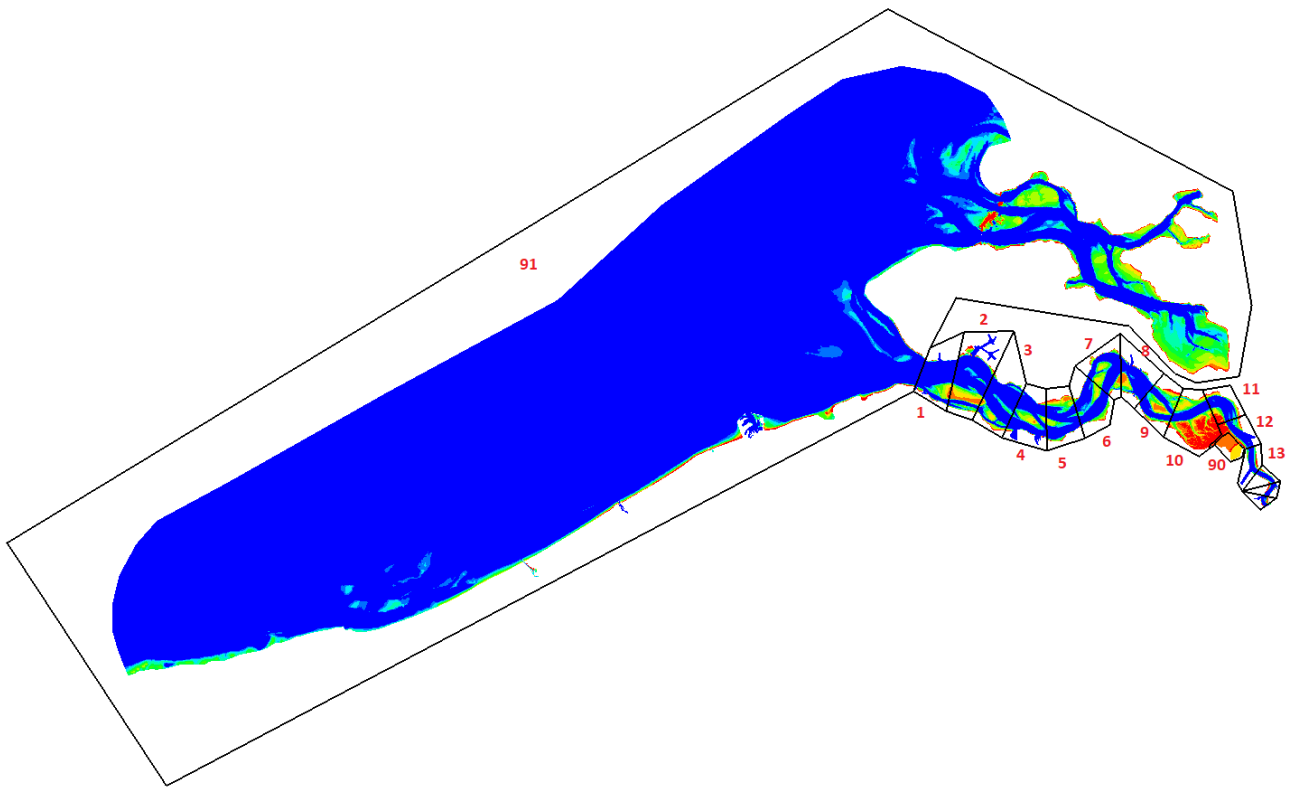


Figure 54 – Polygons for 2050\_C3 (polygons 1-13, 90-91)

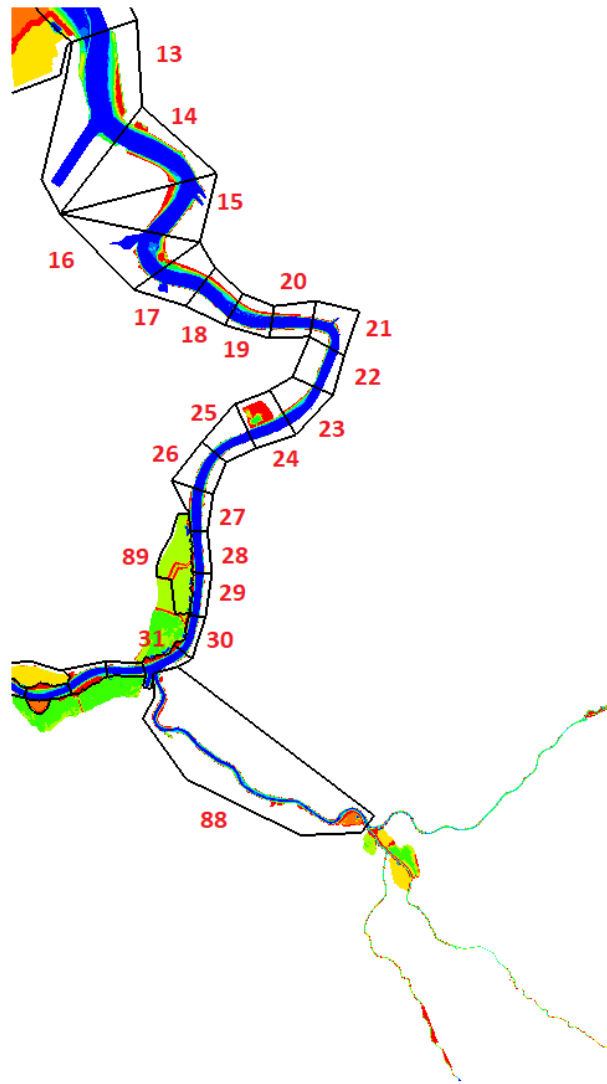


Figure 55 – Polygons for 2050\_C3 (polygons 13-31, 88-89)

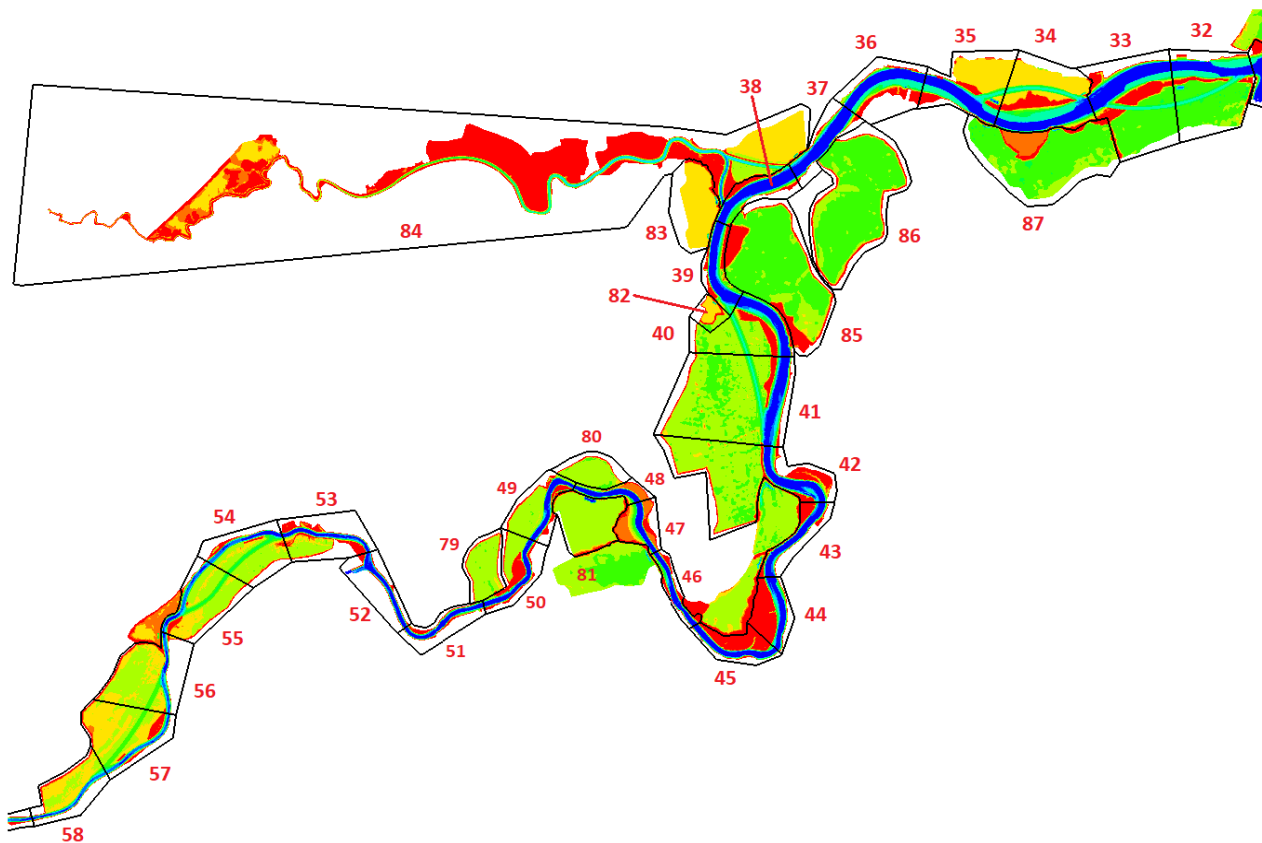


Figure 56 – Polygons for 2050\_C3 (polygons 32-58, 79-87)

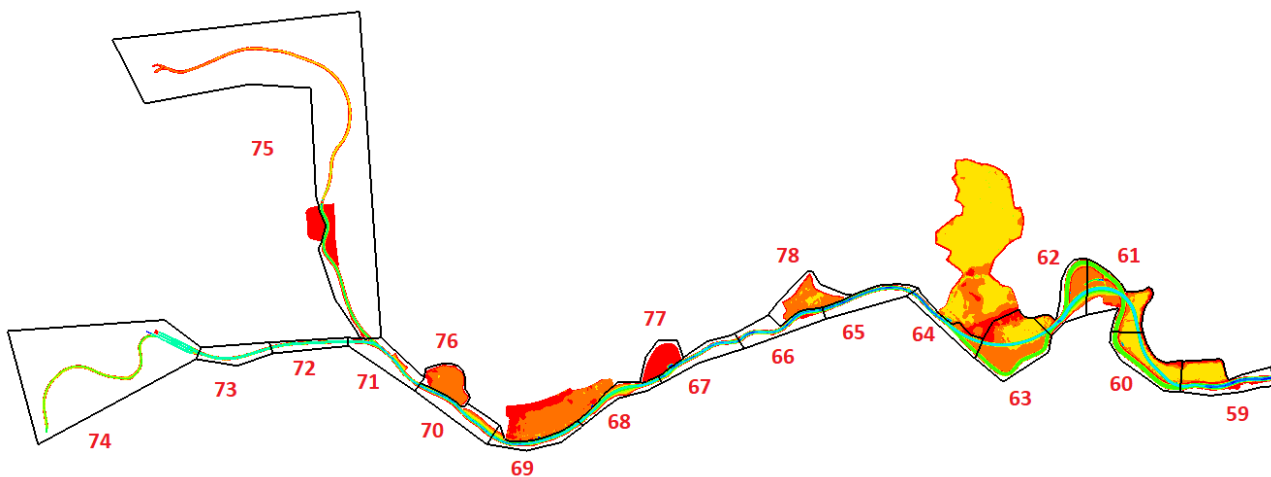


Figure 57 — Polygons for 2050\_C3 (polygons 59-78)

# Appendix 2. Aggregated sedimentation and erosion

2050REF\_C

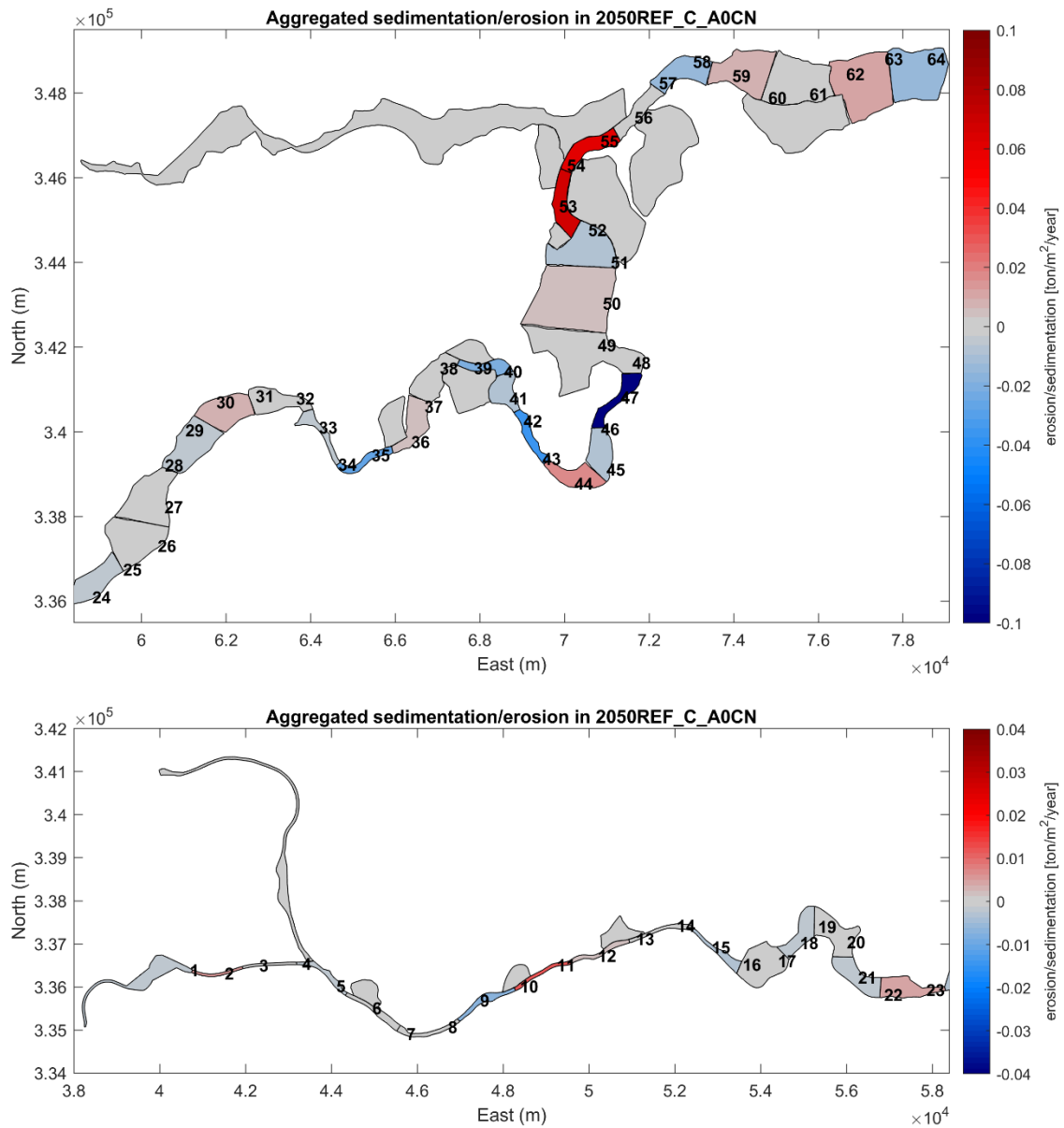


Figure 58 – Potential sedimentation and erosion map for the Upper Sea Scheldt. Scenario 2050REF\_C\_A0CN. Erosion in blue and sedimentation in red. Numbers indicate the distance (km) from Merelbeke.

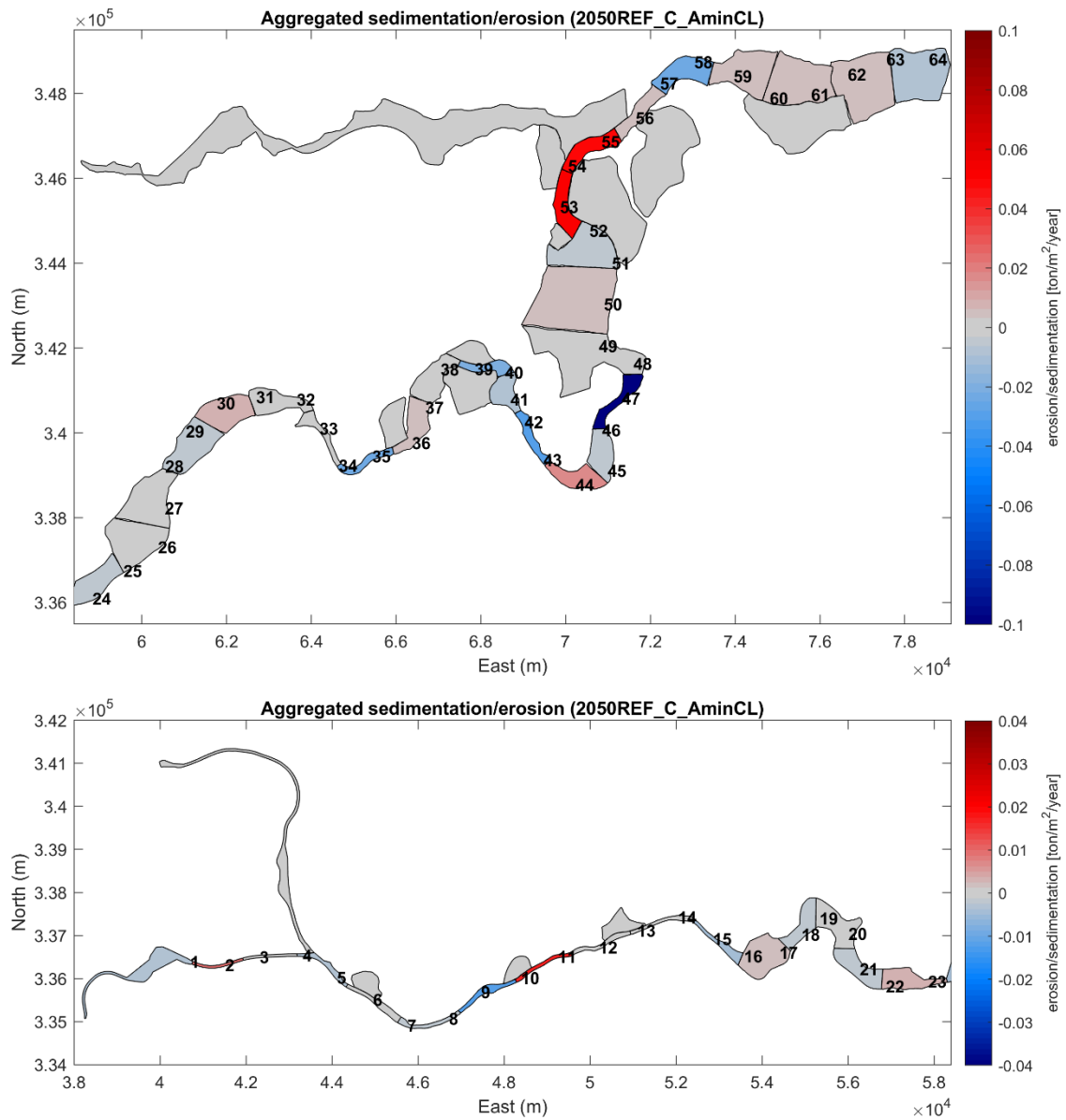


Figure 59 – Potential sedimentation and erosion map for the Upper Sea Scheldt. Scenario 2050REF\_C\_AminCL. Erosion in blue and sedimentation in red. Numbers indicate the distance (km) from Merelbeke.

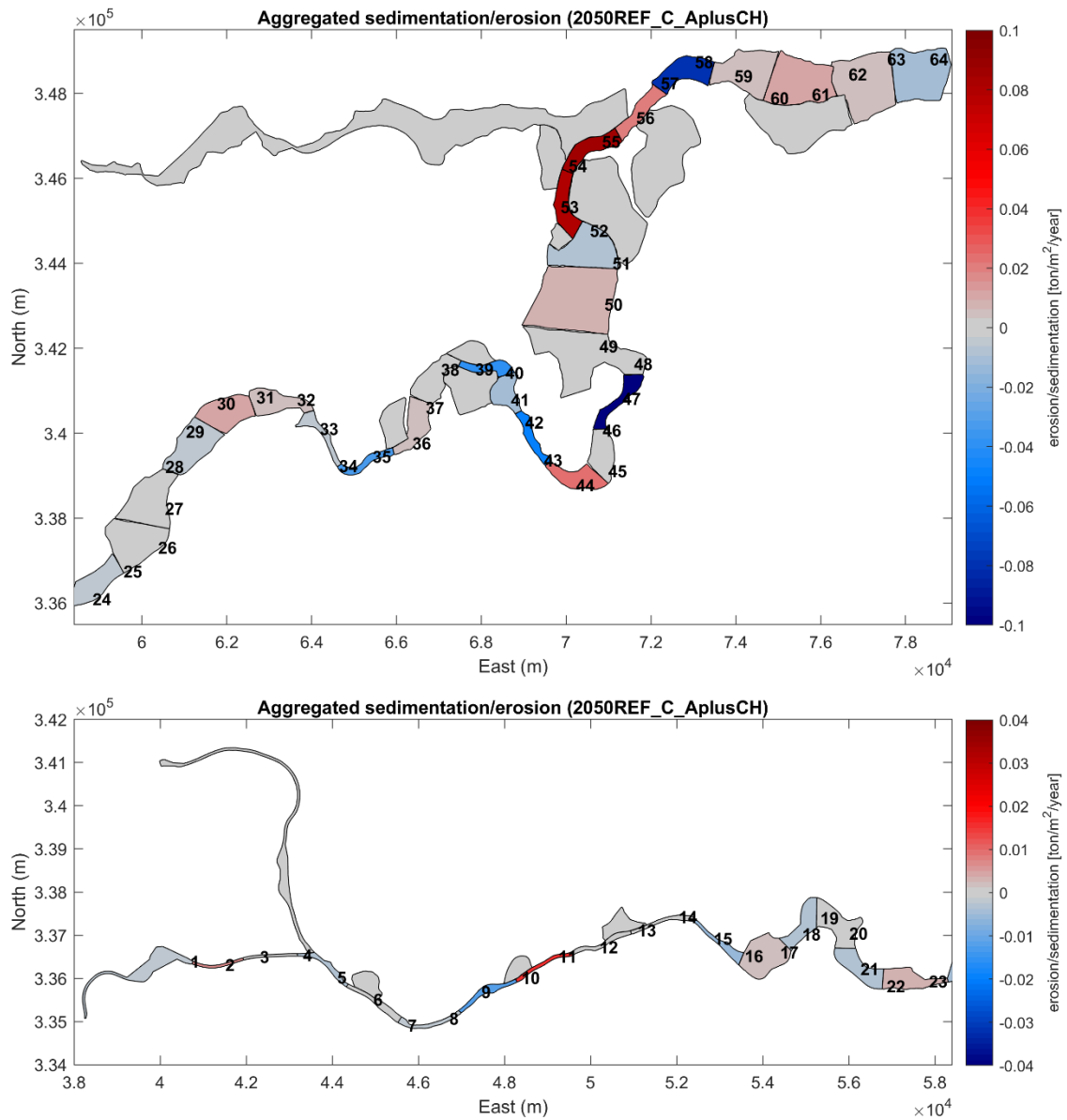


Figure 60 – Potential sedimentation and erosion map for the Upper Sea Scheldt. Scenario 2050REF\_C\_AplusCH. Erosion in blue and sedimentation in red. Numbers indicate the distance (km) from Merelbeke.

2050C1

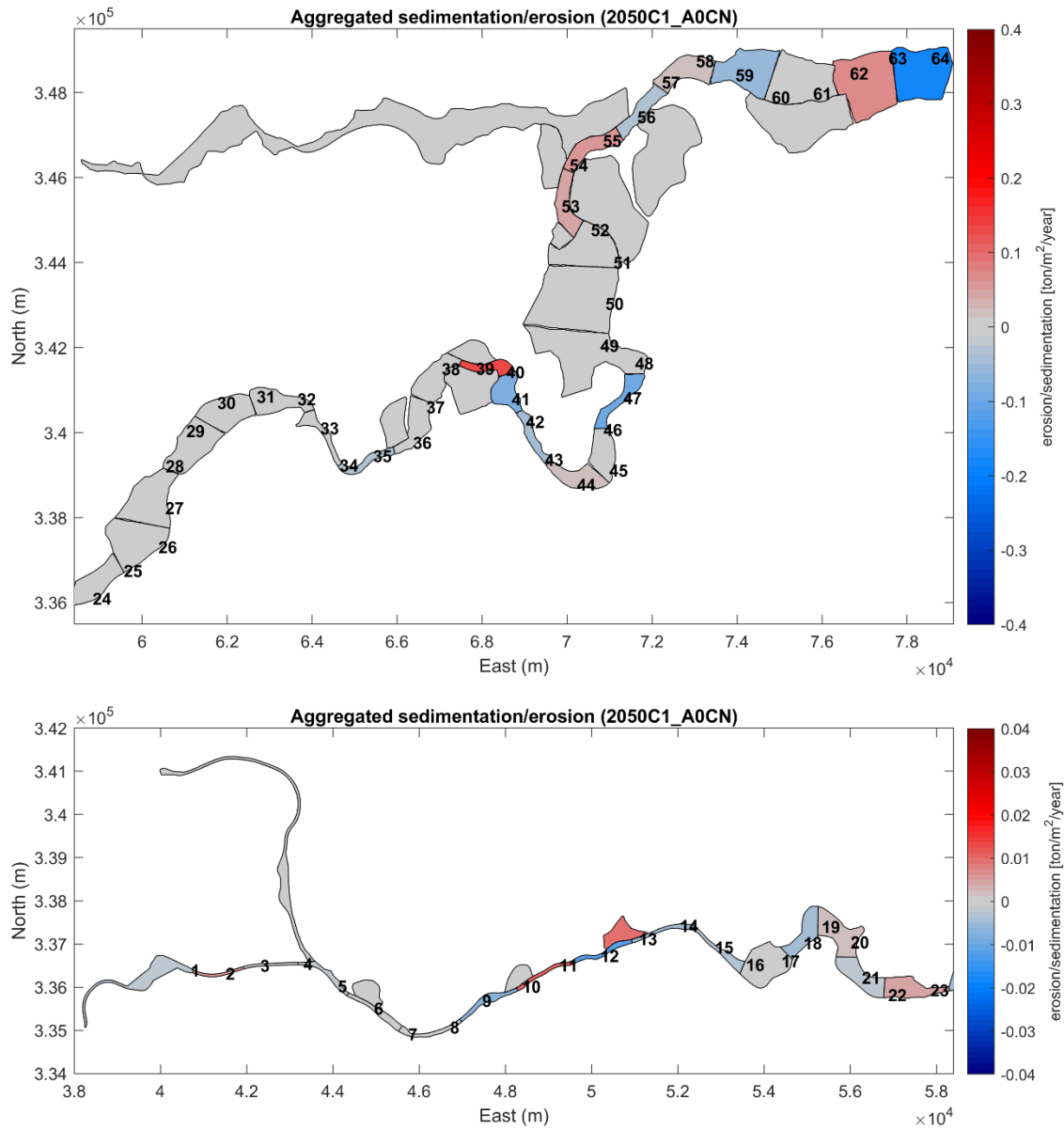


Figure 61 – Potential sedimentation and erosion map for the Upper Sea Scheldt. Scenario 2050C1\_A0CN. Erosion in blue and sedimentation in red. Numbers indicate the distance (km) from Merelbeke.

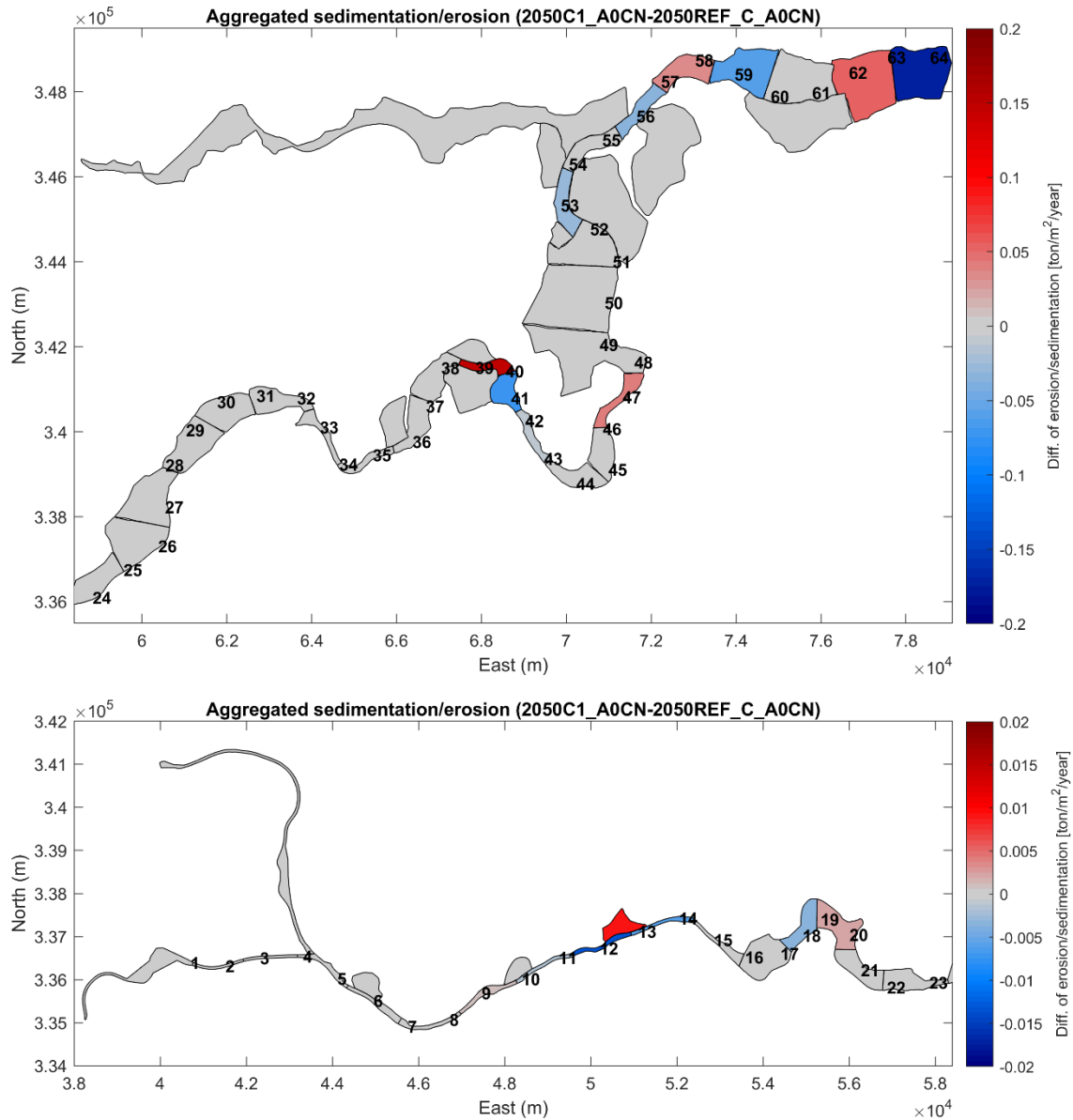


Figure 62 – Effect of C1 alternative on the sedimentation/erosion in the Upper Sea Scheldt under AOCN condition. Red indicates more sedimentation or less erosion. Numbers indicate the distance (km) from Merelbeke.



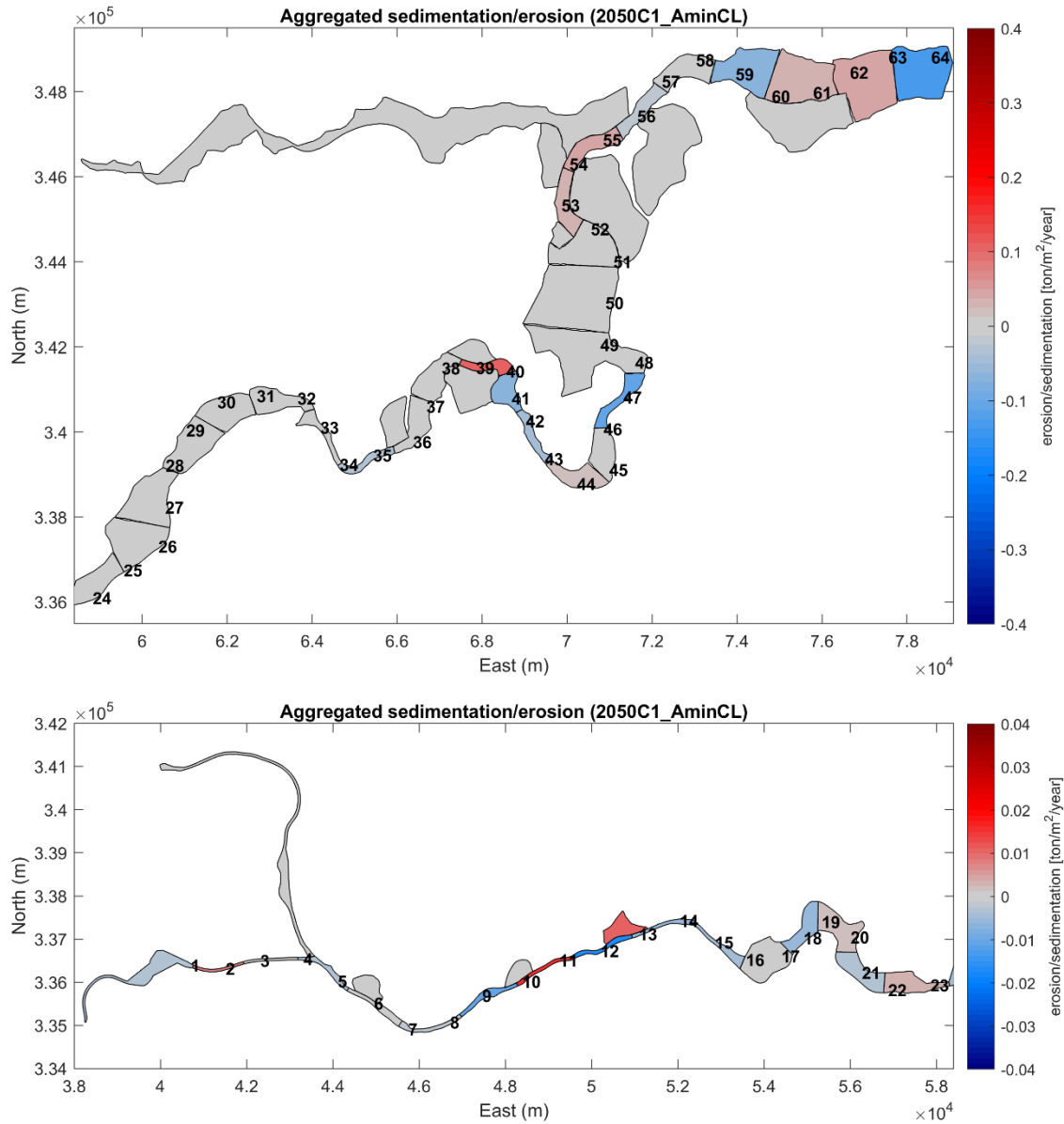


Figure 63 – Potential sedimentation and erosion map for the Upper Sea Scheldt. Scenario 2050C1\_AminCL. Erosion in blue and sedimentation in red. Numbers indicate the distance (km) from Merelbeke.

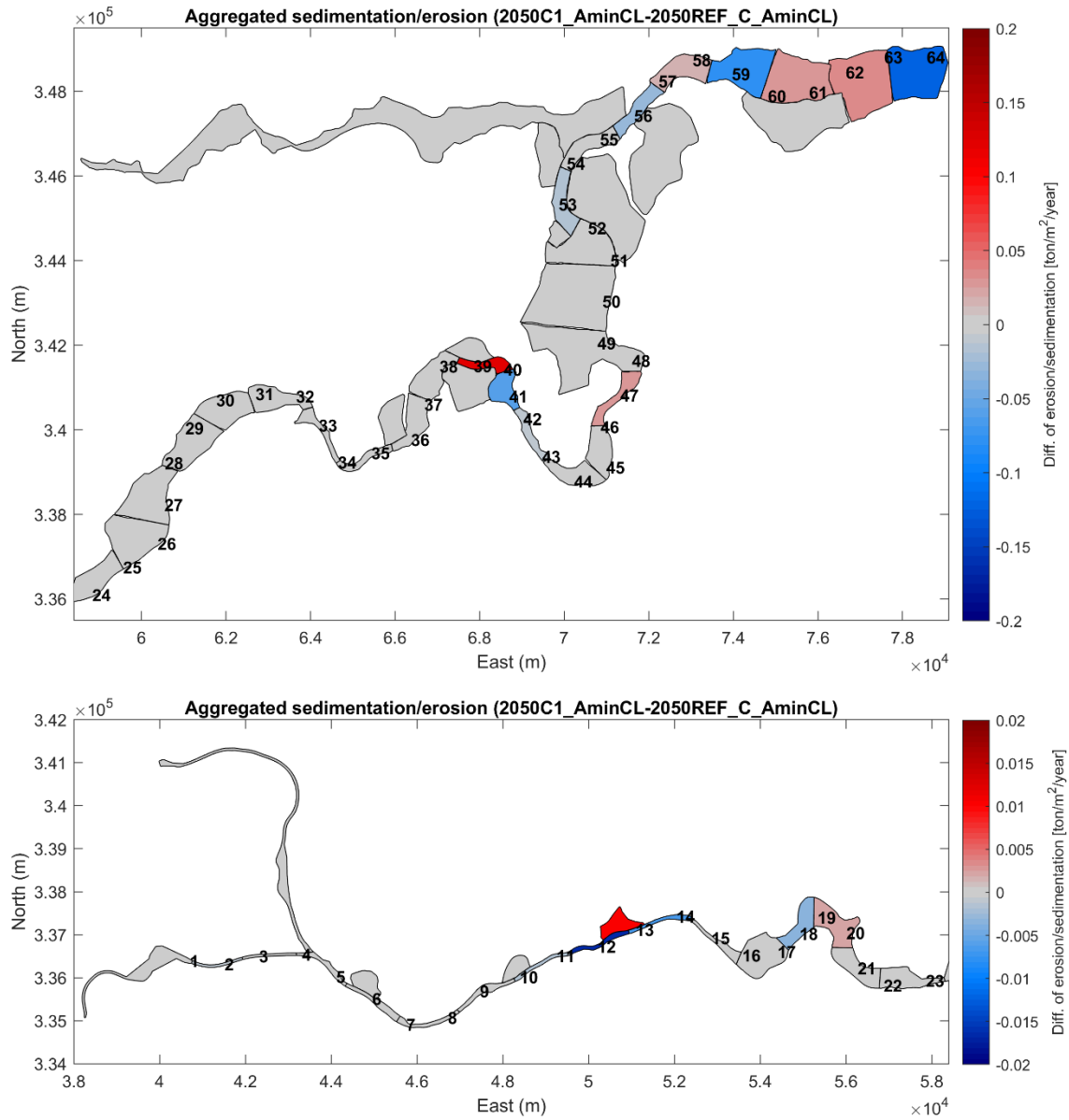


Figure 64 – Effect of C1 alternative on the sedimentation/erosion in the Upper Sea Scheldt under AOCN condition. Red indicates more sedimentation or less erosion.

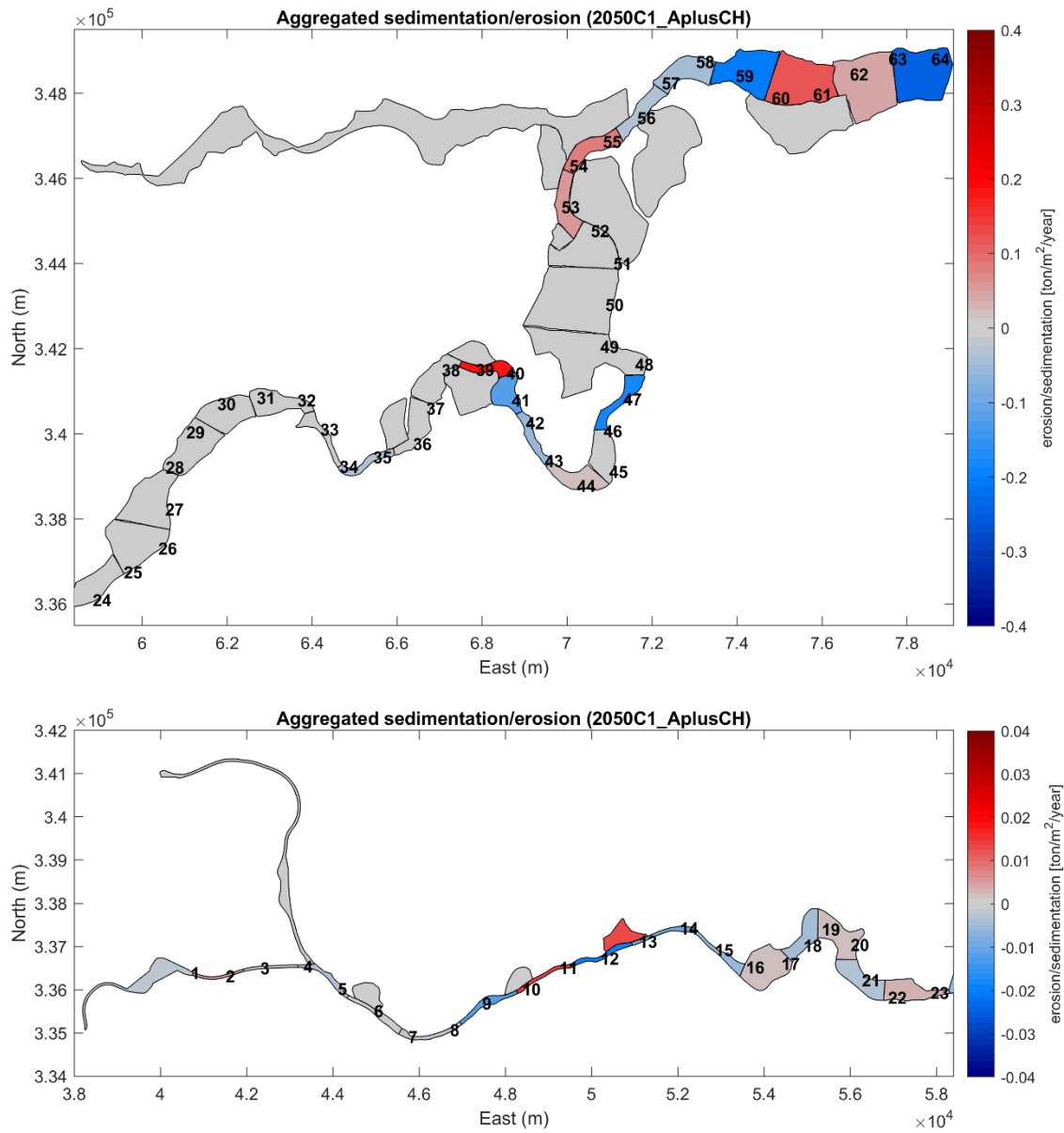


Figure 65 – Potential sedimentation and erosion map for the Upper Sea Scheldt. Scenario 2050C1\_AplusCH. Erosion in blue and sedimentation in red. Numbers indicate the distance (km) from Merelbeke.

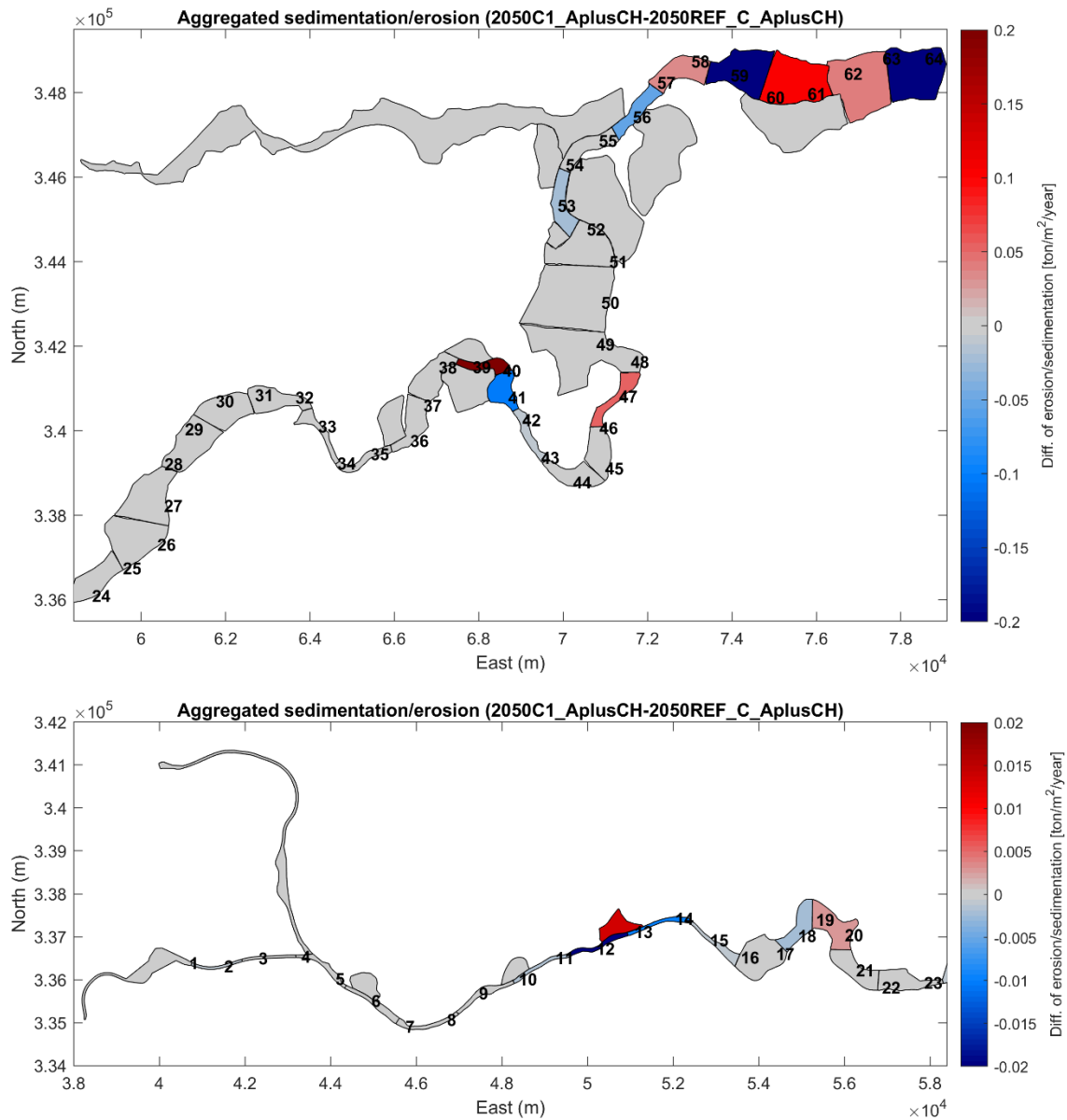


Figure 66 – Effect of C1 alternative on the sedimentation/erosion in the Upper Sea Scheldt under AOCN condition. Red indicates more sedimentation or less erosion.

2050C2

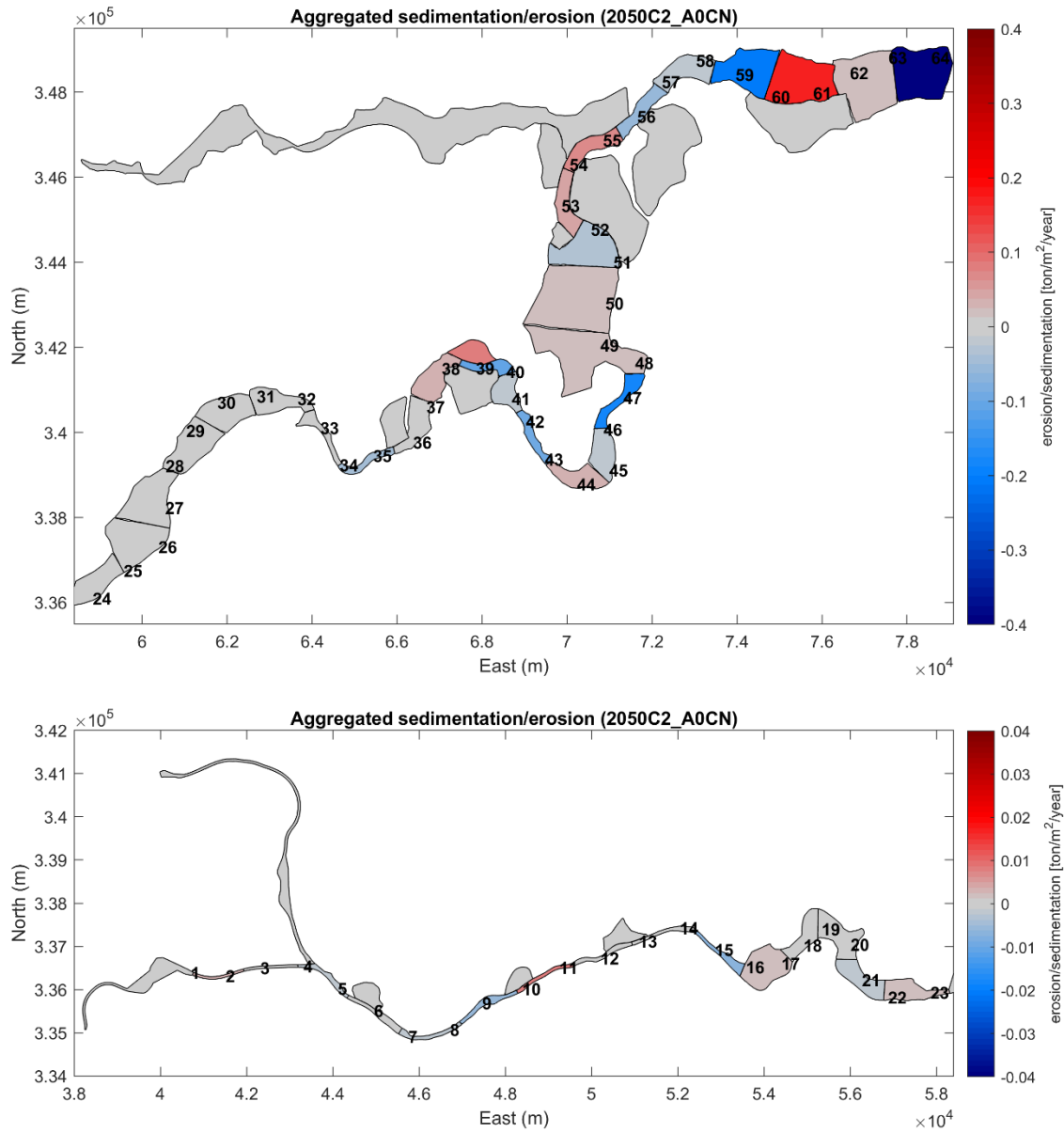


Figure 67 – Potential sedimentation and erosion map for the Upper Sea Scheldt. Scenario 2050C2\_A0CN. Erosion in blue and sedimentation in red. Numbers indicate the distance (km) from Merelbeke.

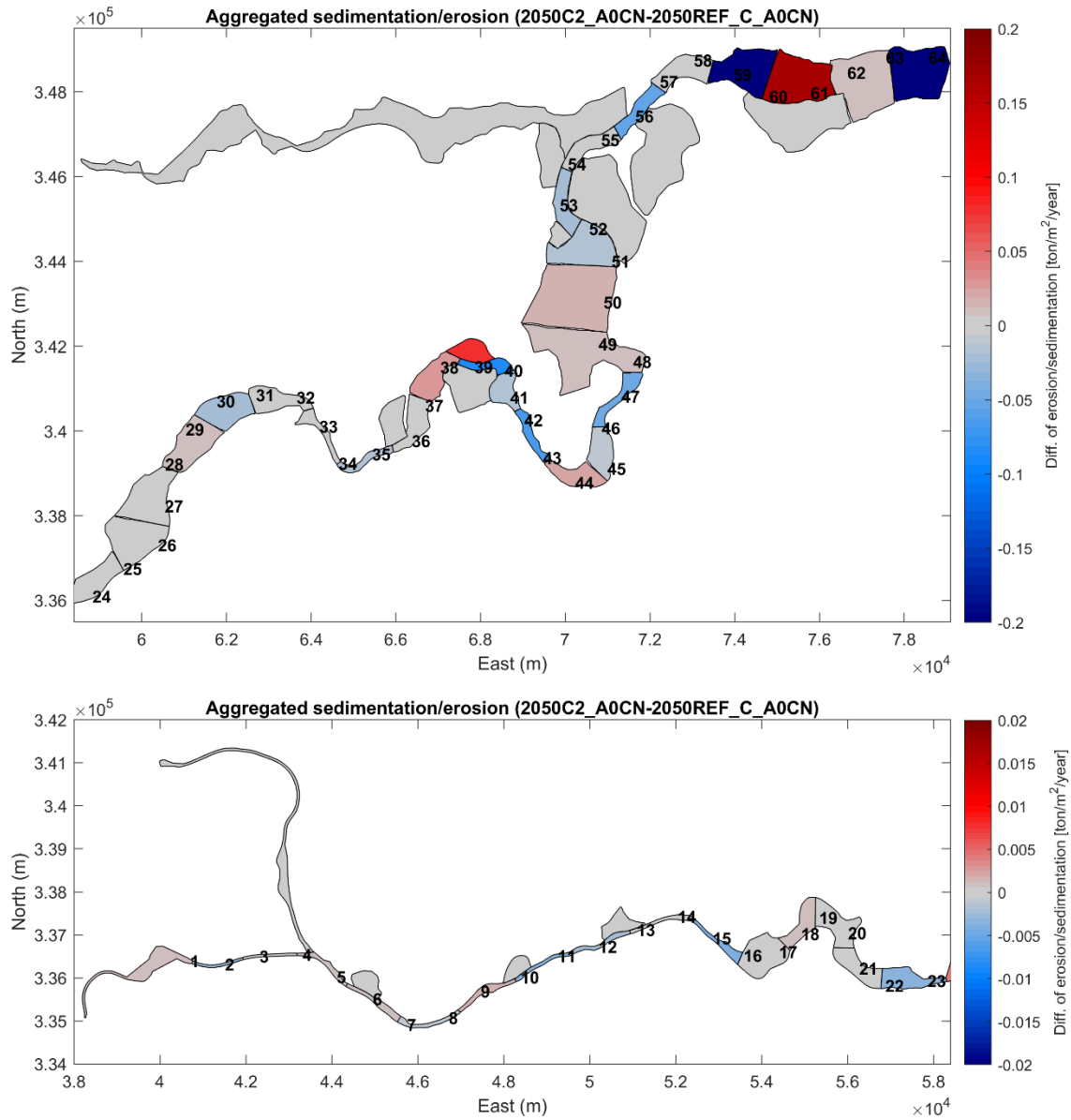


Figure 68 – Effect of C2 alternative on the sedimentation/erosion in the Upper Sea Scheldt under AOCN condition. Red indicates more sedimentation or less erosion.

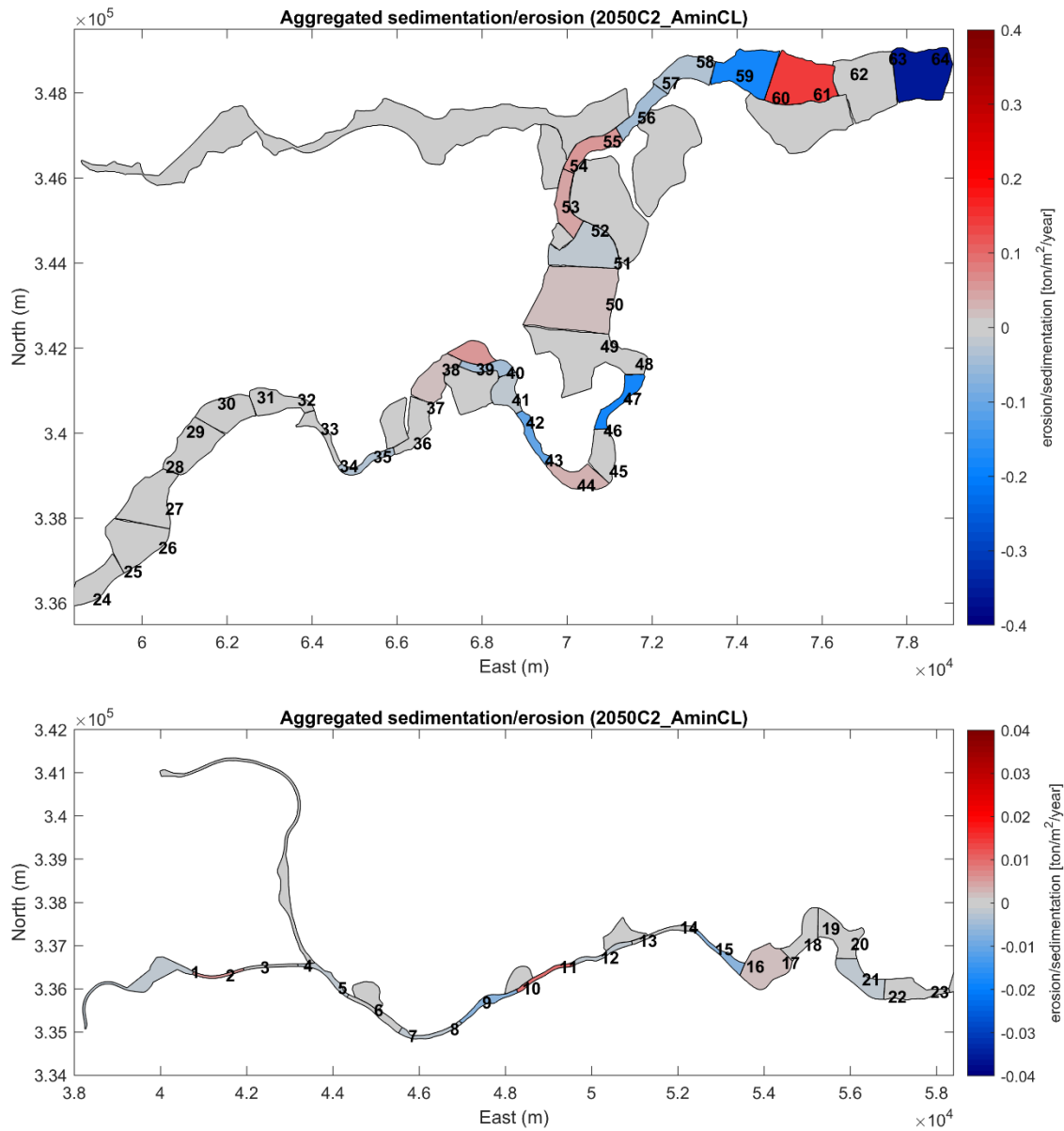


Figure 69 – Potential sedimentation and erosion map for the Upper Sea Scheldt. Scenario 2050C2\_AminCL. Erosion in blue and sedimentation in red. Numbers indicate the distance (km) from Merelbeke.

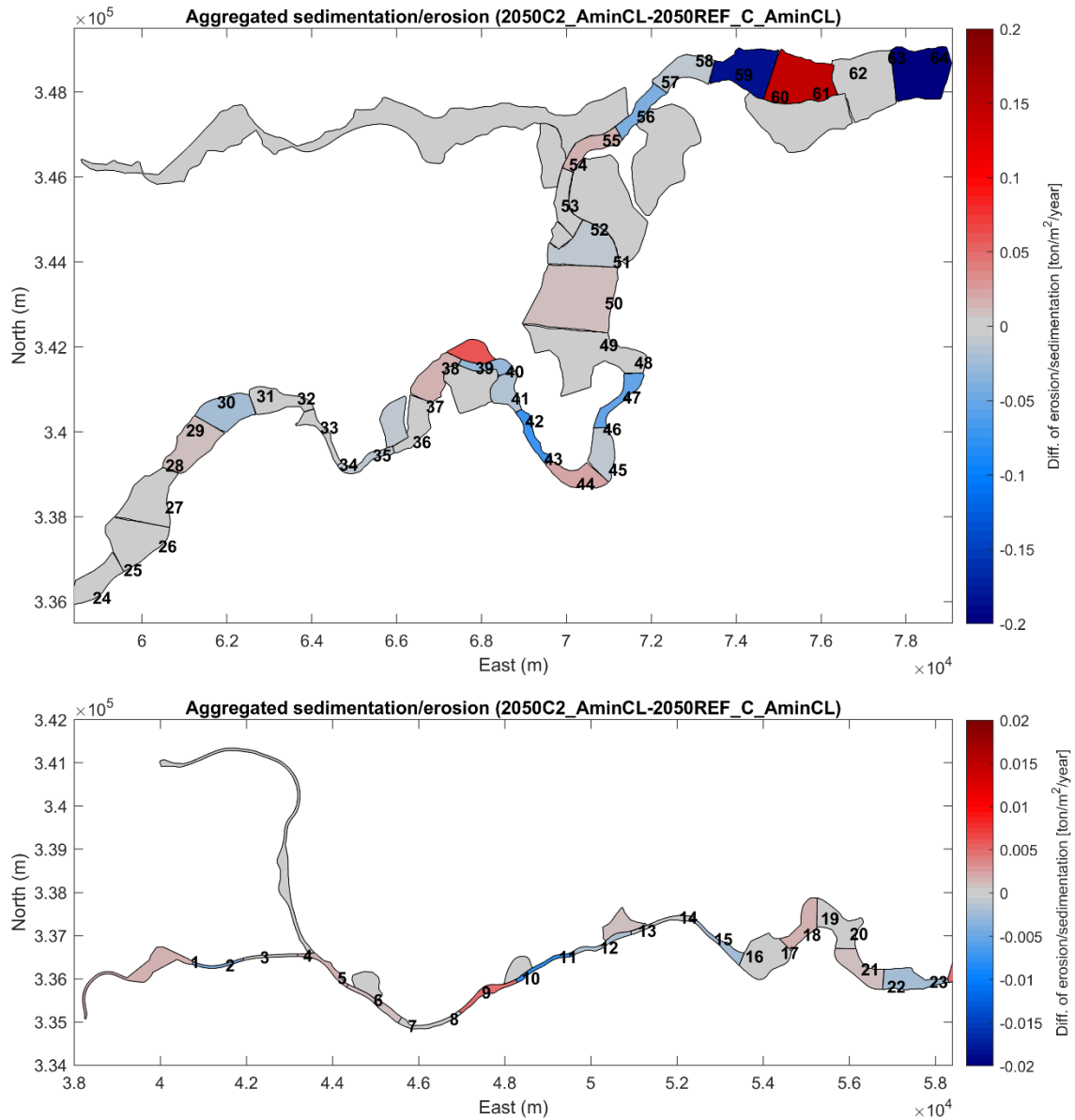


Figure 70 – Effect of C2 alternative on the sedimentation/erosion in the Upper Sea Scheldt under AminCL condition. Red indicates more sedimentation or less erosion.



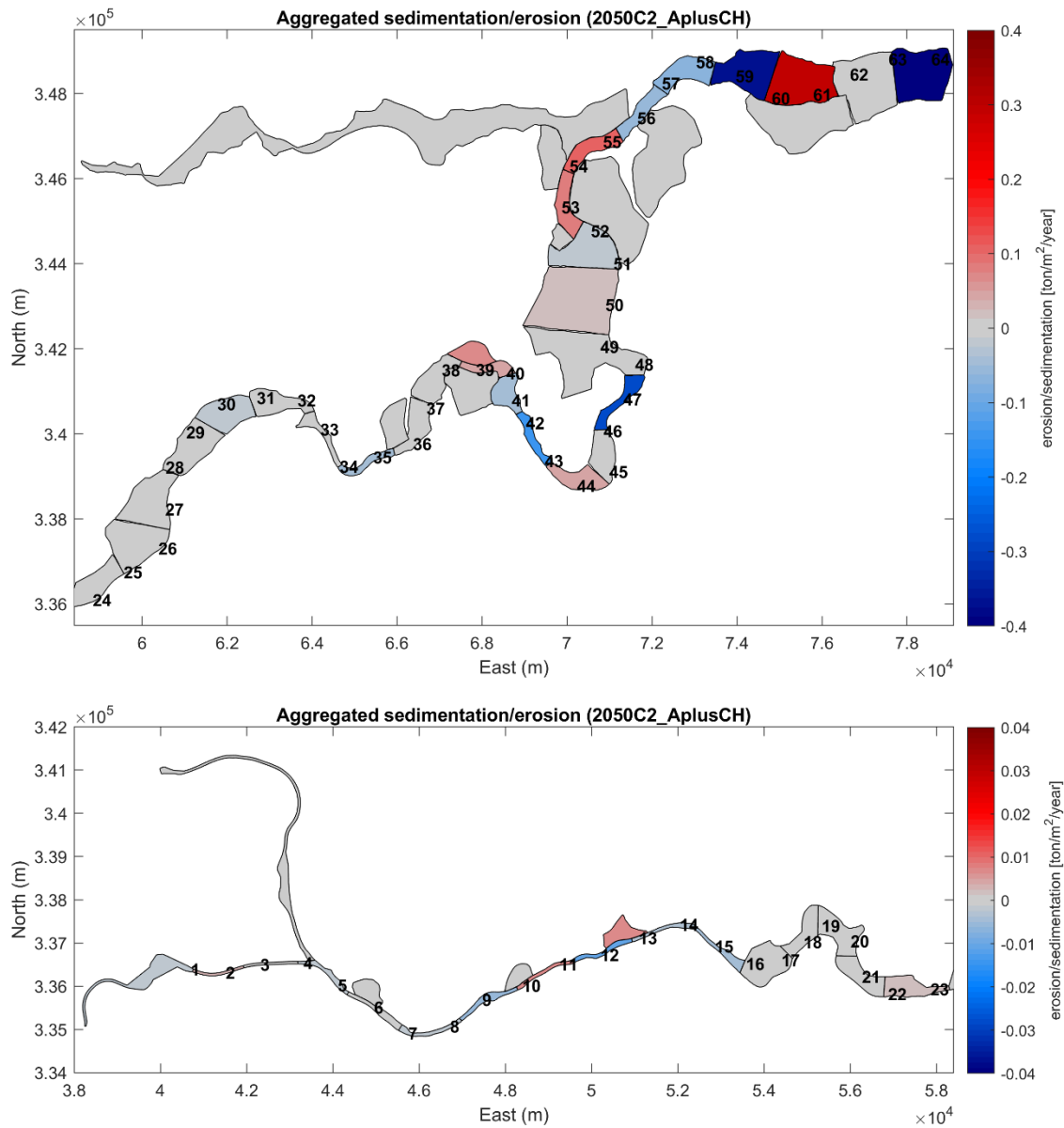


Figure 71 – Potential sedimentation and erosion map for the Upper Sea Scheldt. Scenario 2050C2\_AplusCH. Erosion in blue and sedimentation in red. Numbers indicate the distance (km) from Merelbeke.

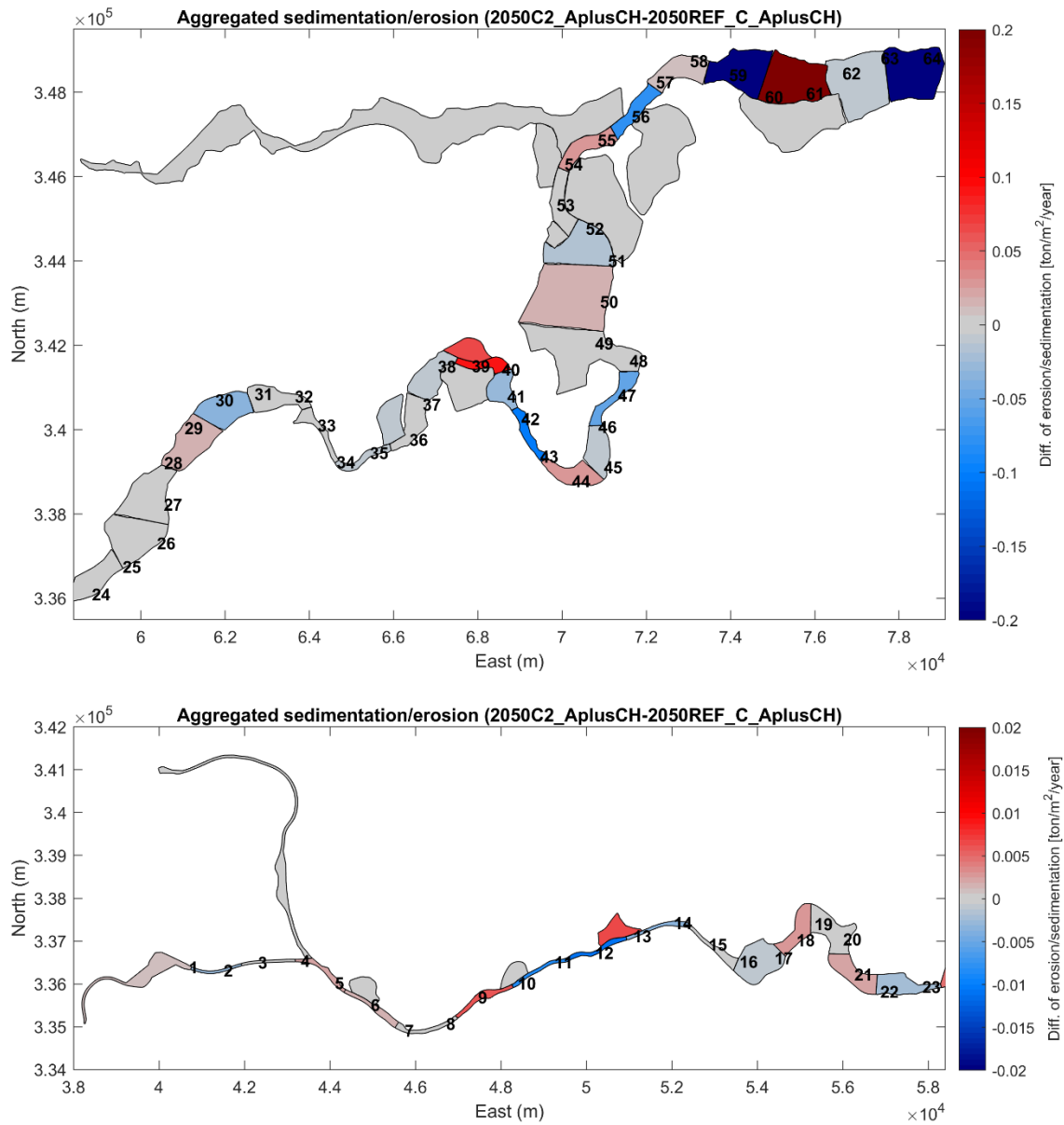


Figure 72 – Effect of C2 alternative on the sedimentation/erosion in the Upper Sea Scheldt under AplusCH condition. Red indicates more sedimentation or less erosion.

2050C3

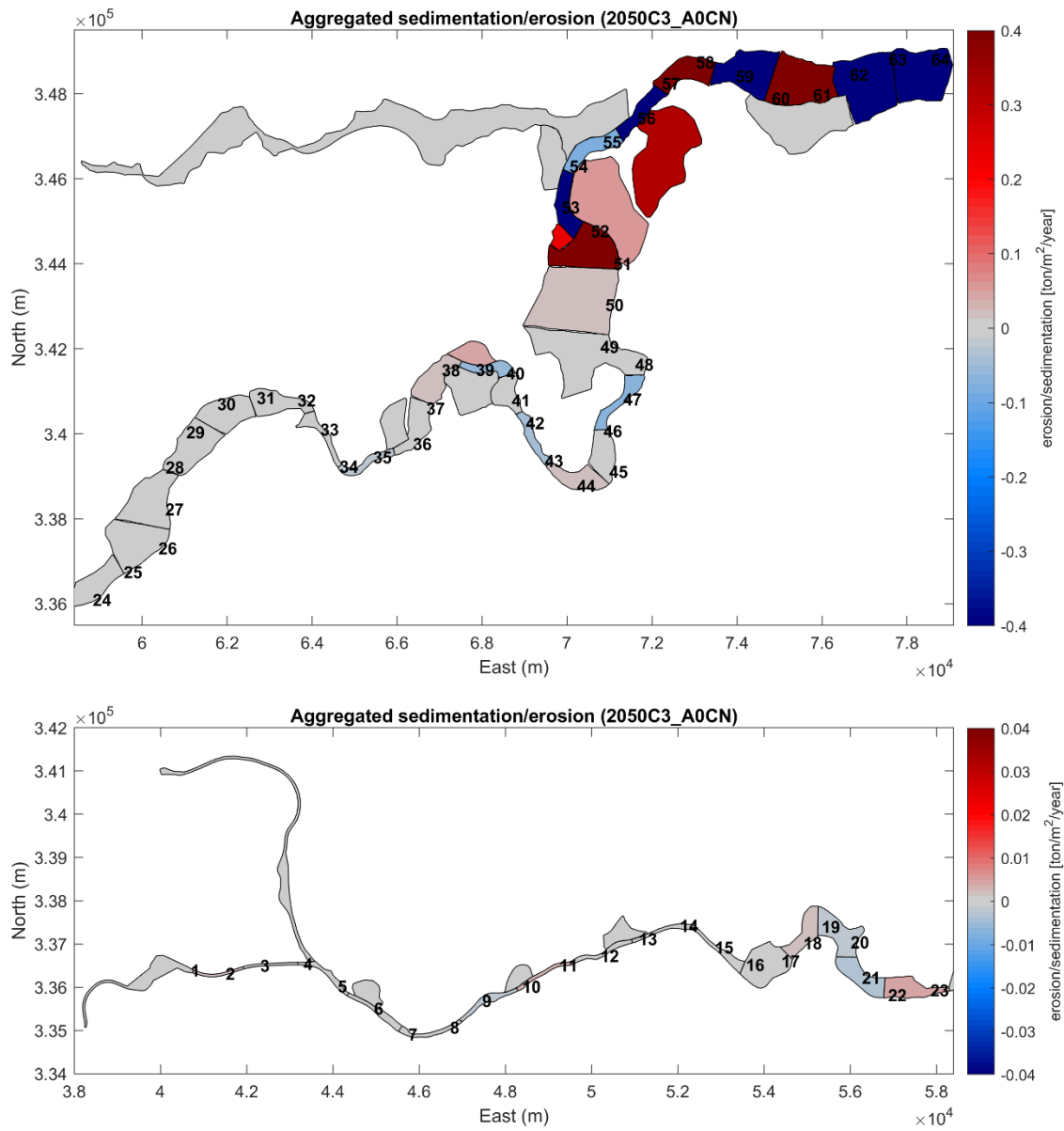


Figure 73 – Potential sedimentation and erosion map for the Upper Sea Scheldt. Scenario 2050C3\_A0CN. Erosion in blue and sedimentation in red. Numbers indicate the distance (km) from Merelbeke.

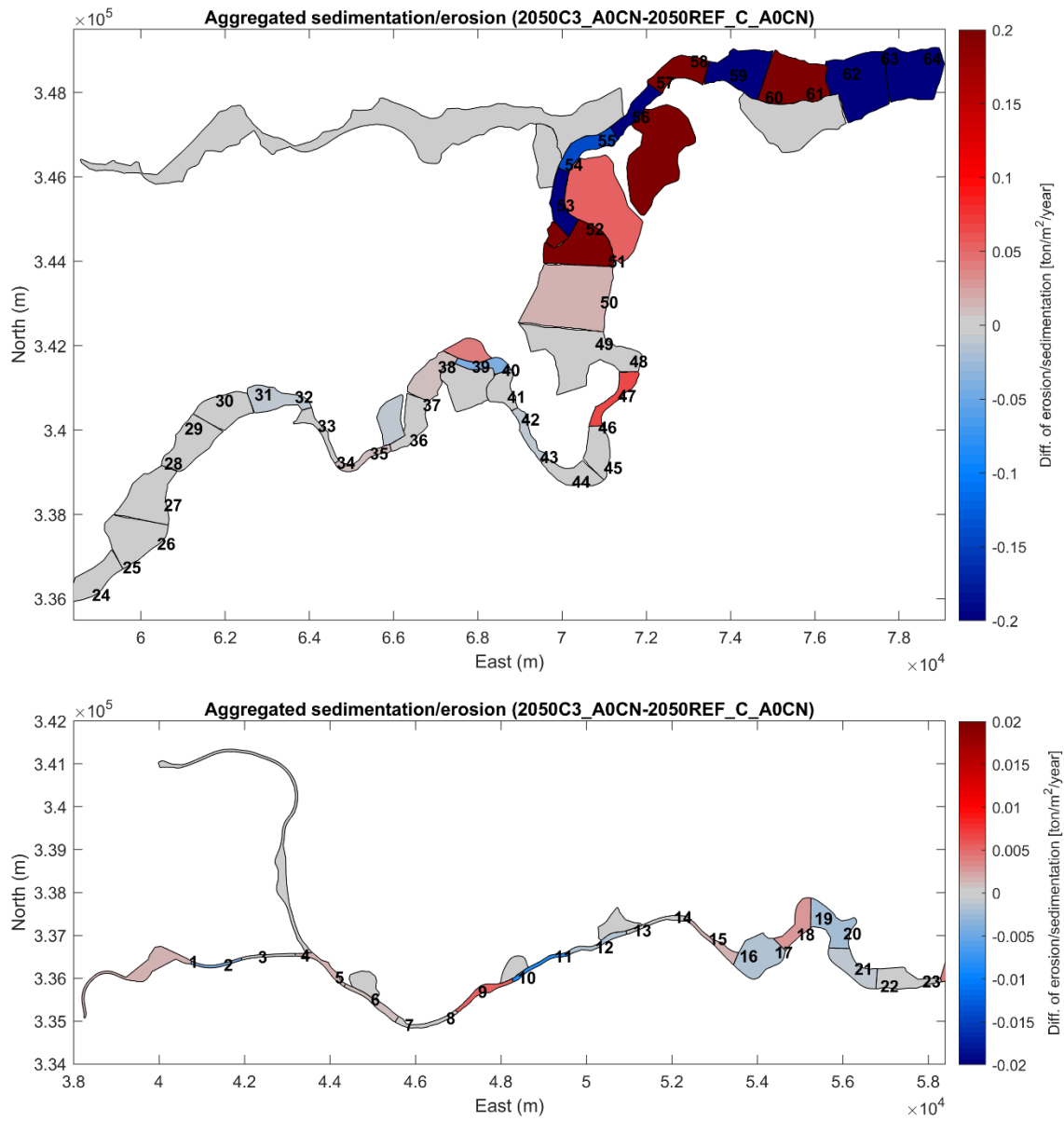


Figure 74 – Effect of C3 alternative on the sedimentation/erosion in the Upper Sea Scheldt under AOCN condition. Red indicates more sedimentation or less erosion.

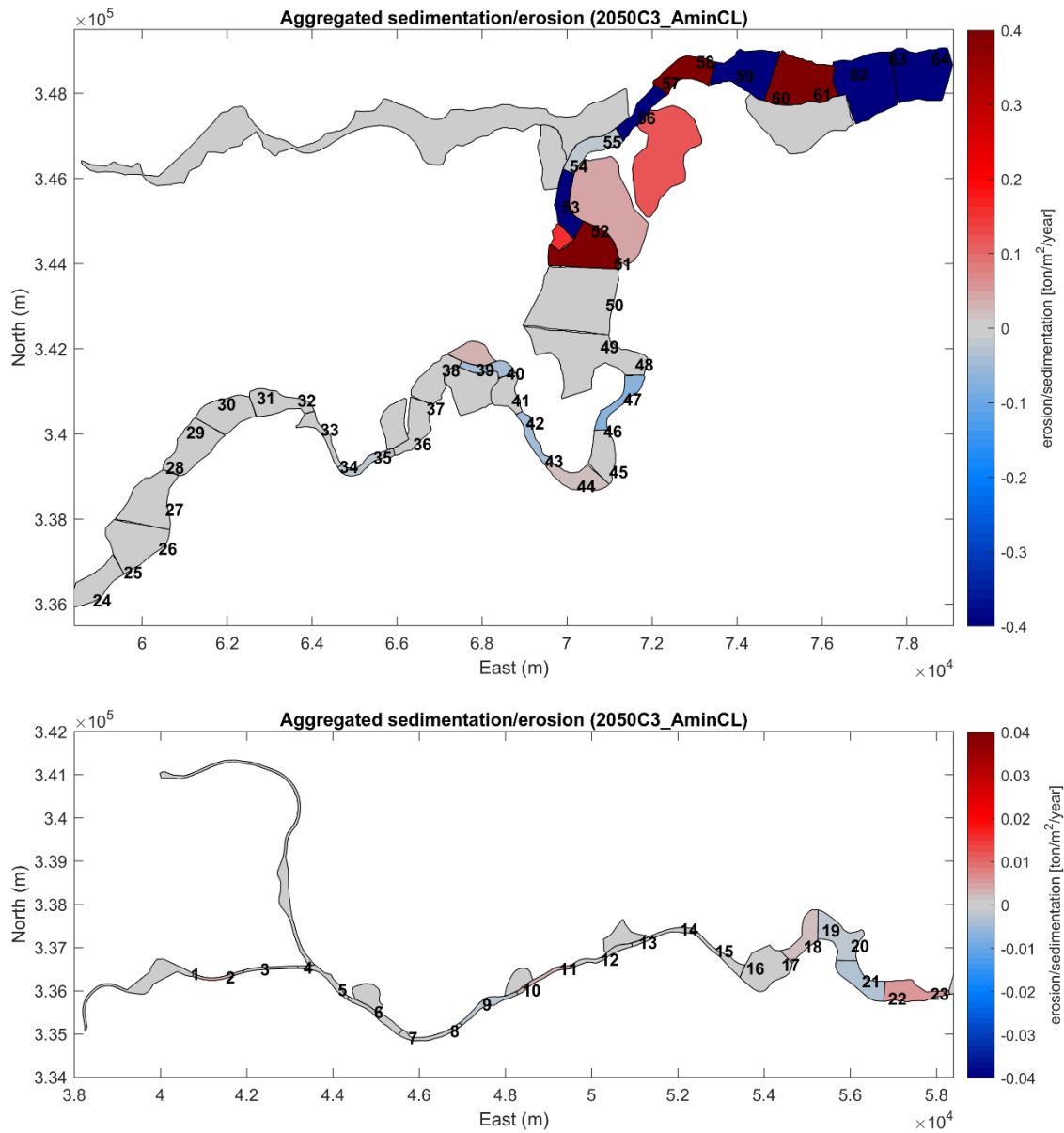


Figure 75 – Potential sedimentation and erosion map for the Upper Sea Scheldt. Scenario 2050C3\_AminCL. Erosion in blue and sedimentation in red. Numbers indicate the distance (km) from Merelbeke.

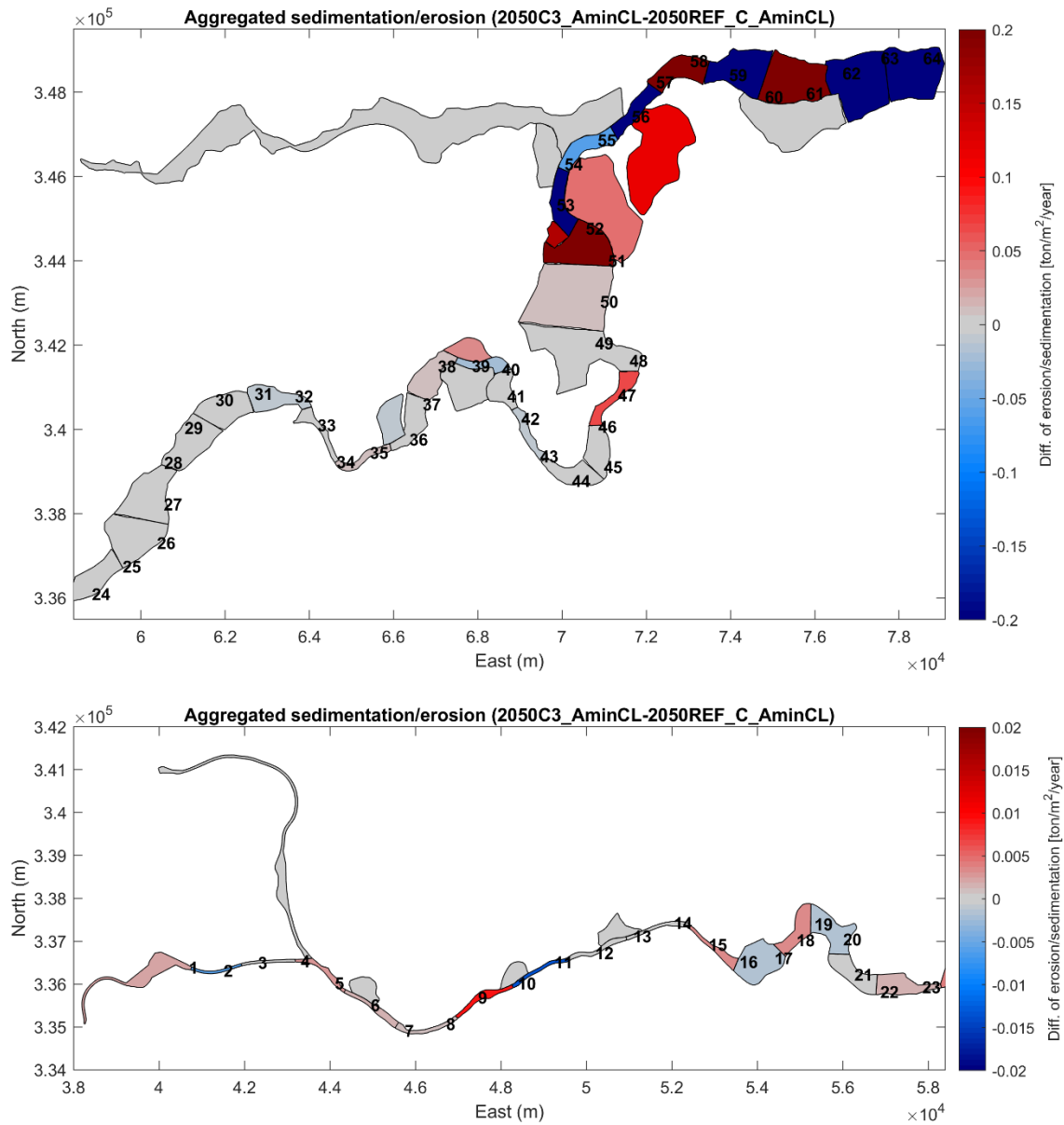


Figure 76 – Effect of C3 alternative on the sedimentation/erosion in the Upper Sea Scheldt under AminCL condition. Red indicates more sedimentation or less erosion.

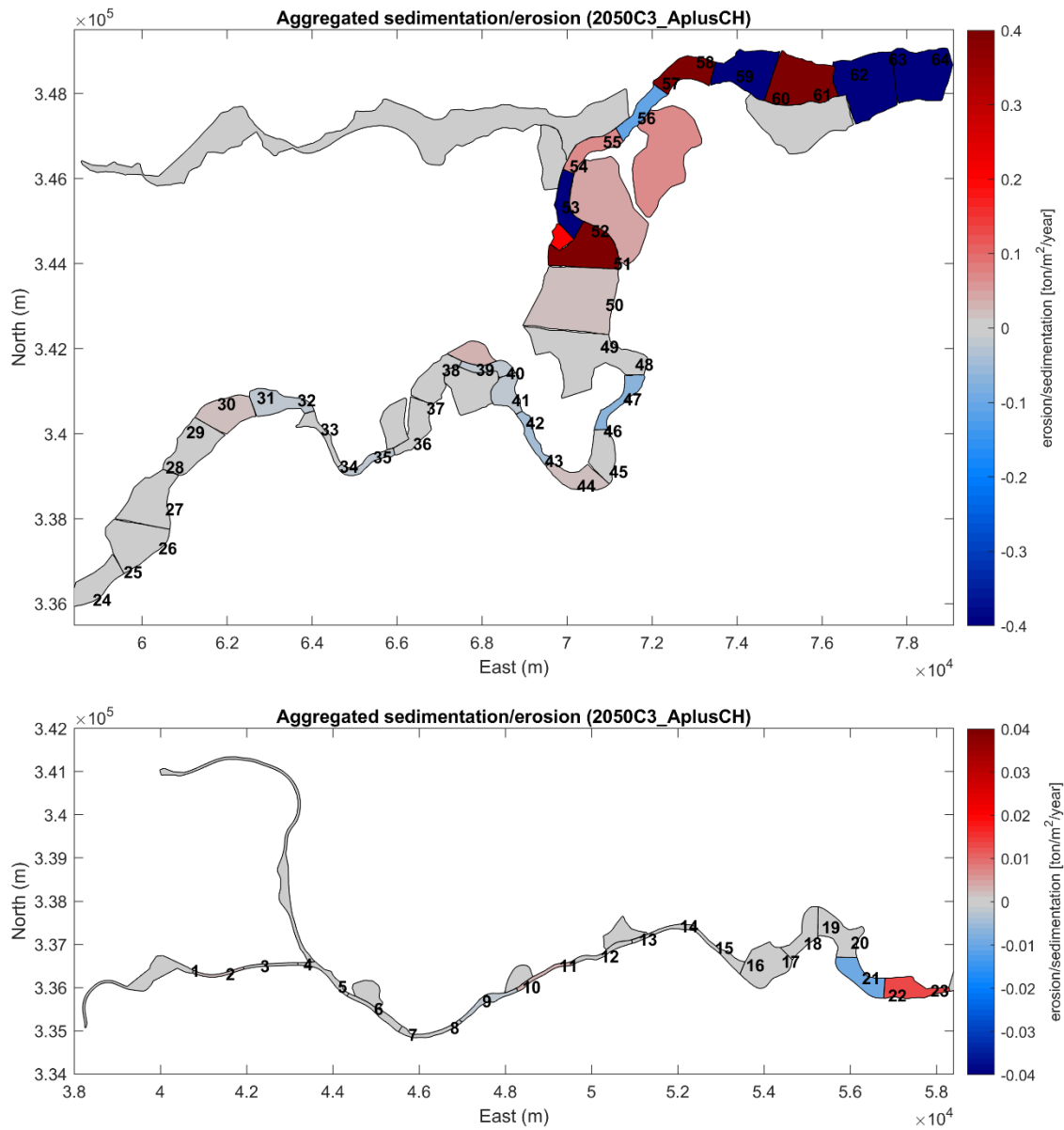


Figure 77 – Potential sedimentation and erosion map for the Upper Sea Scheldt. Scenario 2050C3\_AplusCH. Erosion in blue and sedimentation in red. Numbers indicate the distance (km) from Merelbeke.

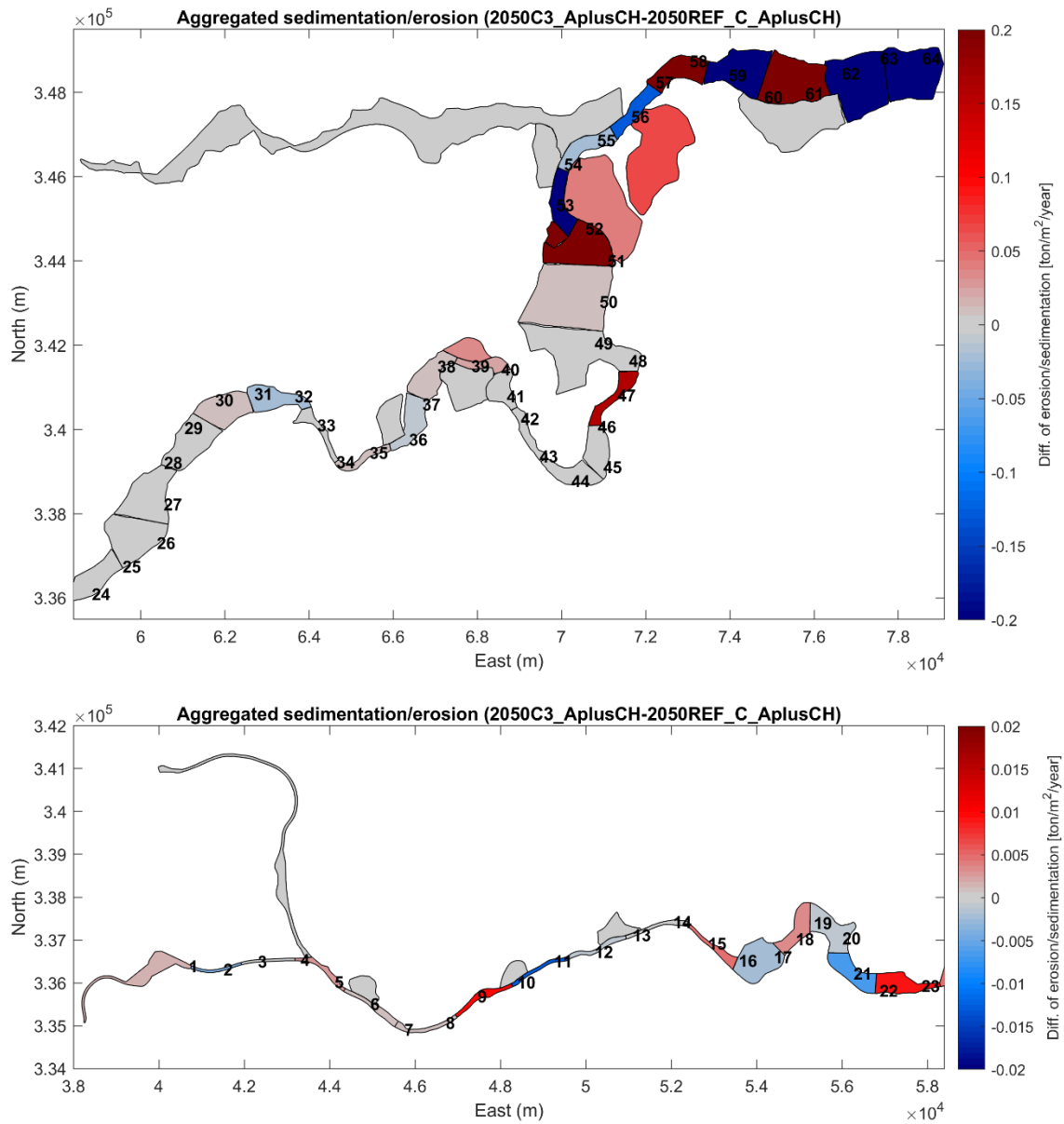


Figure 78 – Effect of C3 alternative on the sedimentation/erosion in the Upper Sea Scheldt under AplusCH condition. Red indicates more sedimentation or less erosion.



# Appendix 3. Bed evolution in the Upper Sea Scheldt

2050REF\_C

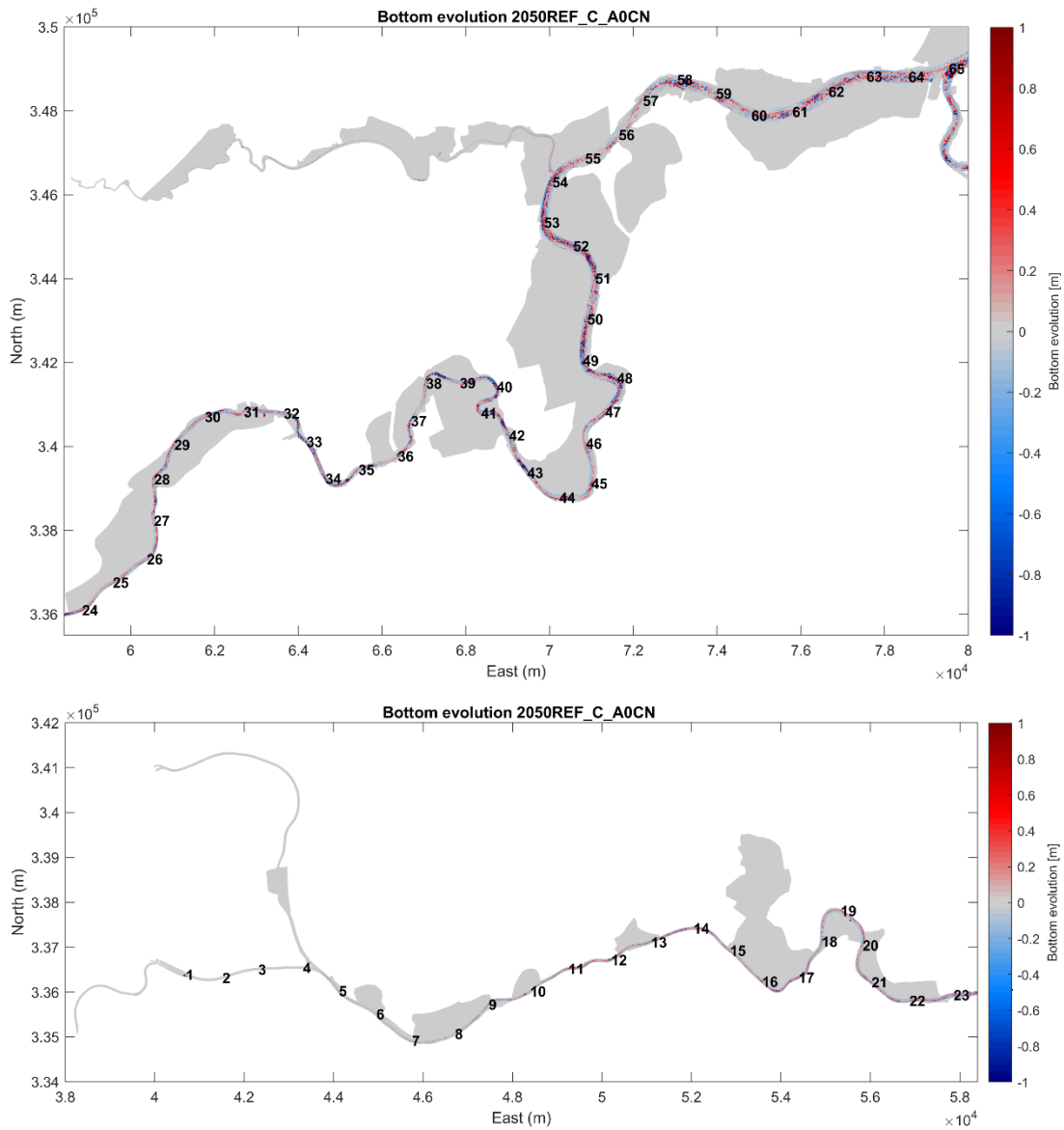


Figure 79 – Bed evolution in the Upper Sea Scheldt after a spring-neap cycle (2050REF\_C\_A0CN)

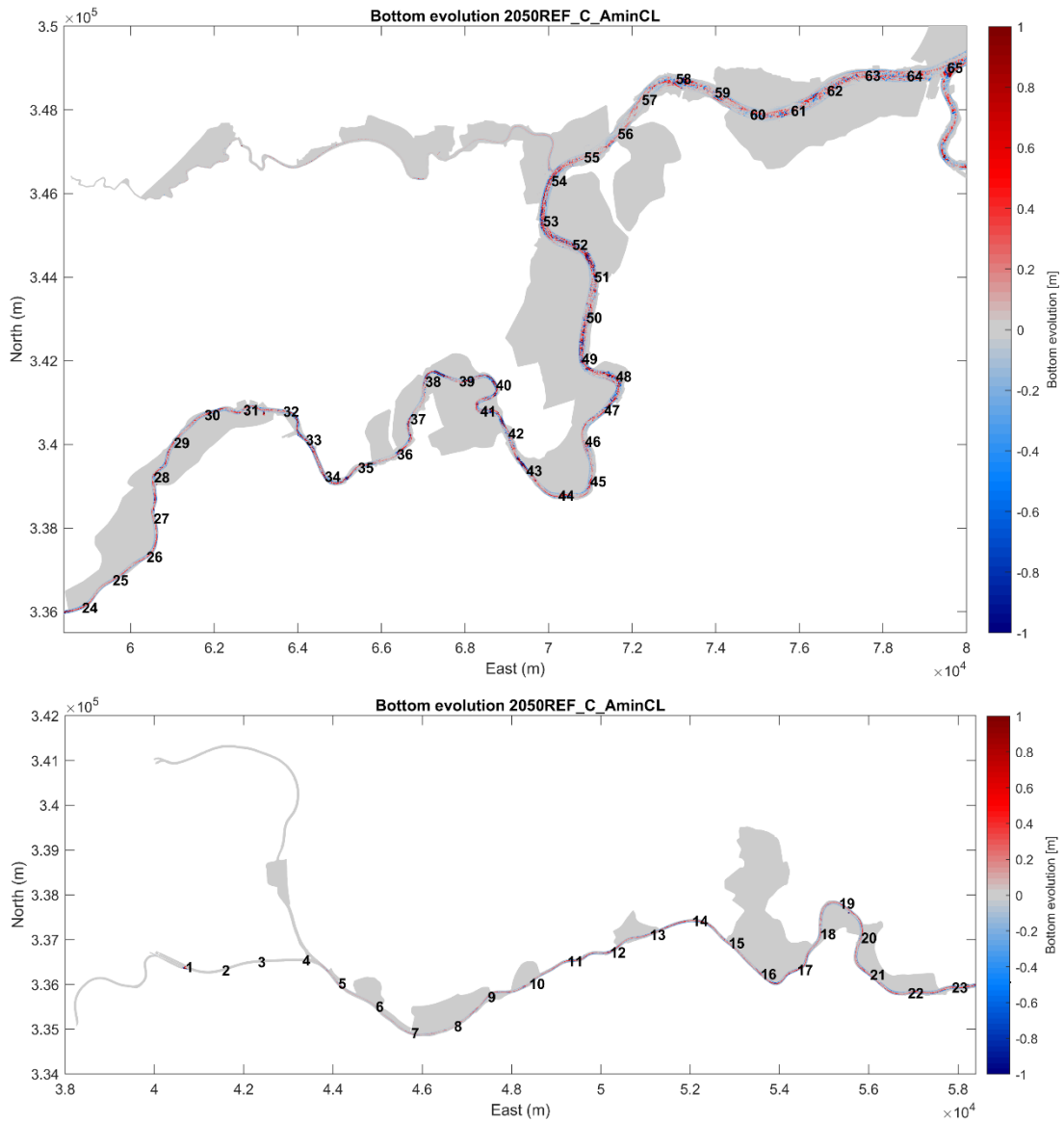


Figure 80 – Bed evolution in the Upper Sea Scheldt after a spring-neap cycle (2050REF\_C\_AminCL)

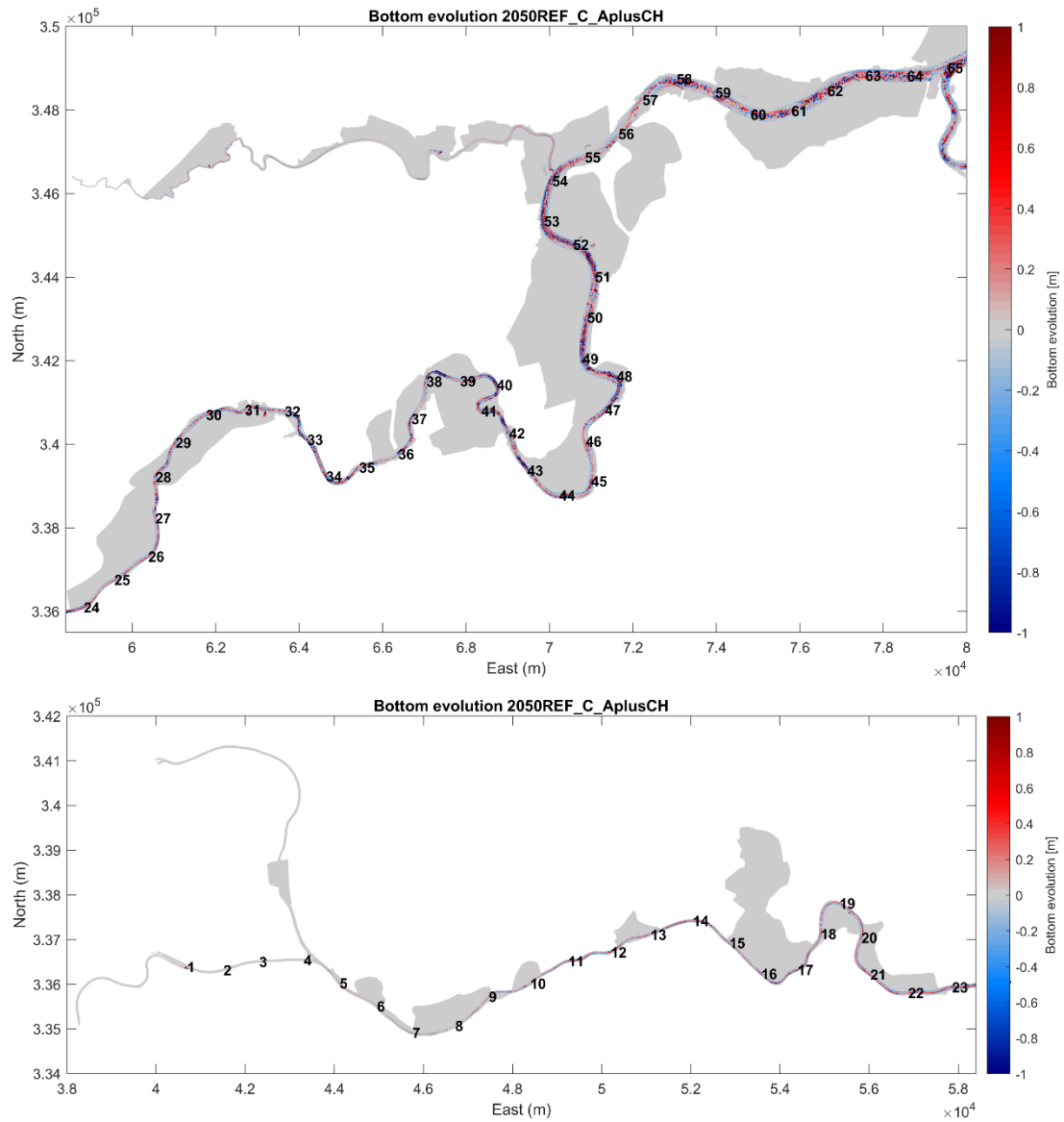


Figure 81 – Bed evolution in the Upper Sea Scheldt after a spring-neap cycle (2050REF\_C\_AplusCH)

2050C1

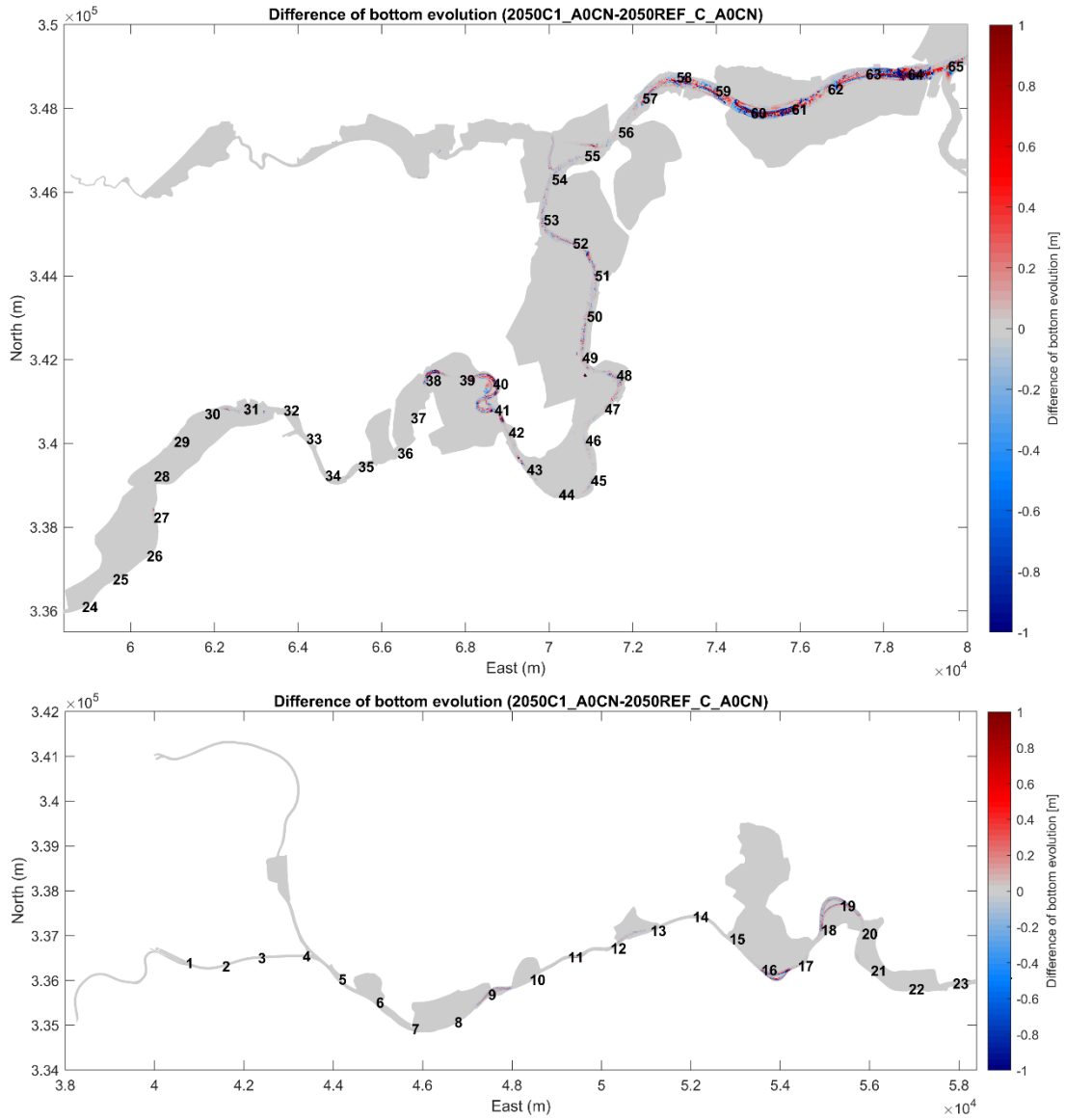


Figure 82 – Difference of bed evolution in the Upper Sea Scheldt after a spring-neap cycle (2050C1\_A0CN-2050REF\_C\_A0CN)

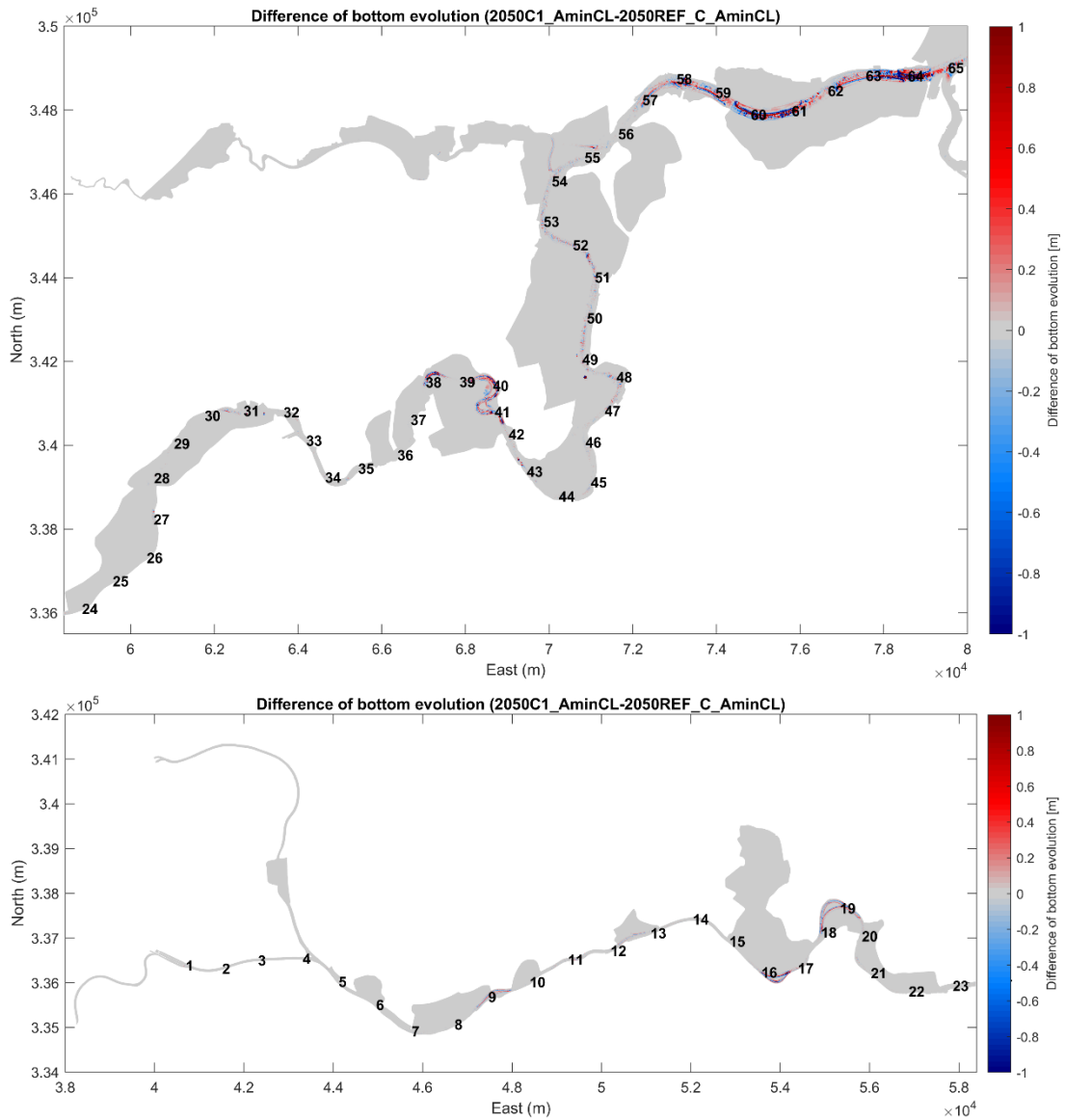


Figure 83 – Difference of bed evolution in the Upper Sea Scheldt after a spring-neap cycle (2050C1\_AminCL-2050REF\_C\_AminCL)

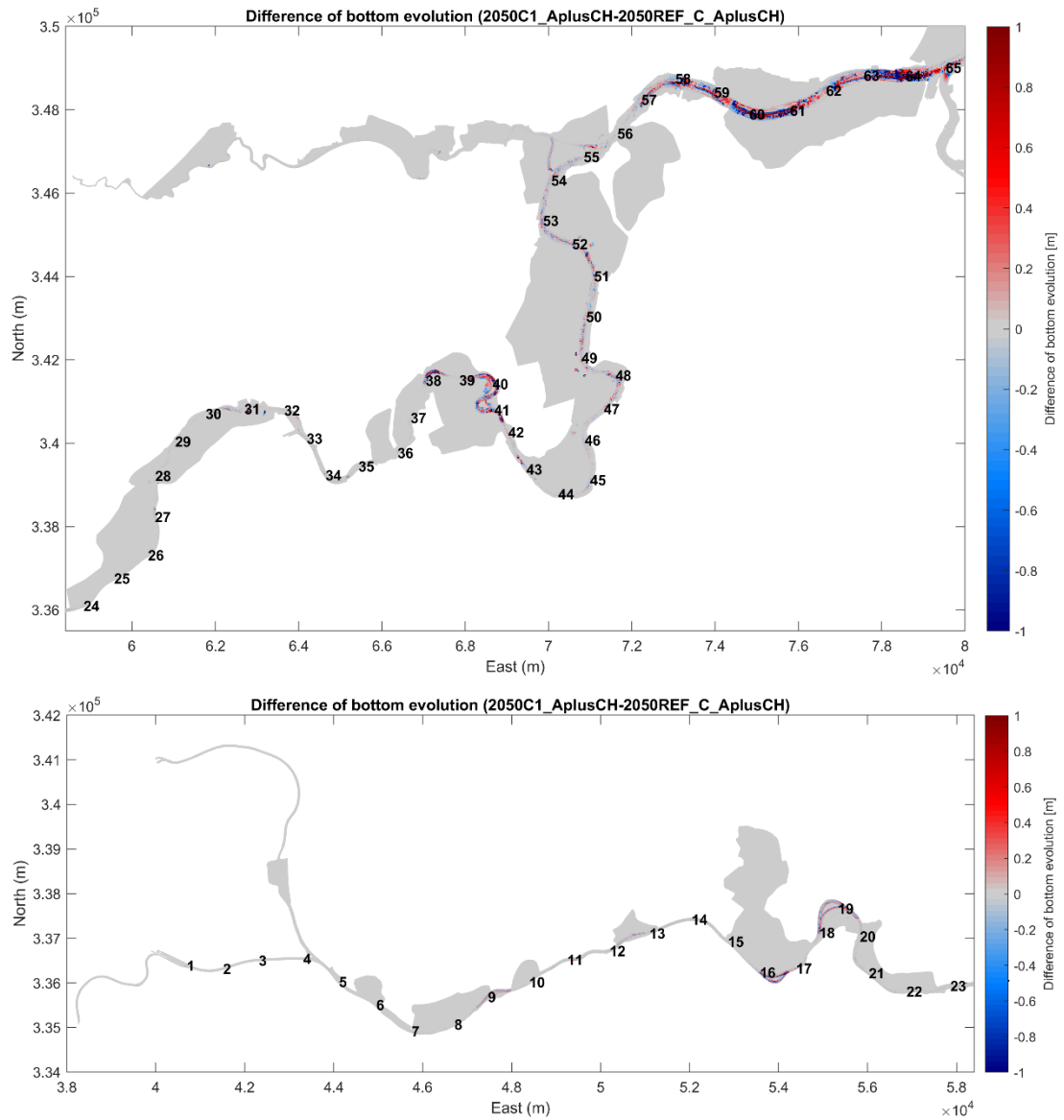


Figure 84 – Difference of bed evolution in the Upper Sea Scheldt after a spring-neap cycle (2050C1\_AplusCH-2050REF\_C\_AplusCH)

2050C2

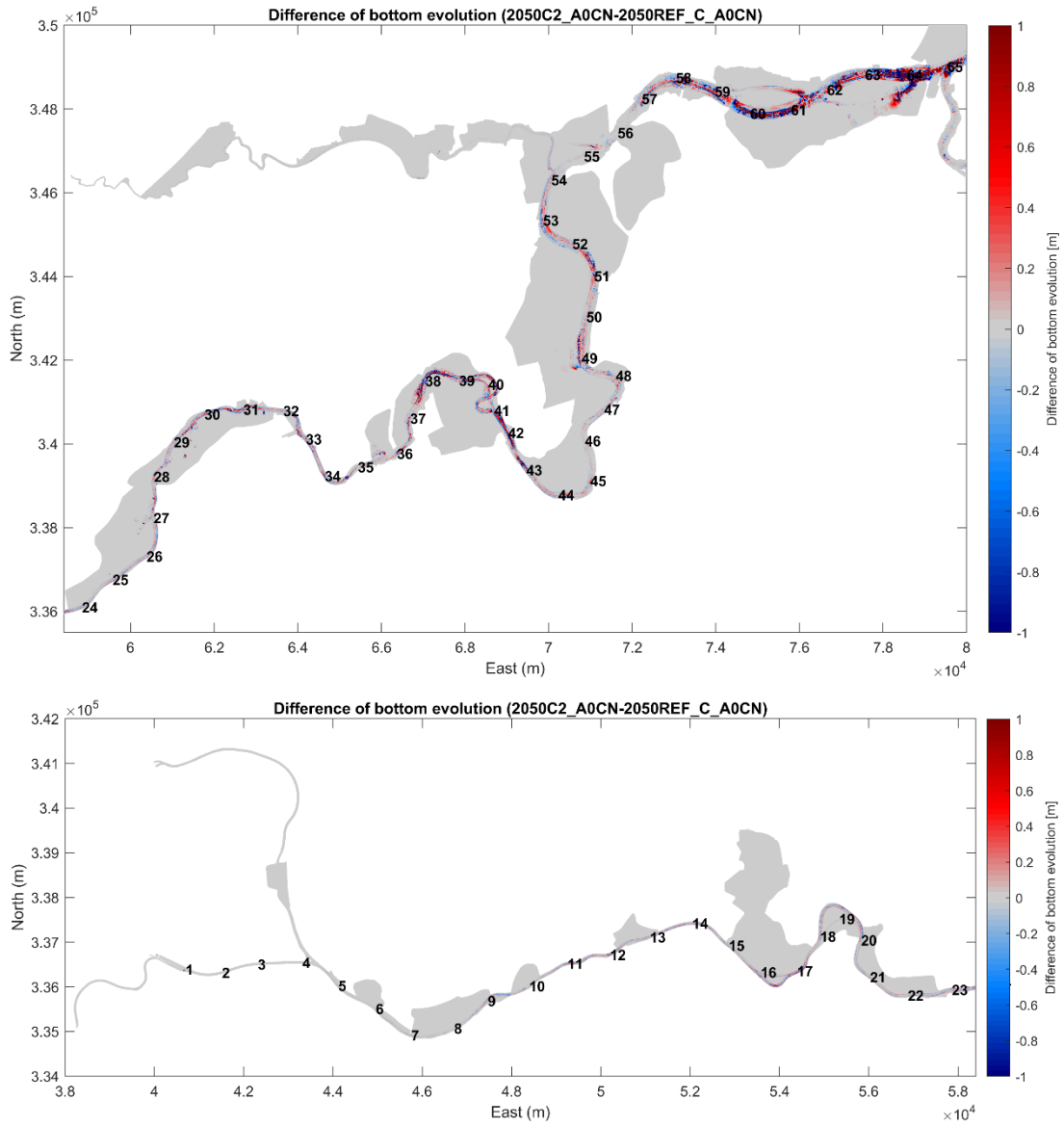


Figure 85 – Difference of bed evolution in the Upper Sea Scheldt after a spring-neap cycle (2050C2\_A0CN-2050REF\_C\_A0CN)

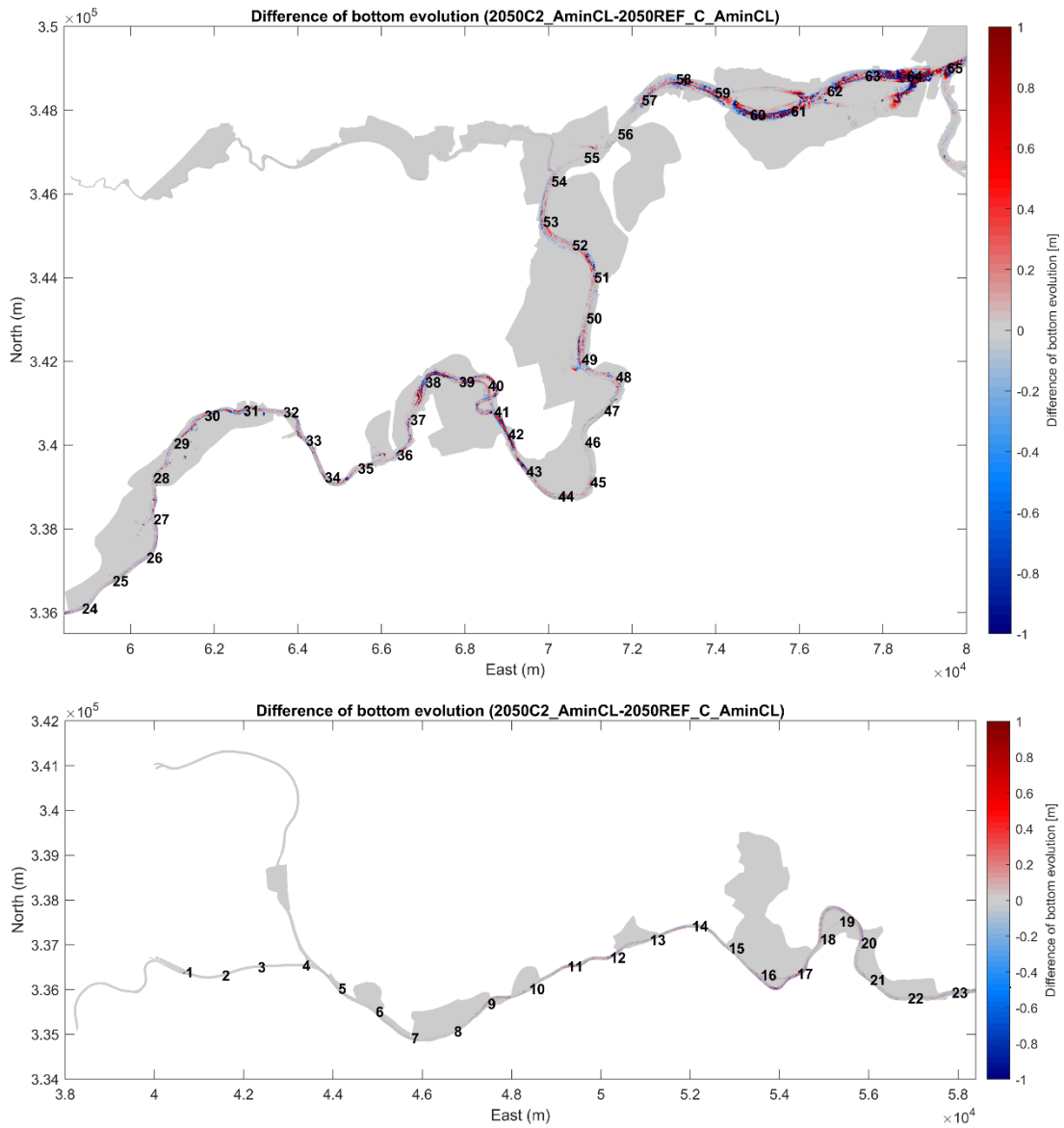


Figure 86 – Difference of bed evolution in the Upper Sea Scheldt after a spring-neap cycle (2050C2\_AminCL-2050REF\_C\_AminCL)



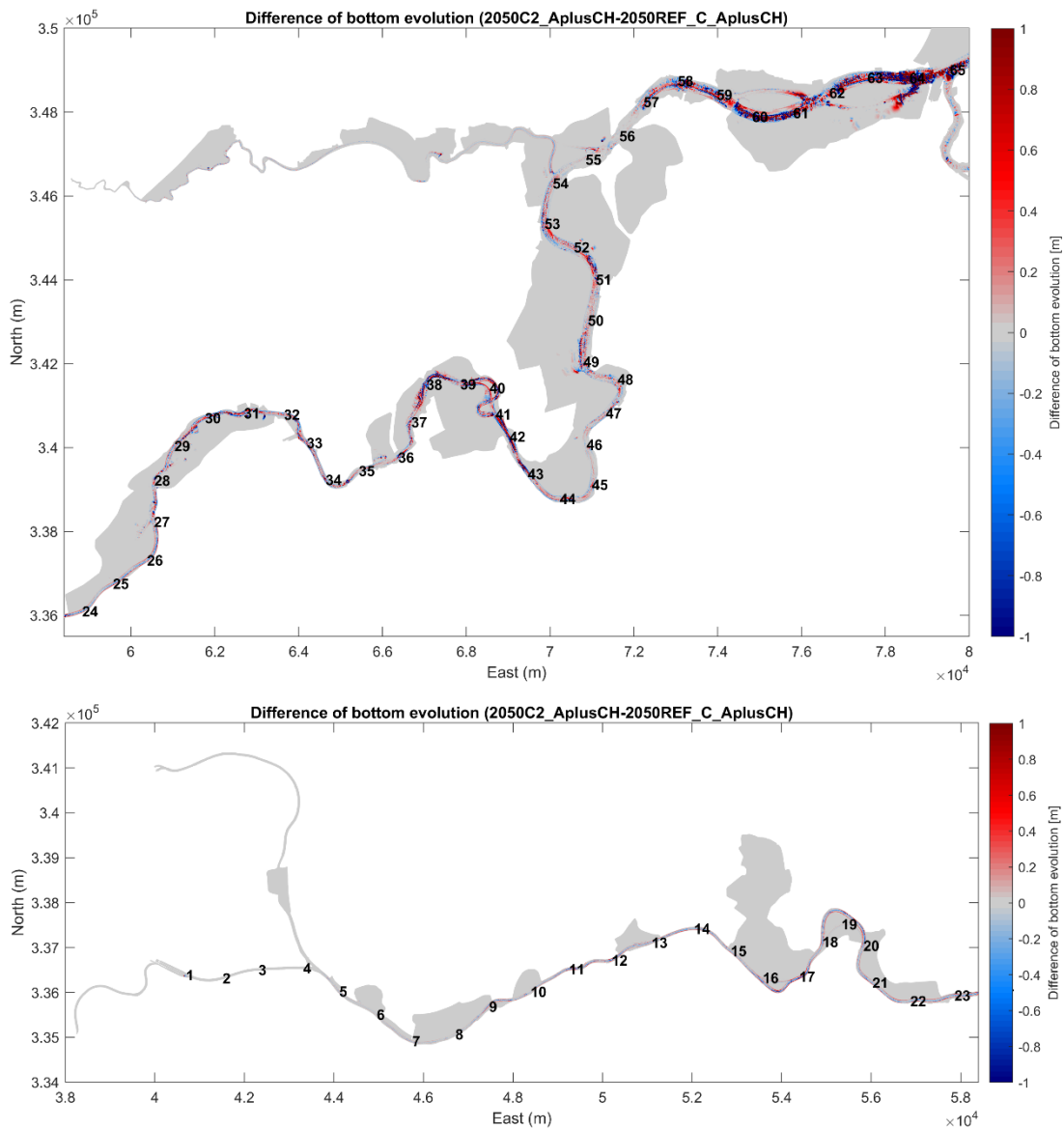


Figure 87 – Difference of bed evolution in the Upper Sea Scheldt after a spring-neap cycle (2050C2\_AplusCH-2050REF\_C\_AplusCH)

2050C3

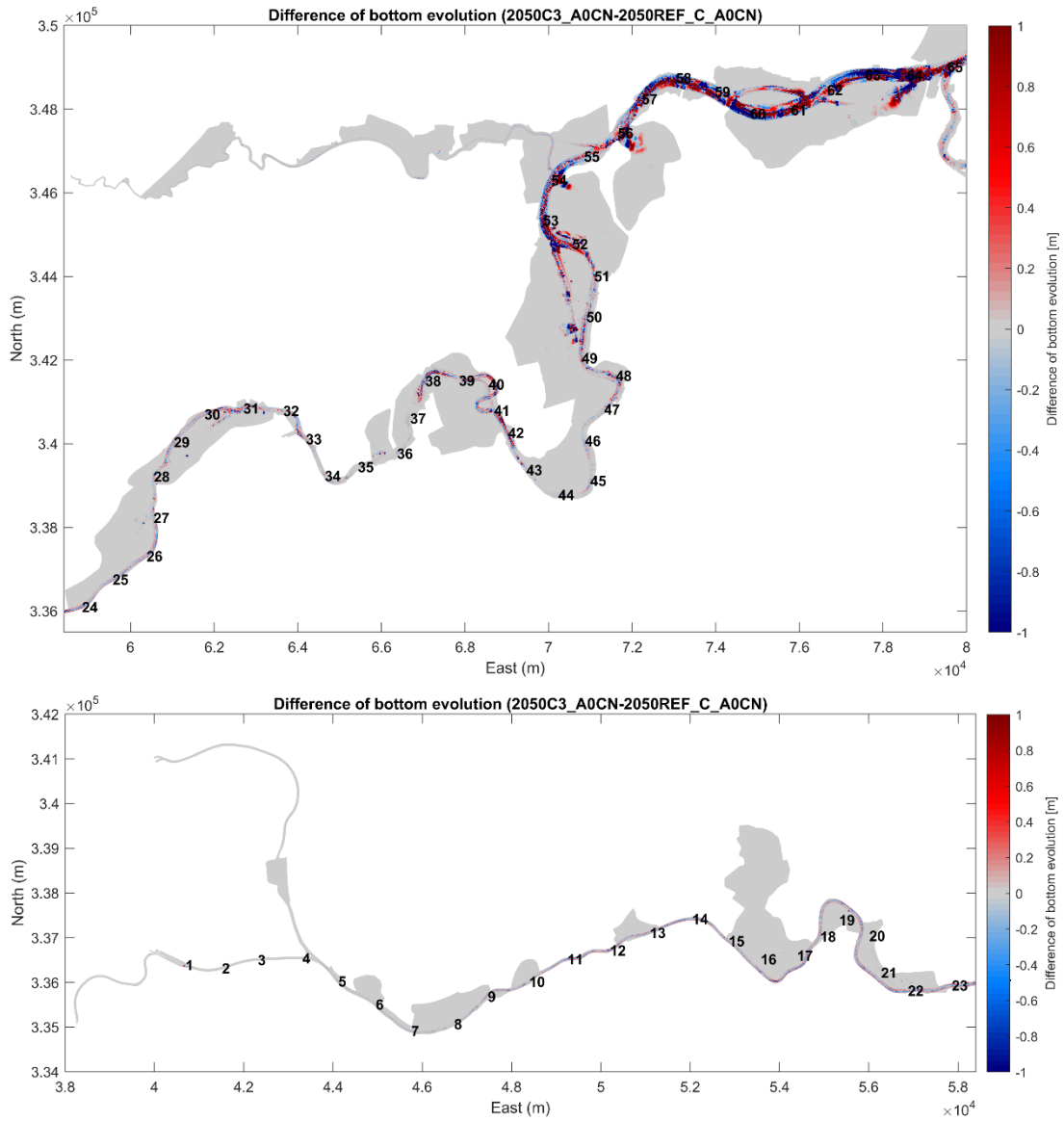


Figure 88 – Difference of bed evolution in the Upper Sea Scheldt after a spring-neap cycle (2050C3\_A0CN-2050REF\_C\_A0CN)

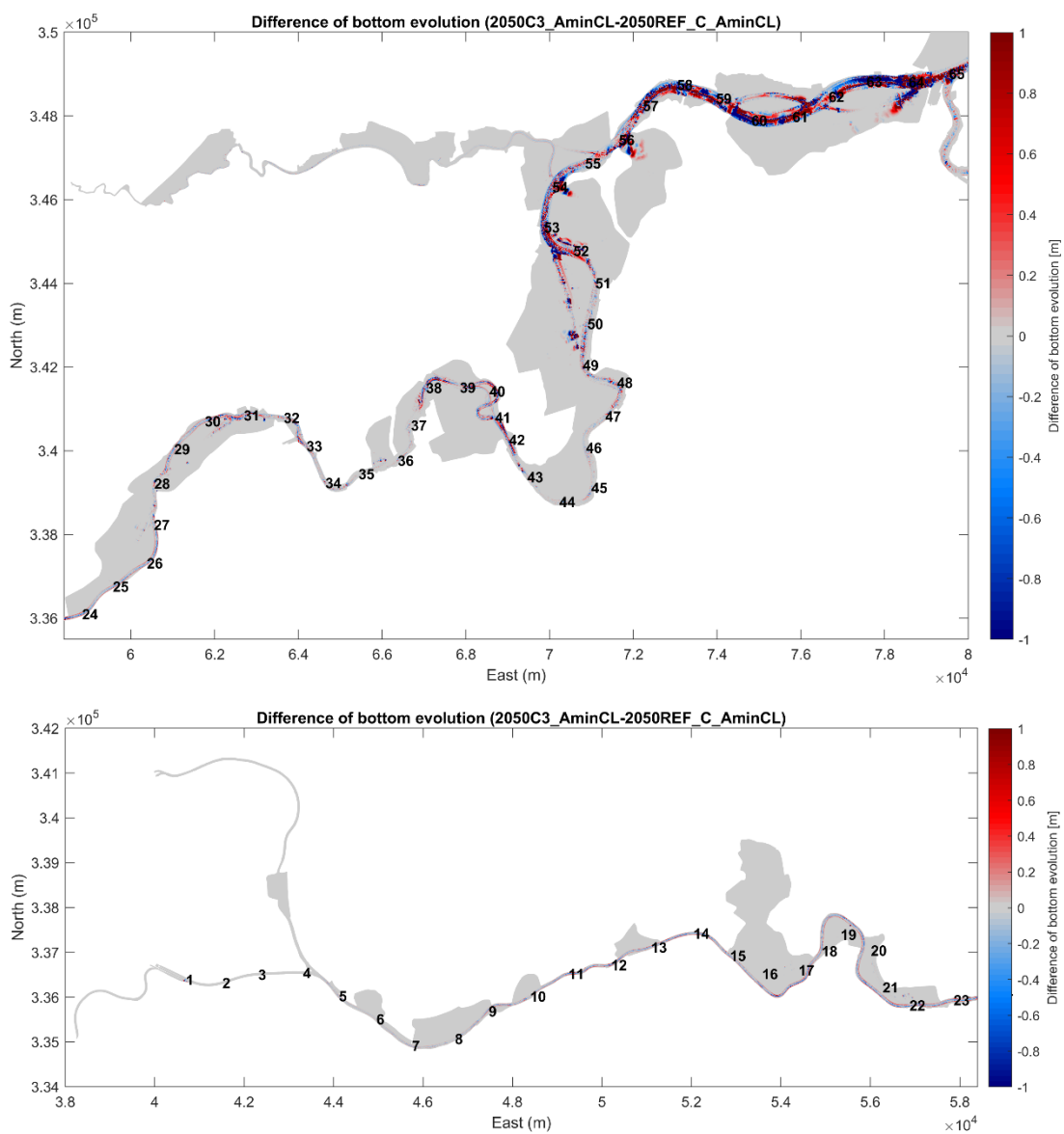


Figure 89 – Difference of bed evolution in the Upper Sea Scheldt after a spring-neap cycle (2050C3\_AminCL-2050REF\_C\_AminCL)

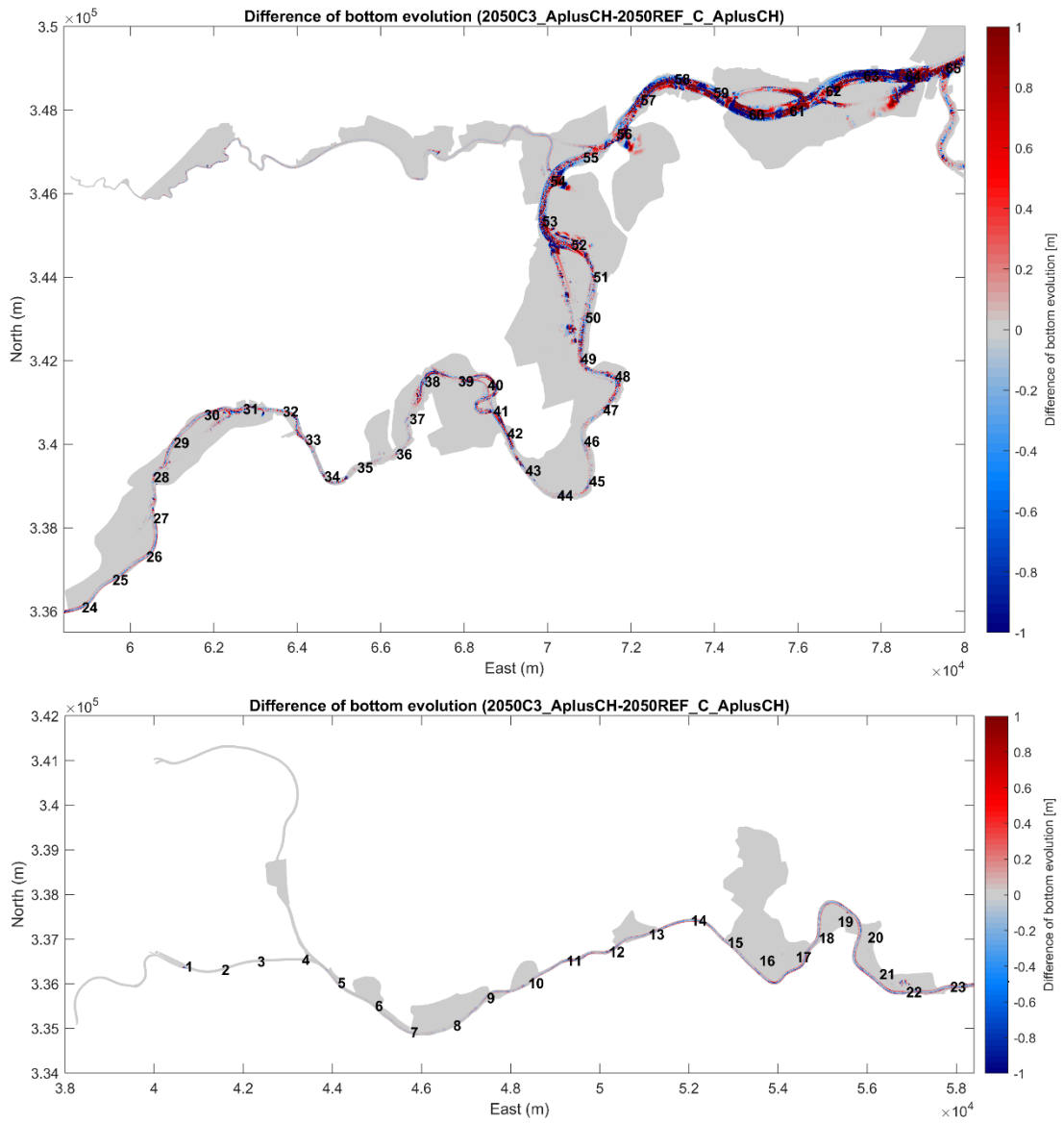


Figure 90 – Difference of bed evolution in the Upper Sea Scheldt after a spring-neap cycle (2050C3\_AplusCH-2050REF\_C\_AplusCH)

DEPARTMENT **MOBILITY & PUBLIC WORKS**  
Flanders hydraulics Research

Berchemlei 115, 2140 Antwerp

T +32 (0)3 224 60 35

F +32 (0)3 224 60 36

[waterbouwkundiglabo@vlaanderen.be](mailto:waterbouwkundiglabo@vlaanderen.be)

[www.flandershydraulicsresearch.be](http://www.flandershydraulicsresearch.be)